UNIVERSITÉ DU QUÉBEC À MONTRÉAL

ENVIRONMENTAL INFLUENCES ON MAJOR BIOEVENTS IN THE EDIACARAN, IN THE ORDOVICIAN AND AT THE PERMIAN-TRIASSIC BOUNDARY

THESIS

PRESENTED

AS PARTIAL REQUIREMENT FOR A

Ph.D IN EARTH AND ATMOSPHERE SCIENCES

BY

TONGGANG ZHANG

MAY 2010

UNIVERSITÉ DU QUÉBEC À MONTRÉAL

INFLUENCES ENVIRONNEMENTALES SUR LES ÉVÈNEMENTS BIOLOGIQUES À L'ÉDIACARIEN, À L'ORDOVICIEN ET À LA LIMITE PERMO-TRIAS

THÈSE
PRÉSENTÉE
COMME EXIGENCE PARTIELLE DU DOCTORAT
EN SCIENCES DE LA TERRE ET DE L'ATMOSPHÈRE

PAR
TONGGANG ZHANG

MAI 2010

REMERCIEMENTS

Mes premiers remerciements vont à mon directeur de thèse, Prof. Yanan Shen et Prof. Daniele L. Pinti qui m'a donné ma chance de faire mon projet de Ph.D au Canada. Pendant ces trois dernières années, ils m'ont beaucoup aidé dans mes recherches et dans ma vie.

Mes sincères remerciements vont aux membres du jury qui ont accepté d'évaluer cette thèse: Prof. Boswell Wing, Prof. Jean-Claude Mashall, Prof. Ross Stevenson. Ils ont soigneusement passé en revue ma proposition de Ph.D et m'ont donné de nombreux conseils pour accomplir mon projet de Ph.D.

Je remercie Renbin Zhan pour les conseils lors des campagnes de terrain dans le Sud de la Chine, ainsi que Wiesław Trela pour les échantillons de carotte de forage. Merci à Agnieszka Adamowicz, Jean-François Hélie, Alen J. Kaufman, Fusong Zhang, Shaoyong Jiang pour leur aide dans les analyses géochimiques.

Mes sincères remerciements vont aussi à Alain Tremblay, Michel Lamothe, Alfred Jaouich, Sophie Bonnet, Lysa Brunet, Sophie Chen, Bianca Fréchette, José Savard, Chantal Gosselin, Nicole Turcot, Micheline Lacroix, et Jinghui Zhao pour leurs aides à mon étude et à ma vie à Montréal.

Merci au GEOTOP pour la bourse de trois ans de Ph.D pendant mon étude. Ce projet a été soutenu par le CRSNG et la Fondation Nationale des Sciences Naturelles de Chine.

RÉSUMÉ

De multiples analyses géochimiques (isotopes du carbone et du soufre, spéciation du fer, contenu en carbone et soufre dans le sédiment et éléments traces) ont été effectuées pour étudier les influences environnementales sur la diversification de la faune d'Édiacara (~570 Ma), à l'Ordovicien inférieur et moyen (~470 Ma), aux extinctions de masse de l'Ordovicen (~445 Ma) et de la limite Permien-Trias (~251 Ma). Les enregistrements haute-résolution de $\delta^{13}C$ et de $\delta^{13}C$ org d'une section provenant de Honghuayuan (Sud de la Chine) ont montré une élévation de +8‰ du $\delta^{13}C$ dans le Floian de l'Ordovicien. Cela implique une hausse du taux d'enfouissement de la matière organique pendant la première partie de l'Ordovicien récent qui aurait pu contribuer au refroidissement climatique et déclencher cet évènement. Les deux valeurs positives du $\delta^{13}C_{org}$ correspondent aux deux pulses de l'extinction de masse de l'Ordovicien. Cela implique des changements dans le cycle biogéochimique du carbone qui sont associés à l'extinction de masse de l'Ordovicien. Les valeurs élevées de $\delta^{34}S$ de la pyrite, le bref passage à des valeurs négatives du $\delta^{34}S$ de 20‰, associés à un ralentissement de la glaciation traduiraient des conditions anoxiques dans l'océan profond pendant la période hirnantienne. Ces conditions anoxiques pourraient avoir pris part à l'extinction de masse à la fin de l'Ordovicien dans le Sud de la Chine et probablement ailleurs. La spéciation des isotopes du Fe et du S, les données de pyrite provenant de la formation de Sheepbed (Canada) et de Doushantuo (Chine) ont suggéré que l'oxygénation progressive des eaux de fond pourrait avoir permis l'apparition burtale des animaux au début de l'Édiacarien et avoir déclenché leur diversification.. Les données isotopiques de C et S, à la limite Pr-T de Nhi Tao (Vietnam), exposent un appauvrissement en ^{34}S, des valeurs négatives du $\delta^{13}C$ des carbonates, et une variation positive significative entre les horizons pyriteux (proxy : $[S]_{py}$ et $\delta^{34}S_{py}$) et $\delta^{13}C$ de carbonate (10-20 cm). Ces données isotopiques suggèrent que la remontée des eaux profondes anoxiques pourrait avoir servie comme mécanisme de déclenchement pour l'extinction de masse du Permien.

Mots clés : diversification, extinction de masse, isotope du carbone, isotope du soufre, spéciation du Fe, procédé de refroidissement, oxique, anoxique

ABSTRACT

Multiple geochemical measurements including stable C- and S-isotopes, Fe speciation, C and S content of sedimentary rocks were performed to investigate environmental influences on the Ediacara biota radiation (~ 570 Ma ago), the Early-Middle Ordovician biodiversification (~ 470 Ma ago), the Late Ordovican mass extinction (~445 Ma ago) and the Permian-Triassic mass extinction (~ 251 Ma ago). High-resolution $\delta^{13}C_{carb}$ and $\delta^{13}C_{org}$ records from a well-exposed section at Honghuayuan in South China exhibited a ~+8‰ excursion in $\delta^{13}C_{org}$ values in the Floian of Early Ordovician. It implies a large increase in the burial rate of organic matter during the mid-Early Ordovician that may have contributed to climatic cooling and played an important role in triggering the GOBE. Two positive $\delta^{13}C_{org}$ excursions corresponding to the two episodes of the Late Ordovician mass extinction suggest the changes in carbon biogeochemical cycle were associated with the Late Ordovician mass extinction. The elevated $\delta^{34}S_{py}$ values of pyrites and a large, short-lived negative $\delta^{34}S_{py}$ excursion of ~20‰ associated with the decay of the glaciation suggest deep-water anoxia may have contributed to the Late Ordovician mass extinction. Fe speciation and S-isotope of pyrite data from the Sheepbed Formation in Canada and the Doushantuo Formation in China suggested that the gradual oxygenation of bottom seawaters could have allowed the abrupt appearance of the earliest animals in the Early Ediacaran and triggered the biodiversification of those animals in Middle-Late Ediacaran. Paired C- and S-isotopic records of the Pr-T boundary at Nhi Tao, Vietnam exhibit strongly ^{34}S-depleted sulfur isotopic compositions, negative carbonate $\delta^{13}C$ excursions, and a significant positive covariation between pyritic horizons (as proxied by $[S]_{py}$ and $\delta^{34}S_{py}$) and carbonate $\delta^{13}C$ at a fine (10–20 cm) stratigraphic scale in Late Permian. These C- and S-isotopic records suggest the upwelling of anoxic deep-waters could have been served as a mechanism for the Late Permian marine mass extinction.

Key words: biodiversification, mass extinction, carbon isotope, sulphur isotope, Fe speciation, cooling process, oxic, anoxic

LISTE DES TABLEAUX

LISTE DES FIGURES

TABLE DES MATIÈRES

General Introduction

The Great Ordovician Biodiversification Event and the Late Ordovician Mass extinction

Profound changes in the biosphere of the Earth occurred during the Ordovician Period (488.3Ma-443.7 Ma). A Great Ordovician Biodiversification Event (GOBE) began ~470 Ma ago during the Early Ordovician and possibly lasted more than 25 Myr into the Late Ordovician (Fig.1, Droser and Sheehan, 1997; Miller, 1997; Webby et al., 2004; Servais et al., 2009). Although the Cambrian explosion resulted in the appearance of nearly all phyla of marine animals, biodiversity at the taxonomic ranks of family, genus and species level remained low until the GOBE (Sepkoski, 1997). By the end of GOBE, biodiversity at the family level had increased to more than three times that in the Cambrian and Early Ordovician (Webby et al., 2004). Following the GOBE, the Great Late Ordovician mass extinction (GOME) occurred ~445 Ma ago (Fig.1, Sepkoski, 1996; timescale of Gradstein et al., 2004), which was the first of the five greatest mass extinctions in the Phanerozoic (Sepkoski, 1991). During the Late Ordovician mass extinction, about 26% of families, 49% of genera and 85% of all species became extinct (Sepkoski, 1996; Jablonski, 1991). On the extinct scale, it is the second largest extinction of the five great extinction events, only next to the end-Permian mass extinction (Fig.1, Sepkoski, 1996).

During the past several decades, the GOBE has received less attention (Bottjer et al., 2001), and the cause of this event remains debated (Servais et al., 2009). It was traditionally proposed that the GOBE occurred during a period of greenhouse conditions and did not coincide with any abrupt environmental changes, and that it simply represented a realization of innate evolutionary potential among early metazoans (Gibbs et al., 1997; Webby et al., 2004). However, recent studies have emphasized the role of environmental changes as a trigger for the GOBE. Trotter et al. (2008) argued on the basis of oxygen-isotopic thermometry of conodonts that climatic cooling may have led to the GOBE. Alternatively, Schmitz et al. (2008) suggested on the basis of changes in the abundance of extraterrestrial chromite grains and the ratio of seawater $^{187}Os/^{188}Os$ that meteorite impacts accelerated the pace of biodiversification during the Early to Middle Ordovician. According to the diversity curve, the Ordovician biodiversification can be divided into two episodes (Fig. 1). The first

episode occurred from the Floian to early Darriwilian, during which number of genera increased from 500 to ~1000, and the second episode occurred from early Sandbian to the onset of the mass extinction, during which number of genera increased from ~1000 to ~1800. However, Trotter et al. (2008) and Schmitz et al. (2008) only investigated the cause of the first episode. In this project, a trigger for the first episode as well as the cause of the second episode will be investigated.

By contrast, the Late Ordovician mass extinction has attracted a lot of studies and a series of documents have been published during the past two decades, including stratigraphy, biostratigraphy, chronology, paleontology, chemostratigraphy (Sheehan 2001 and references therein). At the same interval as the mass extinction, there was an extensive glaciation developed on the Gondwana supercontinent that profoundly influenced on the global environment (Brenchley et al., 1991, 1994). In recent years, C-isotopic chemostratigraphic records worldwide from either brachiopod shells (Qing and Veizer, 1994), or whole-rock limestones and cements, or organic carbon from organic-rich shales, exhibit several remarkable trends in global scale (e.g., Brenchley et al., 2003). The studies of C-isotopic chemostratigraphic records have been conducted in Anticosti Island, Quebec (Orth et al., 1986, Long, 1993; Benchley et al., 1994, 1995), the Selwyn Basin, Northwest Canada (Wang et al., 1993b), the Yukon Territory, Canada (Goodfellow et al., 1992), the Arctic Canada (Melchin and Holmden, 2006), the United Kingdom (Wilde et al., 1986; Underwood et al., 1997), south China (Wang et al., 1993a, 1997), central Nevada (Kump et al., 1999; Finney et al., 1999; Saltzman and Young, 2005; Mitchell et al., 2007), Baltica (Marshall et al., 1997; Brenchley and Marshall, 1999; Kaljo et al., 1999, 2001, 2004; Benchley et al., 1994, 1995, 2003), western Argentina (Marshall et al., 1997).

Integrated with the oxygen isotope data from brachiopod and ostracode calcite, and sedimentological observations, Brenchley et al. (2003) suggested that the carbon isotope excursion started nearly at the same stratigraphic level as the onset of global cooling, sea-level fall, and the first pulse of mass extinction. The later rise in sea-level and decrease in $\delta^{13}C$ values record the end of the glaciation. So the late Ordovician extinction was mainly attributed to consequences of the late Ordovician glaciation. Sea-level change, temperature variations, and reduction in habitats resulting from the late Ordovician glaciation were hypothesized to have killed most marine animals (Sheehan 2001 and references therein).

The Ediacaran animal radiation

Paleontology evidence indicated that the earliest marine animals appeared in the Ediacran(630-542 Ma ago)oceans(Knoll and Carroll, 1999;Narbonne, 2005) that followed the global Neoproterozoic glaciations event called snowball Earth (Hoffman et al., 1998; Hoffman and Schrag, 2002).Fossil studies revealed that those Ediacaran animals were soft-bodied, multicellular organisms(Narbonne,2005 and references therein).In contrast with the microscopic fossils that dominate most Precambrian fossil assemblages, Ediacaran fossils are typically in the centimeter to decimeter size, with some large sizes up to a meter in length (Narbonne, 2005 and references therein). The abrupt appearance of large animals in the Ediacran oceans has inspired the hypothesis that an increase of atmospheric O_2 and the oxygenation of the Ediacaran oceans may have been a trigger for early animal evolution (Cloud, 1972; Knoll et al., 1986; Knoll and Carroll, 1999).

Recent geochemical studies provide some evidences for the oxygenation of the late Ediacaran oceans (<~580 Ma) in Oman (Fike et al., 2006) and the Avalon Peninsula, Newfoundland (Canfield et al., 2007). However, there are few constraints on chemistry of the early Ediacaran oceans (>580 Ma), when earliest animals evolved, and therefore the relationship between ocean chemistry and earliest animal evolution remains unresolved. The well preserved deep ocean sediments deposited under open ocean conditions from China and Canada allow us to investigate chemical evolution of the early Ediacaran ocean and its implications for origin of animals.

The Permain-Triassic boundary mass extinction

The largest mass extinction event in Earth history occurred at Permian-Triassic boundary (PTB), ~252 million years ago (Bowring et al., 1998; Mundil et al., 2004), during which ~90% of marine and ~70% of terrestrial taxa disappeared (Erwin, 1994; Retallack, 1995). Meteorite impact (Becker et al., 2001), the eruption of Siberian basalts (Renne et al., 1995), widespread oceanic anoxia (Knoll et al., 1996; Wignall and Twichett, 1996; Isozaki, 1997; Kump et al., 2005), or perhaps some combination of all these are proposed to explain this biological crisis. The C-isotope chemostratigraphy documented a -3 to -8‰ shift commencing at the Late Permian extinction/event horizon (LPEH) (e.g., Baud et al., 1989; Krull and Retallack, 2000; Twitchett et al., 2001; de Wit et al., 2002; Sephton et al., 2002; Krull et al., 2004; Payne et al., 2004; Korte et al., 2004, 2008). This shift reflects a major

perturbation of the global carbon cycle that has been variously attributed to biomass destruction, reduced organic carbon burial, oxidation of methane from seafloor clathrates, coal, or organic matter from soils, and volcanic CO_2 emissions (see Berner (2002) and Erwin et al. (2002) for reviews). Because the carbon cycle is subject to so many possible influences, C-isotope data alone do not allow for a unique interpretation of causation. S-isotope records (Kaiho et al., 2001, 2006; Newton et al., 2004; Riccardi et al., 2006; Kajiwara et al., 1994; Nielsen and Shen, 2004; Riccardi et al., 2006), frambiodal pyrite size (Wignall and Twitchett, 1996, Nielsen and Shen, 2004), biomarker and Ce anomaly data (Grice et al., 2005; Xie et al., 2005; Kakuwa and Matsumoto, 2006; Hays et al., 2007; Son et al., 2007) suggested that widespread deep-ocean anoxia existed during the Late Permian, and the deep-ocean anoxia together with the subsequent upwelling of anoxic bottom waters could have contributed to the great Pr-T mass extinction (Wignall and Twitchett, 1996, 2002; Isozaki, 1997; Hotinski et al., 2001; Nielsen and Shen, 2004; Kiehl and Shields, 2005). Paired C- and S-isotopic records could provide insights regarding contemporaneous changes in global climate and seawater chemistry (Newton et al., 2004). Well preserved carbonate successions at Meishan section in south China and at the Nhi Tao, northeastern Vietnam containing a series of pyritic horizons allow us to established paired C- and S-isotopic chemostratigraphy to investigate the causation of the PTB.

Research Objectives

The major part of my thesis' work is to investigate the environmental changes and their influences on the end-Ordovician mass extinction and GOBE. Also, as minor part of my thesis, I added research projects on the Ediacaran animal radiation and the P-Tr mass extinction. To constrain the environmental changes and to test these hypotheses, detailed geochemical analyses were performed on sedimentary rocks from south China, western Canada and Northeastern Vietnam. The geochemical analyses include stable C- and S-isotopes, Fe speciation, C and S content in the sediments. These geochemical data when integrated with biostratigraphy and sedimentology provide new insights into environmental changes (atmospheric CO_2 and oxygen concentration, oceanic redox states, and oceanic circulation) and their influences on those major bioevents in the Ordovician, in Neoproterozoic Ediacaran, and at Permian-Triassic boundary.

Experimental and analytical methods

Carbonate and shale samples were collected for carbon isotopic analysis from China. After washing and cutting to remove weathered parts, each sample was crushed and milled to a uniform powder (200 mesh) in an automated agate mortar device in order to analyze carbon and sulphur isotope compositions and element contents.

1) Organic carbon abundance and isotope ($\delta^{13}C_{org.}$)

For organic carbon analysis, about 2 g of powdered sample were treated with 6N HCl for 24 h to remove carbonate minerals, followed by washing and filtering of the residue. The residue was then dried and weighed prior to organic carbon isotope analysis. Organic carbon contents were determined using a NC Instruments NC 2500TM 240 elemental analyzer. Organic carbon isotopic compositions were determined using a VG Micromass IsoprimeTM mass spectrometer coupled to an Elementar Vario Micro CubeTM elemental analyzer with continuous flow. Based on the predetermined organic carbon concentration, 100 μg -10 mg samples were weighed and combusted in the elemental analyzer, and the pure CO_2 gas was sent to the mass spectrometer for $^{13}C/^{12}C$ determination. Organic carbon isotope results are reported in standard per mil δ-notation relative to the V-PDB standard ($\delta^{13}C$). Analytical reproducibility was approximately 0.1‰ based on analysis of IAEA standards. Organic carbon analyses were carried out at University of Quebec at Montreal.

2) Carbonate carbon and oxygen isotopes ($\delta^{13}C_{carb.}$ and $\delta^{18}O_{carb.}$)

Carbon and oxygen isotopic compositions of carbonate samples were determined by a traditional acid-release method (McCrea, 1950). ~15mg powdered samples were reacted with anhydrous H_3PO_4 at 25°C for 24 h under vacuum condition to liberate CO_2, and the CO_2 was purified on a high vacuum extraction line and sealed in Pyrex break-seal tube for carbon isotope analysis. The carbon isotopic ratio was analyzed on a Finnigan MAT 252 mass spectrometer. Results are reported in standard per mil δ-notation relative to the V-PDB standard ($\delta^{13}C$ and $\delta^{18}O$). Analytical precision of these analyses is better than 0.1‰. Analyses of carbonate samples were carried out at the Stable Isotope Lab, institute of Geology and Geophysics, Chinese Academy of Sciences.

3) Pyrite sulfur isotopes ($\delta^{34}S_{py}$) and pyrite concentrations.

Pyrite sulphur was extracted by using chromium reduction methods (Canfield et al., 1986). At first, 1mol/l $CrCl_2$ solution was prepare for pyrite sulphur extraction from shale samples. 266g $CrCl_3 \cdot H_2O$ was dissolved 860ml 1mol/l HCl. Then, the $CrCl_3$ was reacted with Zn under N_2 atmosphere in order to reduce $CrCl_3$ into $CrCl_2$. 0.5-5 g powdered shale samples were reacted with 20 ml 1 mol/l $CrCl_2$ and 20 ml 6 mol/l HCl in a N_2 atmosphere. H_2S gas produced from pyrite reduction by $CrCl_2$ was precipitated as Ag_2S by absorbed with $AgNO_3$. The Ag_2S was centrifuged, washed, dried, and weighed for sulphur isotopic analysis. Pyrite S and Fe concentration were calculated on the basis of Ag_2S weight.

Pyrite sulfur isotopes were determined by elemental analyzer combustion at 1030°C on a continuous-flow GV Isoprime mass spectrometer at University of Maryland. Ag_2S (100 μg) was dropped into a quartz reaction tube packed with quartz chips and elemental Cu for quantitative oxidation and O_2 resorption. Water was removed with a 10 cm magnesium perchlorate trap, and SO_2 was separated from other gases with a 0.8 m polytetrafluoroethylene GC column packed with Porapak 50–80 mesh heated at 90°C. Purified SO_2 was sent into the inlet system of mass spectrometer and $^{34}S/^{32}S$ ratios were measured by mass spectrometer. Sulfur isotope results are reported as per mil (‰) deviation from Vienna-Canyon Diablo triolite $\delta^{34}S$ values. Uncertainties determined from analyses of NBS-127 interspersed with the samples are better than 0.3% for isotope composition.

4) Major, trace and rare earth elements

Major elements including Si, Al, Ti, Mn, Mg, Ca, Na, K, P, and Fe contents were measured by a JEOL JXA-8800 electron microprobe at Nanjing University, China. Element determinations were carried out using a beam size of 3 μm, an accelerating potential voltage of 15 KV, and probe current of 15nA. Standards used were natural minerals and synthetic compounds, including hornblende (Si, Al, Ti, Mg, Ca, Na,) fayalite (Fe, Mn) and K-feldspars (K) in the analytical procedure.

Trace and rare earth elements were measured by inductively coupled plasma source mass spectrometer (ICP-MS) at Nanjing University, China. About 20 mg of sample powders was weighed and transferred into a screw-cap Teflon vial. Powdered samples were leached with 2N HCl in order to remove carbonate and phosphate minerals. Then, the residues were

dissolved with a mixture of 0.5 mL 8 mol/L HNO3 and 1 mL concentrated HF on a hotplate at 130-150℃. After evaporation, samples were redissolved in 5% HNO_3 solution spiked with an internal standard Rh (10ppb) for analysis. Trace metal elements and REE were analyzed on a Finnigan MAT ELEMENT inductively coupled plasma source mass spectrometer (ICP-MS). The analytical precision generally is better than 10% for both trace metal elements and rare earth elements. The concentrations (Table 1) are reported in ppm (μg/g).

References

Baud, A., Holser, W. T., Magaritz, M., 1989. Permian-Triassic of the Tethys: Carbon isotope Studies. Geol. Rundsch. 78, 649–677.

Becker, L., Poreda, R. J., Hunt, A.G., Bunch, T. E., Rampino, M., 2001. Impact event at the Permian-Triassic boundary: Evidence from extraterrestrial noble gases in fullerenes. Science 291, 1530–1533.

Berner, R. A., 2002. Examination of hypotheses for the Permo-Triassic boundary extinction by carbon cycle modeling. Proc. Natl. Acad. Sci. U.S.A. 99, 4172–4177.

Bottjer, D.J., Droser, M.L., Sheehan, P.M., McGhee, G.R., 2001. The ecological architecture of major events in the Phanerozoic history of marine invertebrate life. In: Allmon, W.D., Bottjer, D.J.(eds.), Evolutionary Paleoecology. Columbia Univ. Press, New York, pp.35-61.

Bowring, S. A., Erwin, D. H., Jin, Y. G., Martin, M.W., Davidek, K., Wang, W., 1998. U/Pb zircon geochronology and tempo of the end-Permian mass extinction. Science 280, 1039–1045.

Brenchley, P.J., Romano, M., Young, T.P., Stoch, P., 1991. Hirnatian glaciomarine diamictites-evidence for the spread of glaciation and its effect on Ordovician faunas. Geol. Surv. Can. 90-9,325-336.

Brenchley, P.J., Marshall, J.D., Carden, G.A.F., Robertson, D.B.R., Long, D.G.F., Meidla, T., Hints, L., Anderson, T.F.,1994. Bathymetric and isotopic evidence for a short-lived Late Ordovician glaciation in a greenhouse period. Geology 22, 295-298.

Brenchley, P.J., Carden, G.A.F., Marshall, J.D., 1995. Environmental changes associated with the 'first strike' of the Late Ordovician mass extinction. Modern Geology 20, 69-82.

Brenchley, P.J., Marshall J.D., 1999. Relative timing of critical events during the late Ordovician mass extinction-new data from Oslo. Acta Univ. Carol. Geol. 43,187-190.

Brenchley, P.J., Carden, G.A, Hints, L., Kaljo D, Marshall, J.D., Martma T, Meidla, T.,Nolvak J, 2003. High-resolution stable isotope stratigraphy of Upper Ordovician sequences: Constraints on the timing of bioevents and environmental changes associated with mass extinction and glaciation. GAS Bulletin 115, 89-104.

Canfield, D.E., Raiswell, R., Westrich, J.T., Reaves, C.M., Berner, R.A., 1986. The use of chromium reduction in the analysis of reduced inorganic sulfur in sediments and shale.

Chemical Geology 54,149–155.

Canfield, D.E., Poulton, S.W., Narbonne, G.M., 2007. Late-Neoproterozoic deep-ocean oxygenation and the rise of animal life. Science 315, 92-95.

Cloud, P., 1972, Working model of primitive Earth. Am J Sci 272:537-548.

de Wit, M. J., Ghosh, J. G., de Villiers, S., Rakotosolofo, N., Alexander, J., Tripathi, A., Looy, C., 2002. Multiple organic carbon isotope reversals across the Permo-Triassic boundary of terrestrial Gondwana sequences: Clues to extinction patterns and delayed ecosystem recovery. J. Geol., 110, 227–240.

Droser, M.L., Sheehan, P.M., 1997. Palaeoecology of the Ordovician Radiation; resolution of large- scale patterns with individual clade histories, palaeogeography and environments. Geobios 20, 221– 229.

Erwin, D. H., Bowring, S. A., Jin, Y.G., (2002), End-Permian mass-extinctions: A review. In: Koeberl C., MacLeod K. G. (eds.), Catastrophic Events and Mass Extinctions: Impacts and Beyond. Spec. Pap. Geol. Soc. Am. 356, 353–383.

Erwin, D. H., 1994. The Permo-Triassic extinction. Nature 367, 231–236.

Finney, S.C., Berry, W.B.N., Cooper, J.D., Ripperdan, R.L., Sweet, W.C., 1999. Late Ordovician mass extinction: a new perspective from stratigraphic sections in central Nevada. Geology 27, 215-218.

Fike DA, Grotzinger JP, Pratt LM, Summons RE., 2006. Oxidation of the Ediacaran Ocean. Nature 444:744-747.

Gibbs, M.T., Barron, E.J., Kump, L.R., 1997. An atmospheric pCO_2 threshold for glaciation in the Late Ordovician. Geology 27, 447-450.

Goodfellow, W.D., Nowlan, G.S., McGracken, A.D., Lenz, A.C., Grégoire, D.C., 1992. Geochemical anomalies near the Ordovician-Silurian boundary, north Yukon, Canada. Hist. Biol. 6, 1-23.

Gradstein, F., Ogg, J., Smith, A., 2004. A Geologic Time Scale. Cambridge Univ. Press, 589 pp.

Grice, K., Cao, C., Love, G. D., Böttcher, M. E., Twitchett, R. J., Grosjean, E., Summons, R. E., Turgeon, S. C., Dunning, W., Jin, Y., 2005. Photic zone euxinia during the Permian-Triassic superanoxic event. Science 307, 706–709.

Hays, L.E., Beatty, T., Henderson, C.M., Love, G.D., Summons, R.E., 2007. Evidence for photic zone euxinia through the end-Permian mass extinction in the Panthalassic Ocean (Peace River Basin, Western Canada). Palaeoworld, 16, 39–50.

Hotinski, R. M., Bice, K. L., Kump, L. R., Najjar, R. G., Arthur, M. A., 2001. Ocean stagnation and end-Permian anoxia. Geology, 29, 7–10.

Isozaki, Y., 1997. Permo-Triassic boundary superanoxia and stratified superocean: Records from lost deep sea. Science, 276, 235–238.

Jablonski, D., 1991. Extinctions: a paleontological perspective. Science 253, 754-57.

Kaiho, K., Kajiwara, T., Nakano, T., Muira, Y., Kawahata, H., Tazaki, K., Ueshima, M., Chen, Z., Shi, G. R., 2001. End-Permian catastrophe by a bolide impact: Evidence of a gigantic release of sulfur from the mantle. Geology, 29, 815–818.

Kaiho, K., Chen, Z.Q., Kawahata, H., Kajiwara, Y., Sato, H., 2006. Close-up of the end-Permian mass extinction horizon recorded in the Meishan section, south China: Sedimentary, elemental, and biotic characterization and a negative shift of sulfate sulfur isotope ratio. Palaeogeogr. Palaeoclimatol. Palaeoecol., 239, 396–405.

Kajiwara, Y., Yamakita, S., Ishida, K., Ishiga, H., Imai, A., 1994. Development of a largely anoxic stratified ocean and its temporary massive mixing at the Permian-Triassic boundary supported by the sulfur isotope record. Palaeogeogr. Palaeoclimatol. Palaeoecol. 111, 367–379.

Kakuwa, Y., Matsumoto, R., 2006. Cerium negative anomaly just before the Permian and Triassic boundary event: The upward expansion of anoxia in the water column. Palaeogeogr. Palaeoclimatol. Palaeoecol. 229, 335–344.

Kaljo, D., Hints, L., Hints, O., Martma, T., Nolvok, J., 1999. Carbon isotope excursions and coeval environmental and biotic changes in the Late Caradoc and Ashgill of Estonia. Acta Univ. Carol. Geol. 43, 507-510.

Kaljo, D., Hints, L., Martma, T., Nõlvak, J., 2001. Carbon isotope stratigraphy in the latest Ordovician of Estonia. Chemical Geology 175, 49-59.

Kaljo, D., Hints, L., Martma, T., Nõlvak, J., Oraspõld, A., 2004. Late Ordovician carbon isotope trend in Estonia, its significance in stratigraphy and environmental analysis. Palaeogeography, Palaeoclimatology, Palaeoecology 210, 165-185.

Kiehl, J. T., Shields, C. A., 2005. Climate simulation of the latest Permian: implications for mass Extinction. Geology, 33, 757–760.

Knoll, A.H., Caroll, S.B., 1999. The early evolution of animals: emerging views from comparative biology and geology. Science 284, 2129-2137.

Knoll, A. H., Bambach, R. K., Canfield, D. E., Grotzinger, J. P., 1996. Comparative Earth history and Late Permian mass extinction. Science, 273, 452–457.

Knoll, A.H., Hayes, J.M., Kaufman, J., Swett, K., Lambert, I., 1986. Secular variation in carbon isotope ratios from Upper Proterozoic successions of Svalbard and East Greenland. Nature 321, 832-838.

Korte, C., Kozur, H. W., Joachimski, M. M., Strauss, H., Veizer, J., Schwark, L., 2004. Carbon, sulfur, oxygen and strontium isotope records, organic geochemistry and biostratigraphy across the Permian/Triassic boundary in Abadeh, Iran. Int. J. Earth Sci. 93, 565–581.

Korte, C., Pande, P., Kalia, P., Kozur, H. W., Joachimski, M. M., Oberhänsli, H., 2010. Massive volcanism at the Permian- Triassic boundary and its impact on the isotopic composition of the ocean and atmosphere. J. Asian Earth Sci. 37, 293-311.

Krull, E. S., Retallack G. J., 2000. $\delta^{13}C_{org}$ depth profiles from paleosols across the Permian-Triassic boundary: Evidence for methane release. Geol. Soc. Am. Bull.,112, 1459–1472.

Krull, E. S., Lehrmann, D. J., Druke, D., Kessel, B., Yu,Y., Li, R., 2004. Stable carbon isotope stratigraphy across the Permian-Triassic boundary in shallow marine carbonate platforms, Nanpanjiang Basin, south China. Palaeogeogr. Palaeoclimatol. Palaeoecol. 204, 297–315.

Kump, L.R., Arthur, M.A., Patzkowsky, M.E., Gibbs, M.T., Pinkus, D.S., Sheehan, P.M., 1999. A weathering hypothesis for glaciation at high atmospheric pCO_2 during the Late Ordovician. Palaeogeography, Palaeoclimatology, Palaeoecology 152,173–187.

Kump, L. R., Pavlov, A., Arthur, M. A., 2005. Massive release of hydrogen sulfide to the surface ocean and atmosphere during intervals of oceanic anoxia. Geology, 33, 397–400.

Long, D.G.F., 1993. Oxygen and carbon isotopes and event stratigraphy near the Ordovician—Silurian boundary, Anticosti Island Quebec. Palaeogeography, Palaeoclimatology, Palaeoecology 104, 49-59.

Marshall, J.D., Brenchley, P.J., Mason, P., Wolff, G.A., Astini, R.A., 1997. Global carbon isotopic events associated with mass extinction and glaciation in the Late Ordovician. Palaeogeography, Palaeoclimatology, Palaeoecology 132,195-210.

McCrea J.M, 1950. The isotope chemistry of carbonates and a paleotemperature scale. Journal of Chemical Physics 63:563-566.

Melchin, M.J., Holmden, C., 2006. Carbon isotope chemostratigraphy in Arctic Canada: Sea-level forcing of carbonate platform weathering and implications for Hirnantian global correlation. Palaeogeography, Palaeoclimatology, Palaeoecology 234, 186-200.

Miller, A.I., 1997. Dissecting global diversity trends: examples from the Ordovician radiation. Ann. Rev. Ecology and Systematics 28, 85– 104.

Mitchell, C.E., Sheets, H.D, Belscher, K, Finney, S., Holmden ,C, Laporte, D.F., Melchin, M.J., Patterson W.P., 2007. Species abundance changes during mass extinction and the inverse signor-lipps effect: apparently abrupt graptolite mass extinction as an artifact of sampling. Acta Palaeontologica Sinica 46 (Suppl.), 340-346.

Mundil, R., Ludwig, K. R., Metcalfe, I., Renne, P. R., 2004. Age and timing of the Permian mass extinctions: U/Pb dating of closed-system zircons. Science 305, 1760–1763.

Narbonne, G.M., 2005. The Ediacara biota: Neoproterozoic origin of animals and their ecosystems. *Annu Rev Earth Planet Sci* 33:421-442.

Newton, R. J., Pevitt, E. L., Wignall, P. B., Bottrell, S. H., 2004. Large shifts in the isotopic composition of seawater sulphate across the Permo-Triassic boundary in northern Italy. Earth Planet. Sci. Lett. 218, 331–345.

Nielsen, J. K., Shen, Y., 2004. Evidence for sulfidic deep water during the Late Permian in the East Greenland Basin. Geology, 32, 1037–1040.

Orth, C.J., Gilmore, J.S., Quintana, L.R., Sheehan, P.M., 1986. The terminal Ordovician

extinction: Geochemical analysis of the Ordoviciane/Silurian boundary, Anticosti Island, Quebec. Geology 14, 433-436.

Payne, J. L., Lehrmann, D. J., Wei, J., Orchard, M. J., Schrag, D. P., Knoll, A. H., 2004. Large perturbations of the carbon cycle during recovery from the end-Permian extinction. Science 305, 506–509.

Qing, H., Veizer, J., 1994. Oxygen and carbon isotopic composition of Ordovician brachiopods: Implications for coeval seawater. Geochimica et Cosmochimica Acta 58, 4429-4442.

Renne, P. R., Zheng, Z. C., Richards, M. A., Black, M. T., Basu, A. R., 1995. Synchrony and causal relations between Permian-Triassic boundary crisis and Siberian flood volcanism. Science 269, 1413–1416.

Riccardi, A. L., Arthur, M. A., Kump, L. R., 2006. Sulfur isotopic evidence for chemocline upward excursions during the end-Permian mass extinction. Geochim. Cosmochim. Acta 70, 5740–5752.

Saltzman, M. R., Young, S.A., 2005. Long-lived glaciation in the Late Ordovician? Isotopic and sequence-stratigraphic evidence from western Laurentia. Geology 33, 109-112.

Schmitz, B., Harper D.A.T., Peucker-Ehrenbrink B., Stouge S., Alwmark C., Cronholm A., Bergstrom S.M., Tassinari M., Wang X., 2008. Asteroid breakup linked to the Great Ordovician Biodiversification Event. Nature Geoscience 1, 49-53.

Sephton, M. A., Brinkhuis, H., Looy, C. V., Veefkind, R. J., Visscher, H., de Leeuw, J. W., 2002. Synchronous record of $\delta^{13}C$ shifts in the oceans and atmosphere at the end of the Permian. In: Koeberl, C., MacLeod, K.G. (eds), Catastrophic Events and Mass Extinctions: Impacts and Beyond. Spec. Pap., Geol. Soc. Am. 356, pp.455-462.

Sepkoski, J.J., 1991. Diversity in the Phanerozoic oceans: a partisan review. See Dudley 1, 210-236.

Sepkoski, J.J., 1996. Patterns of Phanerozoic extinction: a perspective from global data bases. In: Walliser O. H. (Ed.), Global Events and Event Stratigraphy in the Phanerozoic. Springer, Berlin, pp. 35-51.

Sepkoski, J.J., 1997. Biodiversity: past, present and future. J. Paleontol. 71, 533–539.

Servais, T., Harper, D.A.T., Li, J., Munnecke, A., Owen, A.W., Sheehan, P.M., 2009. Understanding the Great Ordovician Biodiversification Event (GOBE): Influences of paleogeography, paleoclimate, or paleoecology? GSA Today 19, 4-10.

Sheenhan, P.M., 2001. The Late Ordovician Mass Extinction. Annual Review of Earth and Planetray Sciences 29, 331-364.

Son, T. H., Koeberl, C., Ngoc, N. L., Huyen, D. T., 2007. The Permian-Triassic boundary sections in northern Vietnam (Nhi Tao and Lung Cam sections): Carbon-isotope excursion and elemental variations indicate major anoxic event, Palaeoworld, 16, 51–66.

Trotter, J.A., Williams, I.S., Barnes, C.R., Lecuyer, C., Nicoll, R, S., 2008. Did cooling

oceans trigger Ordovician biodiverisfication? Evidence from conodont thermometry. Science 321, 550-554.

Twitchett, R.J., Looy, C.V., Morante, R., Visscher, H., Wignall., P.B., 2001. Rapid and synchronous collapse of marine and terrestrial ecosystems during the end-Permian biotic crisis, Geology 29, 351–354.

Underwood, C.J., Crowley, S.F., Marshall, J.D., Brenchley, P.J., 1997. High-resolution carbon isotope stratigraphy of the basal Silurian stratotype (Dob's Linn, Scotland) and its global correlation. J. Geol. Soc. London 154, 709-718.

Wang, K., Orth, C.J., Attrep, M., Chatterton, B.D.E., Wang, X., Li, J., 1993a. The great latest Ordovician extinction on the South China Plate: Chemostratigraphic studies of the Ordovician-Silurian boundary interval on the Yangtze platform. Palaeogeography, Palaeoclimatology, Palaeoecology 104, 61-79.

Wang, K., Chatterton, B.D.E., Attrep, M., Orth, C.J., 1993b. Late Ordovician mass extinction in the Selwyn Basin, northwestern Canada. Can. J. Earth Sci. 30, 1870-1880.

Wang, K., Chatterton, B.D.E., Wang, Y., 1997. An organic carbon isotope record of Late Ordovician to Early Silurian marine sedimentary rocks, Yangtze Sea, South China: Implications for CO_2 changes during the Hirnantian glaciation. Palaeogeography, Palaeoclimatology, Palaeoecology 132, 147-158.

Webby, B.D., Paris, F., Droser, M.L.(eds.), 2004. The Great Ordovician Biodiversification Event. Columbia University Press, New York, pp.1-484.

Wignall, P. B., Twitchett, R. J., 1996. Oceanic anoxia and the end Permian mass extinction, Science, 272, 1155–1158.

Wilde, P., Berry, W.B.N., Quinby-Hunt M.S., Orth, C.J., Quintana, L.R., Gilore, J.S., 1986. Iridium abundances across the Ordovician-Silurian stratotype. Science 233, 339-341.

Xie, S., R. D. Pancost, H. Yin, H. Wang, and R. P. Evershed, 2005. Two episodes of microbial change coupled with Permo/Triassic faunal mass extinction, Nature, 434, 494–497.

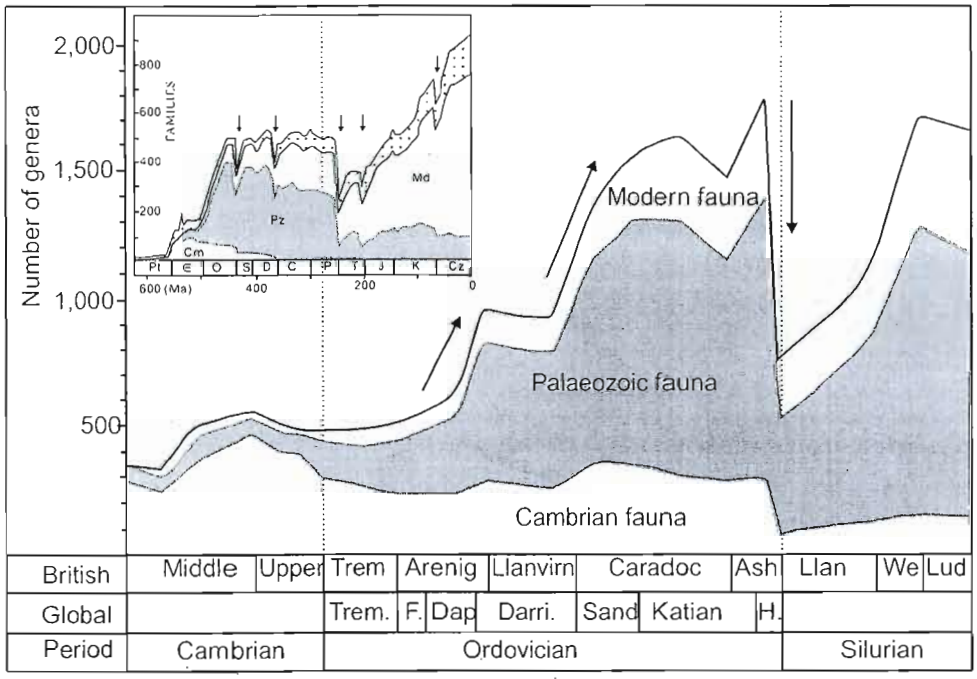

Fig. 1 Biodiversity patterns of marine fauna through geological time (Modified from Sepkoski (1996)), and Middle Cambrian to Silurian taxonomic diversity trends at genus level (Modified from Sepkoski (1995)).

CHAPTER I

High-resolution carbon isotopic records from the Ordovician of South China: Links to climatic cooling and the Great Ordovician Biodiversification Event (GOBE)

Tonggang Zhang, Yanan Shen, Thomas J. Algeo

Manuscript accepted by *Palaeogeography, Palaeoclimatology, Palaeoecology* (2010)

Abstract

The Great Ordovician Biodiversification Event (GOBE) represented the largest expansion of the marine biosphere during the Phanerozoic Eon, yet its causes and consequences remain poorly understood. Patterns of isotopic variation in high-resolution $\delta^{13}C_{carb}$ and $\delta^{13}C_{org}$ records from a well-exposed section at Honghuayuan in South China may provide important insights regarding the GOBE. The Honghuayuan isotopic profiles, which can be correlated with C-isotopic records from contemporaneous sections globally, reveal large perturbations to the global carbon cycle during the Ordovician. A +8‰ increase in $\delta^{13}C_{org}$ values in the Floian implies a large, albeit transient increase in the burial rate of organic matter during the late-Early Ordovician that may have contributed to climatic cooling and played an important role in triggering the GOBE. A +4‰ increase in $\delta^{13}C_{carb}$ and high-frequency variation in $\delta^{13}C_{org}$ in the Darriwilian to Sandbian suggest a second episode of elevated organic carbon burial rates accompanied by substantial instability in the global carbon cycle during the late Middle and early Late Ordovician. This pattern may mark the onset of climate changes culminating in the end-Ordovician Hirnantian glaciation and mass extinction event that terminated the GOBE.

Keywords: $\delta^{13}C_{carb}$, $\delta^{13}C_{org}$, **atmospheric** CO_2, **climate cooling, biodiversification**

I-1. Introduction

The "Great Ordovician Biodiversification Event" (GOBE) began ~470 Ma ago during the Early Ordovician and possibly lasted more than 25 Myr into the Late Ordovician (Droser and Sheehan, 1997; Miller, 1997; Webby et al., 2004; Servais et al., 2009). Whereas the Cambrian explosion resulted in the appearance of nearly all phyla of marine animals, biodiversity at the taxonomic ranks of family, genus and species remained low until the Ordovician (Sepkoski, 1997). By the end of the Ordovician, biodiversity at the family level had increased to more than three times that in the Cambrian and Early Ordovician (Webby et al., 2004). The GOBE was terminated by a major mass extinction at the end of the Ordovician, ~444 Ma ago (Sepkoski, 1996; timescale of Gradstein et al., 2004), which may have been triggered by climatic cooling culminating in the Hirnantian (latest Ordovician) glaciation (Stanley, 1984; Sheehan, 2001), during which icesheets spread across much of Gondwana and part of Laurentia (Crowell, 1999).

Relative to the Cambrian explosion and end-Ordovician mass extinction, the GOBE has received less attention (Bottjer et al., 2001), and the cause of this event remains debated (Servais et al., 2009). It was traditionally proposed that the GOBE did not coincide with any abrupt environmental changes, and that it simply represented a realization of innate evolutionary potential among early metazoans (Webby et al., 2004). However, recent studies have emphasized the role of environmental changes as a trigger for the GOBE. Trotter et al. (2008) argued on the basis of oxygen-isotopic thermometry of conodonts that climatic cooling may have led to the GOBE. Alternatively, Schmitz et al. (2008) suggested on the basis of changes in the abundance of extraterrestrial chromite grains and the ratio of seawater $^{187}Os/^{188}Os$ that meteorite impacts accelerated the pace of biodiversification during the Early to Middle Ordovician.

Warm global climatic conditions have been inferred for the Early to Middle Ordovician on the basis of atmospheric pCO_2 levels that are estimated to have been 14 to 18 times the present atmospheric level (Berner and Kothavala, 2001; Herrmann et al., 2003). Therefore, it has been widely assumed that the GOBE may have occurred during a period of greenhouse conditions (e.g., Gibbs et al., 1997). However, both the onset and termination of this greenhouse period are poorly constrained (Saltzman and Young, 2005), so its temporal relationship to the GOBE remains unclear. Because atmospheric CO_2 is an important greenhouse gas in the atmosphere, variations thereof are commonly suggested to be the main driver of climate change on geological timescales, and at

intermediate timescales, atmospheric pCO_2 is controlled by the input and removal of carbon to the ocean-atmosphere system (e.g., Royer, 2006). Therefore, the carbon isotopic compositions of carbonate and organic carbon have the potential to record changes in the global carbon cycle that may have been associated with changes in atmospheric pCO_2 (Hayes et al., 1999; Kump and Arthur, 1999; Freeman, 2001).

A great number of studies have constructed C-isotopic chemostratigraphic profiles for portions of the Ordovician-Silurian in sections with a global distribution (Wang et al., 1993a; Patzkowsky et al., 1997; Underwood et al., 1997; Kump et al., 1999; Finney et al., 1999; Brenchley et al., 2003; Buggisch et al., 2003; Shields et al., 2003; Saltzman, 2005; Saltzman and Young 2005; Melchin and Holmden, 2006; Kaljo et al., 2007;), including sections in South China (Wang et al., 1993b, 1997; Chen et al., 2006a; Zhang et al., 2009; Fan et al., 2009; Yan et al., 2009; Bergström et al., 2009). Although such records have improved global correlations of Ordovician-Silurian strata (e.g., Sheehan, 2001), most of the sections utilized represent relatively short stratigraphic intervals. In this study, we report high-resolution records for organic carbon ($\delta^{13}C_{org}$) and carbonate carbon ($\delta^{13}C_{carb}$) isotopes from a well-exposed section at Honghuayuan in South China that spans nearly the entire Ordovician. These records exhibit characteristic features that may help to refine the timing of termination of the Cambrian-Ordovician greenhouse climate and that provide insights into relationships between concurrent changes in climate and biodiversity during the Ordovician.

I-2. Geology setting and stratigraphy

I-2.1. Regional geology

During the Ordovician, the China Block consisted of four separate cratons: North China, South China, Tarim, and Chaidam-Tibet (Wang, 1985). On the South China craton, which was covered by a broad epeiric sea, continuous and richly fossiliferous Ordovician-Silurian sequences were widely developed (Chen et al., 2004). By the Late Ordovician, the South China craton had separated from the Gondwanan supercontinent, and it was located at a paleolatitude of about 20°S (e.g., Chen et al., 2004).

During the past several decades, the lithostratigraphy, biostratigraphy, and sedimentary environments of numerous Ordovician sections in South China have been extensively investigated (Mu et al., 1981; Rong and Harper, 1988; Wang and Chen, 1991; Rong et al., 2002; Chen et al., 2004, 2005; 2006a, b; Zhan et al., 2007; Zhan and Jin, 2007, 2008; Hu et al., 2009). Three of these sections were selected as Global Stratotype

Sections and Points (GSSPs) for the base of Dapingian, the base of Darriwilian, and the base of Hirnantian owing to their rich fossil records, especially of graptolites and conodonts that are of great utility for global correlations (Chen et al., 2006a; Zhan and Jin, 2008).

Our samples were collected from the Honghuayuan section located at N28°4′31″, E106°51′45″, about 7 km southeast of Tongzi county, in northern Guizhou Province, China (Fig. I-1). The Honghuayuan section represents a stratigraphically continuous and richly fossiliferous succession extending from the Upper Cambrian to the Lower Silurian. This section has been studied for over 50 years, and the litho-stratigraphy, biostratigraphy, and chronology of the section are well established (Chen et al., 2000; Rong et al., 2002; Zhan and Jin, 2007 and references therein). Paleontological research at Honghuayuan has documented in detail the pattern of biodiversification and mass extinction during the Ordovician, and these observations can be correlated with data from the GSSP section at Wangjiawan in Yichang (Fig. I-1, Chen et al., 2006a). These earlier studies provide the framework within which we have generated new, high-resolution C-isotope record at Honghuayuan for studying the relationship between Ordovician bioevents and major changes in the carbon cycle.

I-2.2. Lithostratigraphy and biostratigraphy at Honghuayuan

At Honghuayuan, the base of the Ordovician section is conformable with underlying carbonates of the Upper Cambrian Loushankuan Group, and the top of the section is conformable with shales of the Lower Silurian Lungmachi Formation. Ordovician strata are subdivided, in ascending order, into the Tungtzu, Hunghuayuan, Meitan, Shihtzupu, Pagoda, Linhsiang, Wufeng, and Kuanyinchiao formations (Fig. I-2). The Tungtzu, Hunghuayuan, and lower Meitan formations comprise the Lower Ordovician, the upper Meitan and Shihtzupu formations comprise the Middle Ordovician, and the Pagoda, Linhsiang, Wufeng, and Kuanyinchiao formations comprise the Upper Ordovician (e.g., Zhan and Jin, 2007). With the exception of the Tungtzu Formation, which was mostly covered, these strata were continuously exposed along a mountainside at Honghuayuan. The detailed litho- and biostratigraphy of the Honghuayuan section have been presented by Zhan and Jin (2007). It should be pointed out that biostratigraphy and fossil assemblages as well as divisions of bizones for the Honghuayuan section in our study were established by previous investigations (Zhan and Jin, 2007 and references therein). A brief description of the six main stratigraphic units at Honghuayuan, from oldest to

youngest, follows:

(1) The Tungtzu Formation (Tremadocian) is 105.4 m thick and consists of gray, thin- to medium-bedded micritic dolostone, bioclastic limestone, oolitic limestone, including a few of yellowish green shales interlayers. The bioclastic limestones contain the trilobites *Asaphellus, Dactylocephalus, Asaphopsis, Wanliangtingia, Psilocephalina, Tungtzuella* (Fu, 1982), and the brachiopods *Apheoorthis, Imbriacatia, Lingulella, Syntrophina, Hesperonomia* (Chen et al., 1995).

(2) The Hunghuayuan Formation (basal Floian) is 34.2 m thick and consists of gray to dark gray, medium- to thick-bedded limestones with a single 2-m-thick shale interbed. The bioclastic limestones contain abundant trilobites (e.g., *Liomegalaspides, Psilocephalina*), brachiopods (e.g., *Trematorthis, Hesperonomia, Apheoorthis, Tritoechia*) (Chen et al., 1995), and conodonts, whereas the shale yielded abundant graptolites (e.g., *Acrograptus saukros, Corymbograptus cf. vacillans*) (Chen et al., 1995; Zhang and Chen, 2003).

(3) The Meitan Formation has a total thickness of ~258 m and is subdivided into lower (Floian) and upper (Dapingian) parts at the base of the limestone bed, which is located ~120 m above the base of the formation. The lower part consists of yellowish green fossil-rich mudstones interbedded with siltstones, and the upper part contains relatively more siltstones and fossil-rich limestones. Brachiopods, the single most abundant fossil group, form several distinct communities, including the Paralenorthid, Sinorthid, and Desmorthid communities, in the lower Meitan. In the upper Meitan, various short-lived brachiopod associations are dominated by opportunistic taxa such as *Methorthis, Lepidorthis, Virgoria*, and *Martellia*. Grapolites are the second most abundant fossil group, allowing subdivision of the formation into eight graptolite biozones (Figs. I-2, I-4; Zhang and Chen, 2003). Trilobites are more variable in occurrence but relatively less abundant than brachiopods and graptolites.

(4) The Shihtzupu Formation (Darriwilian) is 9.3 m thick and characterized by lithologically distinct lower and upper parts. The 2.7-m-thick lower part consists of gray, medium- to thick-bedded micritic, oolitic limestones, and the 6.6-m-thick upper part consists of gray, thin-bedded, calcareous mudstones and argillaceous limestones. Brachiopods, including *Leptellina, Saucrorthis, Glyptorthis, Orthambonites*, and *Bellimurina*, are the most abundant fossils (Fig. I-2), although the upper part also contains trilobites and graptolites, the latter serving for subdivision of the formation into four graptolite biozones (Chen et al., 1995; Zhan et al., 2005).

(5) The Pagoda Formation (Sandbian to lower Katian; = Caradoc) is 36.9 m thick and consists of light gray, medium- to thick-bedded micritic limestones. It is moderately rich in fossils such as trilobites, nautiloids, and brachiopods. Nautiloids are the most important fauna in this formation, especially *Sinoceras chinense* and *Michelinoceras sp.* (Chen et al., 1995). Trilobites and brachiopods, often of diminutive size, are also abundant (Rong et al., 1999).

(6) The Linhsiang Formation (middle Katian) is 4.3 m thick and consists of light gray, argillaceous nodular-like limestones and dark gray, calcareous mudstones. Trilobites and brachiopods are found in the limestones, and graptolites, especially *Dicellograptus complanatus, Amplexograptus latus, Climacograptus sp.*, and *Leptograptus sp.*, are the most abundant fossils in the mudstone beds (Chen et al., 2000).

I-2.3. Ordovician radiation in South China

The GOBE is reflected in diversifications within many marine invertebrate clades during the Early to Middle Ordovician. Though GOBE generated few higher taxa, it did produce a staggering increase in biodiversity at the family, genus and species levels (Webby et al., 2004). As such, in terms of taxonomic terms, GOBE may record the greatest interval of biodiversification of life over the last 3.8 billion years. The detailed paleonotological studies show that changes in the number of species and ecological dominance of marine animals of different ecotypes in the South China has provided a representative example of macroevolutionary patterns during the GOBE. For example, brachiopods underwent not only a sharp increase in taxonomic abundance but also a dramatic change in the range of habitats occupied and ecological roles played (e.g., Zhan and Jin, 2007). In terms of biodiversity and ecological dominance, orthids and pentamerids probably became the most important orders of brachiopods (Zhan et al., 2005; Zhan and Harper, 2006).

The Honghuayuan section preserved one of the best records of the GOBE in south China. The detailed paleontological investigations revealed macroevolutionary patterns of marine animals of different ecotypes during the diversification event (e.g., Zhan et al., 2005). At Honghuayuan, the Early Ordovician radiation resulted in a small increase in the number of brachiopod orders and a larger increase in the number of families (from 6 to 24) and genera (from 8 to 57) (Zhan and Jin, 2007). The diversification began slowly within the *Tetragraptus* biozone of the Tremadocian and accelerated within the *Acrograptus filiformis* Biozone at the base of the Meitan Formation (Fig. I-2).

Brachiopod biodiversity reached its first peak within the *Didymograptus eobifidus* Biozone of the lower Meitan Formation, about four graptolite biozones earlier than in North America and in Baltic (Zhan and Jin, 2007, 2008) (Fig. I-2).

I-3. Sample collection and analytical methods

Carbonate and shale samples were collected for carbon isotopic analysis. After washing and cutting to remove weathered parts, each sample was crushed and milled to a uniform powder in an automated agate mortar device. For organic carbon analysis, about 2 g of powdered sample were treated with 6N HCl for 24 h to remove carbonate minerals, followed by washing and filtering of the residue. The residue was then dried and weighed prior to organic carbon isotope analysis. Organic carbon contents were determined using a NC Instruments NC 2500™ elemental analyzer. Organic carbon isotopic compositions were determined using a VG Micromass Isoprime™ mass spectrometer coupled to an Elementar Vario Micro Cube™ elemental analyzer with continuous flow. Based on the predetermined organic carbon concentration, from 100 μg to 10 mg samples were weighed and combusted in the elemental analyzer, and the pure CO_2 gas was sent to the mass spectrometer for $^{13}C/^{12}C$ determination. Analytical reproducibility was approximately 0.1‰ based on analysis of IAEA standards.

Carbon isotopic compositions of carbonate samples were determined by a traditional acid-release method. ~10 mg powdered samples were treated with anhydrous H_3PO_4 at 25°C for 24 h to liberate CO_2, and the purified CO_2 was sealed for carbon isotope analysis. The carbon isotopic ratio was analyzed on a Finnigan MAT 252 mass spectrometer. Results are reported in standard per mil δ-notation relative to the V-PDB standard. Analytical precision of these analyses is better than 0.1‰. Geochemical data (TOC, $\delta^{13}C_{org}$ and $\delta^{13}C_{carb}$) are given in Table I-1.

I-4. Results and discussion

I-4.1. Evaluation of secondary effects on isotopic records at Honghuayuan

The C isotopic signature of organic matter ($\delta^{13}C_{org}$) is potentially influenced by a number of environmental and diagenetic factors. Where the isotopic composition of bulk organic matter is analyzed (as in the present study), admixture of terrestrial organic matter can result in $\delta^{13}C_{org}$ values that deviate from those of pure marine organic matter to varying degrees (e.g., Cramer and Saltzman, 2007). However, the influence of terrestrial organic carbon input on the $\delta^{13}C_{org}$ values of Ordovician samples was limited at

most owing to an absence of higher land plants at that time (Algeo and Scheckler, 1998). Bryophytes were present but probably in low abundance and their non-woody tissues probably decayed rapidly, leading to little contribution to bulk organic matter in contemporaneous marine sediments.

Bacterial and thermogenic destruction of specific fractions of organic matter in early to late diagenesis can lead to a shift in the C-isotopic composition of bulk organic matter (Freeman, 2001). Recrystallization plays an important role in the preservation of organic matter in carbonate sediments (Ingalls et al., 2004). Organic matter that enters the oil window generally yields ^{12}C-enriched hydrocarbons, so the isotopic composition of the residual kerogen becomes enriched in ^{13}C (Hayes et al., 1989). The degree of thermal maturation of the sediment thus influences its bulk organic $\delta^{13}C$ composition. For the study units, there are several important considerations regarding the potential effects of thermal alteration. First, Ordovician sedimentary rocks in South China are relatively immature thermally, as shown by low conodont colour alteration indices (CAI = 2.0-2.5) and low vitrinite reflectance (R_0) for graptolites (1.0-1.1%), chitinozoans (1.28), scolecodonts (1.04-1.23), bitumen (1.0-1.22), and kerogen (0.9) (Wang et al., 1993). Second, although systematic correlation between $\delta^{13}C_{org}$ and organic carbon content (C_{org}) may develop through diagenesis (e.g., Kump et al., 1999; Shen and Schidlowski, 2000), no systematic relationship was observed between $\delta^{13}C_{org}$ and organic carbon content (C_{org}) at either the biozone or formation level in the Honghuayuan section (Fig. 1-3A). These observations suggest at most limited diagenetic alteration of primary marine organic $\delta^{13}C$ values in the Honghuayuan section.

The C isotopic compositions of carbonates can also potentially be altered through diagenetic reactions, especially at high water/rock ratios (>~20) or where inorganic carbon sources with markedly different isotopic compositions (e.g., DIC produced through oxidation of methane) are present in sediment porewaters. Water/rock ratios in the diagenetic environment of the study section can be estimated from O-isotopic ratios and burial temperatures. Most $\delta^{18}O_{carb}$ values at Hunghuayuan are between -8‰ and -10‰ (Table I-1), which are equivalent to water/rock ratios of 3-10 (Algeo et al., 1992) at burial temperatures of 60-80 °C (Wang et al., 1993). The Honghuayuan section exhibits only a limited range of $\delta^{13}C_{carb}$ values (-2‰ to +4‰), which is consistent with a primary marine signature and with estimates of low diagenetic water/rock ratios. A lack of systematic correlation between $\delta^{13}C_{carb}$ and $\delta^{18}O_{carb}$ at either the biozone or formation level in the studied section (Fig. 1-3B) provides further evidence of only minimal

secondary alteration of the carbonate C-isotopic record at Honghuayuan. On the other hand, the O-isotopic composition of carbonates is commonly altered at water/rock ratios as low as 1-3 (Algeo et al., 1992), and the range of $\delta^{18}O_{carb}$ values observed at Hunghuayuan (-8‰ and -10‰; Fig. I-3B) implies at least a modest negative shift from contemporaneous primary marine values (Lohmann and Walker, 1989). Thus, most of the carbonate O-isotopic record at Honghuayuan can be regarded as of secondary origin.

I-4.2. C-isotopic chemostratigraphy of the Honghuayuan section

The organic C-isotope chemostratigraphy of the Honghuayuan section shows several remarkable changes from the middle Floian to the lower Katian (Fig. I-4B). At Honghuayuan, the first large shift of $\delta^{13}C_{org}$ occurred in the Floian stage. From the middle of the *Acrograptus filiformis* biozone to the top of the *Didymograptus eobifidus* biozone, $\delta^{13}C_{org}$ values rise from -29.4‰ to -21.1‰, then $\delta^{13}C_{org}$ values show a decreased trend from -21.1‰ to -27.2‰ towards the top of the *Azygograptus suecicus* biozone of the Dapingian stage. It is evident that $\delta^{13}C_{org}$ exhibits an increase of ~8‰ in the Floian stage at Honghuayuan (Fig. I-4B). The Middle and Upper Ordovician also exhibit significant variation in $\delta^{13}C_{org}$ values: the Dapingian through Katian stages show several large (~4‰) fluctuations, accompanied by a shift in average $\delta^{13}C_{org}$ values of ~-26.5‰ in the Dapingian to ~-29‰ in the upper Katian (Fig. I-4B).

The carbonate C-isotope chemostratigraphy for Honghuayuan also shows a few major features (Figs. I-4A, I-5A). $\delta^{13}C_{carb}$ values rise from -1.1 ‰ to +1.5‰, and exhibit a ~3‰ positive increase from the upper part of carbonate sequence of the Meitan Formation to the lower part of the Shihtzupu Formation. This $\delta^{13}C_{carb}$ increase is followed by a ~1.5‰ decrease towards the topmost of the Shihtzupu Formation. Biostratigraphically, the $\delta^{13}C_{carb}$ increase of ~3‰ and subsequent decrease of ~1.5‰ from the top of the Meitan to the topmost of the Shihtzupu Formation occur in the Darriwilian Stage. It appears that $\delta^{13}C_{carb}$ rises from +0.3‰ to +2.7‰ from the topmost of the Shihtzupu Formation to the lowermost Pagoda Formation of the early Sandbian (Fig. I-5A). For the most of the Pagoda Formation (i.e., from Sandbian to middle Katian), $\delta^{13}C_{carb}$ values vary between +1‰ and +2‰ and they show little stratigraphic change. However, it appears that the $\delta^{13}C_{carb}$ values of the Pagoda carbonates decrease from +2.7‰ to +0.8‰ in the upper Katian (Fig. I-5A).

I-4.3. C-isotope excursions and global correlations

At Honghuayuan, a large (+8‰) excursion in $\delta^{13}C_{org}$ is observed over a 75-m-thick

stratigraphic interval in the lower to mid-Floian, from the *Acrograptus filiformis* through the *Didymograptus eobifidus* biozones of the Meitan Formation (Fig. I-4B). The relatively smooth character of this excursion (as reflected in limited sample-to-sample variance) suggests that it represents a perturbation to the global carbon cycle rather than a response to local environmental factors or to post-depositional processes. This excursion may be correlative with C-isotopic excursions identified in age-equivalent sections elsewhere. In southwestern Argentina, $\delta^{13}C_{carb}$ values rise from -2.8‰ to 0.3‰ from the *P proteus* to the *O. evae* conodont biozones of the Arenigian, which is probably equivalent to the Floian (Buggisch et al., 2003) (Fig. I-4C). Upwardly, the C-isotope data show a decreased trend towards the Early Darriwilian (Buggisch et al., 2003) (Fig. I-4C). Within the same interval of the Argentinian section, $\delta^{13}C_{org}$ values show a parallel increase of ~+2.8‰ (Buggisch et al., 2003). There is no $\delta^{13}C_{carb}$ data for the lower to mid-Floian at Honghuayuan because of a lack of carbonate deposits. However, the correlative biostratigraphy based on conodont and graptolite biozones between South China and southwestern Argentina allow us to correlate the positive $\delta^{13}C_{org}$ excursions observed from the two areas.

The positive increase of ~3‰ for $\delta^{13}C_{carb}$ (i.e., -1‰ to +2‰) in the Darriwilian stage at Honghuayuan has been reported from elsewhere (Fig. I-5A). For example, in central Nevada, $\delta^{13}C_{carb}$ increase from -2‰ to 0‰ was observed at the middle Chazyan stage (Saltzman and Young, 2005) (Fig. I-5B). In Estonia, $\delta^{13}C_{carb}$ values rise from -0.5‰ to +1.5‰ from Kunda stage to Aseri stage at Valga-Mehikoorma, exhibiting a ~2‰ positive increase in mid-Darriwilian (Kaljo et al., 2007). Also, a positive excursion of ~1.5‰ for $\delta^{13}C_{carb}$ was reported in the Darriwilian stage of southwestern Argentina (Buggisch et al., 2003). These C-isotopic data suggest that the Darriwilian carbon isotope excursion may be of global significance and provide evidence of a major perturbation to the global carbon cycle at that time.

Saltzman and Young (2005) observed positive C-isotopic excursions of 1-2‰ in the Turinian stage of the Mohawkian in Nevada (western United States) (Fig. I-5B). The age of the boundary between the Turinian and Chatfieldian is 454 Ma (Ludvigson et al., 2004), which may be equivalent to the Sandbian stage. If so, the increase of ~2‰ for $\delta^{13}C_{carb}$ in the lowermost Sandbian stage at Honghuayuan probably can be correlated to that in the Turinian stage in North America (Fig. I-5).

At Honghuayuan, $\delta^{13}C_{carb}$ data show little apparent stratigraphic trend for the Pagoda Formation spanning lower Sandbian to Katian (Fig. I-5A). It has been reported that a

positive C-isotopic increase occurred globally in the early Katian, which was known as the Guttenberg Inorganic Carbon Excursions (GICE). GICE has been observed from North America (Pancost et al., 1999, Saltzman and Young, 2005), Baltic (Kaljo et al., 2007), and from the Pagoda Formation in South China (Bergström et al., 2009). The apparent lack of GICE in the Honghuayuan section may reflect possible preservation biases of the isotopic record at this locale.

I-4.4. Implications of C-isotopic variation for the GOBE

Various explanations have been offered for C-isotopic excursions in the stratigraphic record, among which one of the most common interpretations of positive excursions is that they reflect increases in organic carbon burial rate that may be associated with concurrent decreases in atmospheric pCO_2 (Arthur et al., 1988; Patzkowsky et al., 1997; Kump and Arthur, 1999). Because photosynthesis fractionate in favor of ^{12}C relative to their source of inorganic carbon (by ~20‰ to 25‰ for plants using the Hatch-Slack photosynthetic cycle), higher rates of primary productivity probably driven by increased availability of nutrients and light and subsequent burial of ^{12}C-enriched organic matter cause the dissolved inorganic carbon (DIC) reservoir in seawater to become enriched in ^{13}C. Based on these relationships, concurrent large positive C-isotopic excursions in the mid-Floian of South China and southwestern Argentina (Fig. I-4B, I-4C) are inferred to be indicative of a major organic carbon burial event and a probable simultaneous decrease in atmospheric pCO_2 during the Early Ordovician (cf. Saltzman, 2005).

Paleontologic studies of the Early Ordovician radiation in South China have documented a rapid diversification commencing in the *Acrograptus filiformis* biozone at the base of the Meitan Formation and reaching the first peak at the top of the *Didymograptus eobifidus* biozone (Fig. I-2). Thus, the beginning of the diversification event was concurrent with the onset of the extended +8‰ excursion in $\delta^{13}C_{org}$ in the Floian stage at Honghuayuan (Fig. I-4B). Based on relationships between the $\delta^{13}C$ of seawater DIC and atmospheric pCO_2 discussed above, this excursion provides evidence of probable strong climatic cooling during the Early Ordovician that may have been an important factor in the GOBE (c.f. Trotter et al., 2008).

At Honghuayuan, the $\delta^{13}C_{carb}$ record exhibits episodic increases within the middle Darriwilian and basal Sandbian (Fig. I-4A, Fig. I-5A). These $\delta^{13}C_{carb}$ increases suggest that enhanced burial rates of organic matter continued to occur episodically during the late Middle and early Late Ordovician in South China. The elevated burial rates of

organic matter could have led to a further decline in the atmospheric pCO_2 and global climatic cooling. This interpretation is consistent with the results of an oxygen-isotopic thermometry study of contemporaneous conodonts, which documented a probable decrease in global temperatures from 42°C in the early Tremadocian to 28°C in the middle Darriwilian (Trotter et al., 2008). We suggest that episodes of enhanced organic carbon burial, as evidenced by C-isotopic increases observed at Honghuayuan (Fig. I-4), may have been an important factor in contributing to the late Middle and early Late Ordovician cooling trend that culminated in the Hirnantian glaciation.

I-5. Conclusions

High-resolution organic carbon and carbonate carbon isotopic records from a well-exposed section at Honghuayuan in South China provide one of the most complete records through the Ordovician. Detailed C-isotopic chemostratigraphic study of this section reveals large perturbations that can be correlated with C-isotopic records from other basins and, hence, may be indicative of perturbations to the global carbon cycle. The episodic increases in $\delta^{13}C_{org}$ and $\delta^{13}C_{carb}$ values observed at Honghuayuan in South China suggest enhanced burial rates of organic matter during the Early to early Late Ordovician. The elevated burial of organic matter could have contributed to climatic cooling that played an important role in triggering both the GOBE and the end-Ordovician mass extinction. Although biodiversification may have been promoted during the Early to Middle Ordovician by climatic cooling, intensified cooling during the Late Ordovician had a harmful effect on contemporaneous marine biotas.

Acknowledgments

We thank Renbin Zhan for help in the field work. This study was supported by Natural Sciences and Engieering Research Council of Canada, National Natural Science Foundation of China. TJA acknowledges support from the National Science Foundation.

References

Algeo, T.J., Scheckler, S.E., 1998. Terrestrial-marine teleconnections in the Devonian: links between the evolution of land plants, weathering processes and marine anoxic events. Philos. Trans. R. Soc. Lond. (B) Biol. Sci. 353, 113-128.

Algeo, T.J., Wilkinson, B.H., Lohmann, K.C., 1992. Meteoric-burial diagenesis of Pennsylvanian carbonate: water/rock interactions and basin geothermics. J. Sediment. Petrol. 62, 652-670.

Arthur, M.A., Dean, W.E., Pratt, L. M., 1988. Geochemical and climatic effects of

increased marine organic carbon burial at the Cenomanian/Turonian boundary. Nature 335, 714-717.

Berner, R.A., Kothavala, Z., 2001. GEOCARB III: A revised model of atmospheric CO_2 over Phanerozoic time. Am. J. Sci. 301, 182-204.

Bergström, S.M., Chen, X., Schmitz, B., Young, S., Rong, J., Saltzman, M.R., 2009. First documentation of the Ordovician Guttenberg $\delta^{13}C$ excursion (GICE) in Asia: chemostratigraphy of the Pagoda and Yanwashan formations in southeastern China. Geol. Mag. 146, 1-11.

Bottjer, D.J., Droser, M.L., Sheehan, P.M., McGhee Jr., G.R., 2001. The ecological architecture of major events in the Phanerozoic history of marine life. In: Allmon, W.D., Bottjer, D.J. (Eds.), Evolutionary Paleoecology. The Ecological Context of Macroevolutionary Change. Columbia Univ. Press, pp. 35–61.

Brenchley, P.J., Carden, G.A, Hints, O., Kaljo, D, Marshall, J.D., Martma, T, Meidla, T., Nolvak, J, 2003. High-resolution stable isotope stratigraphy of Upper Ordovician sequences: Constraints on the timing of bioevents and environmental changes associated with mass extinction and glaciation. Geol. Soc. Am. Bull. 115, 89-104.

Buggisch, W., Keller, M., Lehnert, O., 2003. Carbon isotope record of Late Cambrian to Early Ordovician carbonates of the Argentine Precordillera. Palaeogeogr.

Palaeoclimatol. Palaeoecol. 195, 357-373.

Chen, X., Rong, J., Wang, X., Wang, Z., Zhang, Y., Zhan, R., 1995. Correlation of Ordovician Rocks of China. International Union of Geol. Sci. Publ. 31, 104pp.

Chen, X., Rong, J., Mitchell, C.E., Harper, D.A.T., Fan, J., Zhan, R., Zhang, Y., Li, R., Wang, Y., 2000. Late Ordovician to earliest Silurian graptolite and branchiopod zonation from Yangtze Region, South China with global correlation. Geol. Mag. 137, 623-650.

Chen, X., Rong, J., Li, Y., Boucot, A. J., 2004. Facies patterns and geography of the Yangtze region, South China, through the Ordovician and Silurian transition. Palaeogeogr. Palaeoclimatol. Palaeoecol. 204, 353-372.

Chen, X., Melchin, M.J., Sheets, H.D., Mitchell, C.E., Fan, J.X., 2005. Patterns and processes of latest Ordovician graptolite extinction and recovery based on data from south China. J. Paleontol. 79, 842-861.

Chen, X., Rong, J., Fan, J., Zhan, R., Mitchell, C., Harper, D.A.T, Melchin, M.J., Peng, P., Finney, S.C., Wang, X., 2006a. The global boundary stratotype section and point for the base of the Hirnantian Stage (the uppermost of the Ordovician System). Episodes 29, 183-196.

Chen, X., Zhang, Y., Fan, J., 2006b. Ordovician graptolite evolutionary radiation: a review. Geo. J. 41, 289–301.

Cramer, B.D., Saltzman, M.R., 2007. Early Silurian paired analyses from the Midcontinent of North America: Implications for paleoceanography and paleoclimate. Palaeogeogr. Palaeoclimatol. Palaeoecol. 256, 195-203.

Crowell, J.C., 1999. Pre-Mesozoic Ice Ages: Their Bearing on Understanding the Climate System. Geol. Soc. Am. Memoir 192, 106 pp.

Droser, M.L., Sheehan, P.M., 1997. Palaeoecology of the Ordovician Radiation; resolution of large-scale patterns with individual clade histories, palaeogeography and

environments. Geobios 20, 221–229.

Fan, J., Peng, P., Melchin, M.J., 2009. Carbon isotopes and event stratigraphy near the Ordovician-Silurian boundary, Yichang, South China. Palaeogeogr. Palaeoclimatol. Palaeoecol. 276, 160-169.

Finney, S.C., Berry, W.B.N., Cooper, J.D., Ripperdan, R.L., Sweet, W.C., 1999. Late Ordovician mass extinction: a new perspective from stratigraphic sections in central Nevada. Geology 27, 215-218.

Freeman, K.H., 2001. Isotopic biogeochemistry of marine organic carbon. Rev. in Mineral. and Geochem. 43, 579-605.

Fu, K., 1982. The Ordovician of the Yangtze region. In: Lai, C. (Ed.), The Ordovician System of China. Stratigraphy of China 5. Geol. Publ. House, Beijing, pp. 92-131.

Gibbs, M.T., Barron, E.J., Kump, L.R., 1997. An atmospheric pCO_2 threshold for glaciation in the Late Ordovician. Geology 27, 447-450.

Gradstein, F., Ogg, J., Smith, A., 2004. A Geologic Time Scale. Cambridge Univ. Press, 589 pp.

Hayes, J.M., Popp, B.N., Takigiku, R., Johnson, M.W., 1989. An isotopic study of biogeochemical relationships between carbonates and organic carbon on the Greenhorn Formation. Geochim. Cosmochim. Acta 68, 4363-4379.

Hayes, J.M., Strauss, H., Kaufman, A.J, 1999. The abundance of ^{13}C in marine organic matter and isotopic fractionation in the global biogeochemical cycle of carbon during the past 800 Ma. Chem. Geol. 161, 103-125.

Herrmann, A.D., Patkowsky, M.E., Pollard, D., 2003. Obliquity forcing with 8-12 times preindustrial levels of atmospheric pCO_2 during the Late Ordovician glaciation. Geology 31, 485-488.

Hu, Y. H., Zhou, J.B., Song, B., Li, W., Sun, W.D., 2008. SHRIMP zircon U-Pb dating from K-bentonite in the top of Ordovician of Wangjiawan Section, Yichang, Hubei, China. Science in China (Series D): Earth Sciences 51, 493-498.

Ingalls, A.E, Aller, R.C., Lee, C., Wakeham, S.G., 2004. Organic matter diagenesis in shallow water carbonate sediments. Geochim. Cosmochim. Acta 68, 4363-4379.

Kaljo, D., Martma, T., Saadre, T., 2007. Post-Hunnebergian Ordovician carbon isotope trend in Baltoscandia, its environmental implications and some similarities with that of Nevada. Palaeogeogr. Palaeoclimatol. Palaeoecol. 245, 138–155

Kump, L.R., Arthur, M.A., 1999. Interpreting carbon-isotope excursions: carbonates and organic matter. Chem. Geol. 161, 181-198.

Kump, L.R., Arthur, M.A., Patzkowsky, M.E., Gibbs, M.T., Pinkus, D.S., Sheehan, P.M., 1999. A weathering hypothesis for glaciation at high atmospheric pCO_2 during the Late Ordovician. Palaeogeogr. Palaeoclimatol. Palaeoecol. 152, 173-187.

Lohmann, K.C, Walker, J.C.G., 1989. The $\delta^{18}O$ record of Phanerozoic abiotic marine calcite cements. Geophys. Res. Lett. 16, 319-322.

Ludvigson, G.A., Witzke, B.J., Gonzalez, L.A., Carpenter, S.J., Schneider, C.L., Hasiuk, F., 2004. Late Ordovician (Turinian-Chatfieldian) carbon isotope excursions and their stratigraphic and paleoceanographic significance. Palaeogeogr. Palaeoclimatol. Palaeoecol. 210, 187-214.

Melchin, M.J., Holmden, C., 2006. Carbon isotope chemostratigraphy in Arctic Canada: Sea-level forcing of carbonate platform weathering and implications for Hirnantian global correlation. Palaeogeogr. Palaeoclimatol. Palaeoecol. 234, 186-200.

Miller, A.I., 1997. Dissecting global diversity trends: examples from the Ordovician radiation. Ann. Rev. Ecology and Systematics 28, 85– 104.

Mu, E., Li, J., Ge, M., Chen, X., Ni, Y., Lin, Y., 1981. Late Ordovician paleogeography of South China. Acta Stratigraphy Sinica 5, 165-170.

Pancost, R.D., Freeman, K.H., Patżkowsky, M.E., 1999. Organic-matter source variation and the expression of a late Middle Ordovician carbon isotope excursion. Geology 27, 1015-1018.

Patzkowsky, M.E., Slupik, L.M., Arthur, M.A., Pancost, R.D., Freeman, K.H., 1997. Late Middle Ordovician environmental change and extinction: Harbinger of the Late Ordovician or continuation of Cambrian patterns? Geology 25, 911-914.

Rong, J., Chen, X., Harper, D.A.T., 2002. The latest Ordovician Hirnantia Fauna (Brachiopoda) in time and space. Lethaia 35, 231-249.

Rong, J., Harper, D.A.T., 1988. A global synthesis of the latest Ordovician Hirnantian brachiopod faunas. Trans. Roy. Soc. Edinburgh (Earth Sci.) 79, 383-402.

Rong, J., Zhan, R., Harper, D.A.T., 1999. Late Ordovician (Caradoc-Ashgill) brachiopod faunas with Foliomena based on data from China. Palaios 14, 412-431.

Royer, D.L., 2006. CO_2-forced climate thresholds during the Phanerozoic. Geochim. Cosmochim. Acta 70, 5665-5675.

Saltzman, M.R., 2005. Phosphorus, nitrogen, and the redox evolution of the Paleozoic oceans. Geology 33, 573-576.

Saltzman, M. R., Young, S.A., 2005. Long-lived glaciation in the Late Ordovician? Isotopic and sequence-stratigraphic evidence from western Laurentia. Geology 33, 109-112.

Schmitz, B., Harper, D.A.T., Peucker-Ehrenbrink, B., Stouge, S., Alwmark, C., Cronholm, A., Bergstrom, S.M., Tassinari, M., Wang, X., 2008. Asteroid breakup linked to the Great Ordovician Biodiversification Event. Nature Geoscience 1, 49-53.

Sepkoski, J.J., 1996. Patterns of Phanerozoic extinction: a perspective from global data bases. In: Walliser O. H. (Ed.), Global Events and Event Stratigraphy in the Phanerozoic. Springer, Berlin, pp. 35-51.

Sepkoski, J.J., 1997. Biodiversity: past, present and future. J. Paleontol. 71, 533–539.

Servais, T., Harper, D.A.T., Li, J., Munnecke, A., Owen, A.W., Sheehan, P.M., 2009. Understanding the Great Ordovician Biodiversification Event (GOBE): Influences of paleogeography, paleoclimate, or paleoecology? GSA Today 19, 4-10.

Sheehan, P.M., 2001. The Late Ordovician mass extinction. Ann. Rev. Earth and Planetary Sci. 29, 331-364.

Shen, Y., Schidlowski, M., 2000. New C isotope stratigraphy from southwest China: Implications for the placement of the Precambrian-Cambrian boundary on the Yangtze Platform and global correlations. Geology 28, 623-626.

Shields, G.A., Garden, G.A.F., Veizer, J., Meidla, T., Rong, J., Li, R., 2003. Sr, C, and O

isotope geochemistry of Ordovician brachiopods: A major isotope event around the Middle-Late Ordovician transition. Geochim. Cosmochim. Acta 67, 2005-2025.

Stanley, S.M., 1984. Temperature and biotic crises in the marine realm. Geology 12, 205-208.

Trotter, J.A., Williams, I.S., Barnes, C.R., Lecuyer, C., Nicoll, R,S., 2008. Did cooling oceans trigger Ordovician biodiverisfication? Evidence from conodont thermometry. Science 321, 550-554.

Underwood, C.J., Crowley, S.F., Marshall, J.D., Brenchley, P.J., 1997. High-resolution carbon isotope stratigraphy of the basal Silurian stratotype (Dob's Linn, Scotland) and its global correlation. J. Geol. Soc. London 154, 709-718.

Wang, H., 1985. Atlas of the Paleogeography of China. Cartographic Publ. House, Beijing, 143 pp.

Wang, H., Chen, J., 1991. Late Ordovician and early Silurian rugose coral biogeography and world reconstruction of palaeocontinents. Palaeogeogr. Palaeoclimatol. Palaeoecol. 86, 3-21.

Wang, K., Orth, C.J., Attrep, M., Chatterton, B.D.E., Wang, X., Li, J., 1993a. The great latest Ordovician extinction on the South China Plate: Chemostratigraphic studies of the Ordovician-Silurian boundary interval on the Yangtze platform. Palaeogeogr. Palaeoclimatol. Palaeoecol. 104, 61-79.

Wang, K., Chatterton, B.D.E., Attrep, M., Orth, C.J., 1993b. Late Ordovician mass extinction in the Selwyn Basin, northwestern Canada. Can. J. Earth Sci. 30, 1870-1880.

Wang, K., Chatterton, B.D.E., Wang, Y., 1997. An organic carbon isotope record of Late Ordovician to Early Silurian marine sedimentary rocks, Yangtze Sea, South China: Implications for CO_2 changes during the Hirnantian glaciation. Palaeogeogr. Palaeoclimatol. Palaeoecol. 132, 147-158.

Wang, X., Hoffknecht, A., Xiao, J., Chen, S., Li, Z., Broche, R.B., Erdtmamm, B.D., 1993. Graptolite, chitinozoan and scolecodont reflectances and their use as indicators of thermal maturity. Acta Geol. Sinica 6, 93-105.

Webby, B.D., Paris, F., Droser, M.L., 2004. The Great Ordovician Biodiversification Event. Columbia Univ. Press, New York, 484 pp.

Yan, D., Chen, D., Wang, Q., Wang, J., Wang, Z., 2009. Carbon and sulfur isotopic anomalies across the Ordovician–Silurian boundary on the Yangtze Platform, South China. Palaeogeogr. Palaeoclimatol. Palaeoecol. 274, 32-39.

Zhan, R., Rong, J., Cheng, J., Chen, P., 2005. Early-Mid Ordovician brachiopod diversification in South China. Science in China (Series D): Earth Sciences 48, 662-675.

Zhan, R., Harper, D.A.T., 2006. Biotic diachroneity during the Ordovician radiation: evidence from South China. Lethaia 39, 211-226.

Zhan, R., Jin, J., 2007. Ordovician-Early Silurian (Llandovery) Stratigraphy and Palaeontology of the Upper Yangtze Platform, South China. Science Press, Beijing, 169 pp.

Zhan, R., Jin, J., 2008. Aspects of recent advances in the Ordovician stratigraphy and palaeontology of China. Paleoworld 17, 1-11.

Zhan, R., Jin, J., Chen, P., 2007. Brachiopod diversification during the Early-Middle

Ordovician: an example from Dawan Formation, Yichang, central China. Can. J. Earth Sci. 44, 9-24.

Zhang, T., Shen, Y., Zhan, R., Shen, S., Chen, X., 2009. Large perturbations of the carbon and sulfur cycle associated with the Late Ordovician mass extinction in South China. Geology 37, 299-302.

Zhang, Y., Chen X., 2003. The Early Ordovician graptolite sequence of the Upper Yangtze region, South China. INSUGEO Serie Correlacion Geologia 17, 173-180.

Figure captions:

Fig. I-1. Location and paleogeography map for the Honghuayuan section in South China (Modified from Zhan and Jin, 2007).

Fig. I-2. Brachiopod radiation in Early to Middle Ordovician at Honghuayuan in South China (Modified from Zhan et al. 2005).

Fig. I-3. Evaluation of the diagenetic influence on C-isotope compositions: (A) $\delta^{13}C_{org}$ versus C_{org}; (B) $\delta^{13}C_{carb}$ versus $\delta^{18}O_{carb}$.

Fig. I-4. C-isotopic chemostratigraphy of the Honghuayuan section in South China and its correlation to that in Argentina. (A) $\delta^{13}C_{carb}$; (B) $\delta^{13}C_{org}$; and (C) correlation to $\delta^{13}C_{carb}$ profile for southwestern Argentina. (Buggisch et al., 2003). Graptolite taxonomic abbreviations: *D. compla.* = *Dicellograptus complanatus, E.c.* = *Exigraptus clavus, G.l.* = *Gymnograptus linnarssoni, U.a.* = *Undulograptus austrodentatus.* Conodont taxonomic abbreviations: *B.n.*, = *B. navis, C.a.* = *C. angulatus, C.l.* = *C. lindstromi, E.s.* = *E. suecicus, L.v.* = *L. variabilis, M.d.* = *Macerodus dianae, M.p.* = *M. parva, O.e.* = *O. evae, P.o.* = *P. originalis, P.e.* = *P. elegans, P.p.* = *P. proteus, R.m.* = *R. manitouensis.*

Fig. I-5. Detailed C-isotopic chemostratigraphy of Middle to Upper Ordovician interval at Honghuayuan: (A) $\delta^{13}C_{carb}$; and (B) correlation to $\delta^{13}C_{carb}$ profile for Nevada (Saltzman and Young, 2005).

Table 1-1 Geochemical data (TOC, $\delta^{13}C_{org}$ and $\delta^{13}C_{carb}$) of Ordovician samples from the Honghuayuan section in South China

Sample	Fm.	Stage	Grapt.	Litho.	H (m)	$\delta^{13}C_{org}$ (‰)	C_{org} (%)	$\delta^{13}C_{carb}$ (‰)	$\delta^{18}O_{carb}$ (‰)
GZ04	Hung.	Floian	A.filifor	carb.	0.50	-29.08	0.04	-1.02	-9.14
GZ05	Hung.	Floian	A.filifor	carb.	1.50	-28.52	0.05	-1.25	-8.92
GZ06	Hung.	Floian	A.filifor	carb.	3.00	-28.85	0.05	-1.64	-9.07
GZ07	Hung.	Floian	A.filifor	carb.	5.00	-29.12	0.06	-2.05	-9.40
GZ08	Hung.	Floian	A.filifor	carb.	7.50	-29.01	0.06	-1.67	-9.63
GZ09	Hung.	Floian	A.filifor	carb.	12.81	-29.36	0.04	-1.50	-9.89
GZ10	Hung.	Floian	A.filifor	carb.	15.00	-27.68	0.06	-1.31	-9.98
GZ11	Hung.	Floian	A.filifor	carb.	16.00	-24.96	0.03	-1.60	-9.96
GZ12	Hung.	Floian	A.filifor	carb.	17.50	-28.27	0.04	-1.62	-9.99
GZ13	Hung.	Floian	A.filifor	carb.	20.00	-28.92	0.03	-1.25	-9.62
GZ14	Hung.	Floian	A.filifor	carb.	22.41	-27.53	0.07	-1.23	-10.12
GZ15	Hung.	Floian	A.filifor	carb.	24.55	-28.32	0.06	-1.25	-10.06
GZ16	Hung.	Floian	A.filifor	carb.	27.75	-27.13	0.07	-1.28	-9.37
GZ17	Hung.	Floian	A.filifor	carb.	30.74	-27.38	0.03	-1.20	-9.99
GZ18	Hung.	Floian	A.filifor	carb.	32.87	-25.42	0.03	-1.27	-8.55
GZ19	Hung.	Floian	A.filifor	carb.	33.30	-26.81	0.03	-1.73	-9.02
GZ20	Hung.	Floian	A.filifor	carb.	33.72	-27.04	0.02	-2.03	-9.50
GZ21	Hung.	Floian	A.filifor	carb.	34.15	-26.45	0.02	-2.21	-10.02
GZ23	Meitan	Floian	A.filifor	carb.	35.27	-26.50	0.02	-1.65	-10.10
GZ26	Meitan	Floian	A.filifor	carb.	42.73	-24.34	0.02	-2.51	-9.47
GZ27	Meitan	Floian	A.filifor	carb.	43.33	-26.57	0.03	-1.48	-10.03
GZ159	Meitan	Floian	D.eobif.	mud.	48.53	-23.16	0.08		
GZ160	Meitan	Floian	D.eobif.	mud.	53.59	-22.92	0.10		
GZ161	Meitan	Floian	D.eobif.	mud.	57.63	-22.45	0.07		
GZ162	Meitan	Floian	D.eobif.	mud.	62.71	-22.71	0.10		
GZ163	Meitan	Floian	D.eobif.	mud.	67.73	-22.45	0.10		
GZ164	Meitan	Floian	D.eobif.	mud.	72.81	-22.53	0.10		
GZ165	Meitan	Floian	D.eobif.	mud.	77.87	-21.63	0.09		
GZ166	Meitan	Floian	D.eobif.	mud.	85.93	-21.37	0.07		

Table I-1 continued

Sample	Fm.	Stage	Grapt.	Litho.	H (m)	$\delta^{13}C_{org}$ (‰)	C_{org} (%)	$\delta^{13}C_{carb}$ (‰)	$\delta^{18}O_{carb}$ (‰)
GZ167	Meitan	Floian	C.defl.	mud.	92.01	-21.12	0.09		
GZ168	Meitan	Floian	C.defl.	mud.	100.93	-22.71	0.09		
GZ169	Meitan	Floian	C.defl.	mud.	107.39	-22.50	0.12		
GZ170	Meitan	Floian	C.defl.	mud.	115.92	-22.44	0.06		
GZ171	Meitan	Floian	C.defl.	mud.	120.51	-22.75	0.06		
GZ172	Meitan	Floian	C.defl.	mud.	125.04	-22.93	0.06		
GZ173	Meitan	Floian	C.defl.	mud.	132.50	-23.88	0.07		
GZ174	Meitan	Floian	C.defl.	mud.	137.16	-24.40	0.08		
GZ175	Meitan	Floian	C.defl.	mud.	142.69	-24.48	0.08		
GZ176	Meitan	Floian	A.sueci	mud.	147.21	-24.26	0.08		
GZ177	Meitan	Floian	A.sueci	mud.	149.03	-22.74	0.06		
GZ178	Meitan	Floian	A.sueci	mud.	150.50	-21.86	0.10		
GZ179	Meitan	Floian	A.sueci	mud.	152.07	-25.32	0.09		
GZ180	Meitan	Floian	A.sueci	mud.	155.09	-25.62	0.10		
GZ181	Meitan	Floian	A.sueci	mud.	159.13	-25.31	0.12		
GZ32	Meitan	Floian	A.sueci	carb.	159.20	-26.72	0.05	-1.18	-10.27
GZ33	Meitan	Floian	A.sueci	carb.	159.91	-25.65	0.03	-1.15	-9.76
GZ34	Meitan	Floian	A.sueci	carb.	159.26	-24.72	0.05	-0.99	-9.79
GZ35	Meitan	Floian	A.sueci	carb.	160.84	-23.84	0.04	-0.89	-9.14
GZ36	Meitan	Floian	A.sueci	carb.	161.33	-23.26	0.02	-0.66	-8.51
GZ37	Meitan	Floian	A.sueci	carb.	162.42	-25.73	0.03	-1.18	-10.12
GZ182	Meitan	Dapin.	A.sueci	mud.	167.93	-25.04	0.11		
GZ183	Meitan	Dapin.	A.sueci	mud.	173.39	-25.34	0.11		
GZ184	Meitan	Dapin.	A.sueci	mud.	178.84	-25.66	0.21		
GZ185	Meitan	Dapin.	A.sueci	mud.	182.30	-27.98	0.31		
GZ186	Meitan	Dapin.	A.sueci	mud.	187.50	-23.08	0.04		
GZ41	Meitan	Dapin.	A.sueci	carb.	194.28	-24.34	0.03	-1.27	-10.19
GZ42	Meitan	Dapin.	A.sueci	carb.	195.37	-25.65	0.04	-1.25	-9.86
GZ187	Meitan	Dapin.	A.sueci	carb.	202.66	-24.37	0.08		

Table I-1 continued

Sample	Fm.	Stage	Grapt.	Litho.	H (m)	$\delta^{13}C_{org}$ (‰)	C_{org} (%)	$\delta^{13}C_{carb}$ (‰)	$\delta^{18}O_{carb}$ (‰)
GZ44	Meitan	Dapin.	A.sueci	carb.	209.28	-25.25	0.04	-1.25	-10.26
GZ45	Meitan	Dapin.	A.sueci	carb.	209.82	-26.38	0.05	-1.79	-10.34
GZ188	Meitan	Dapin.	A.sueci	mud.	213.66	-26.95	0.18		
GZ189	Meitan	Dapin.	A.sueci	mud.	221.30	-26.84	0.17		
GZ190	Meitan	Dapin.	A.sueci	mud.	229.93	-27.21	0.25		
GZ191	Meitan	Dapin.	E.Hiru.	mud.	241.48	-26.54	0.19		
GZ193	Meitan	Dapin.	E.Hiru.	mud.	254.57	-25.40	0.12		
GZ194	Meitan	Dapin.	E.Hiru.	mud.	263.30	-25.25	0.10		
GZ47	Meitan	Dapin.	E.Hiru.	carb.	278.46	-25.34	0.05	-1.11	-8.75
GZ48	Meitan	Dapin.	E.Hiru.	carb.	281.73	-26.89	0.04	-0.73	-9.22
GZ196	Meitan	Darri.	E.clav.	mud.	276.39	-27.99	0.07		
GZ197	Meitan	Darri.	E.clav.	mud.	289.20	-28.58	0.10		
GZ49	Shihtz.	Darri.	U.aust.	carb.	292.15	-26.23	0.07	1.53	-8.48
GZ50	Shihtz.	Darri.	U.aust.	carb.	294.27	-26.58	0.06	1.39	-8.88
GZ51	Shihtz.	Darri.	U.aust.	carb.	294.95	-27.92	0.05	1.21	-8.76
GZ52	Shihtz.	Darri.	U.aust.	carb.	295.10	-27.51	0.09	0.80	-8.58
GZ53	Shihtz.	Darri.	U.aust.	carb.	295.25	-27.16	0.07	0.89	-8.33
GZ54	Shihtz.	Darri.	U. inte.	carb.	295.85	-27.32	0.08	0.92	-8.23
GZ55	Shihtz.	Darri.	U. inte.	carb.	296.31	-26.44	0.07	1.00	-8.67
GZ56	Shihtz.	Darri.	U. inte.	carb.	296.76	-27.37	0.08	0.96	-8.80
GZ57	Shihtz.	Darri.	U. inte.	carb.	297.52	-27.22	0.06	1.12	-8.90
GZ58	Shihtz.	Darri.	U. inte.	carb.	297.97	-26.87	0.05	0.96	-8.90
GZ59	Shihtz.	Darri.	D.artus	carb.	298.73	-27.09	0.06	0.63	-8.90
GZ60	Shihtz.	Darri.	D.artus	carb.	299.03	-26.89	0.04	0.90	-8.86
GZ61	Shihtz.	Darri.	D.artus	carb.	299.94	-26.53	0.06	0.35	-8.79
GZ62	Shihtz.	Darri.	D.artus	carb.	300.69	-26.38	0.05	0.50	-8.83
GZ63	Shihtz.	Darri.	D.artus	carb.	301.45	-27.15	0.04	0.72	-8.89
GZ64	Pago.	Sand.	N.grac.	carb.	301.64	-29.82	0.10	0.85	-8.64
GZ65	Pago.	Sand.	N.grac.	carb.	303.50	-28.99	0.07	2.22	-8.40

Table I-1 continued

Sample	Fm.	Stage	Grapt.	Litho.	H (m)	$\delta^{13}C_{org}$ (‰)	C_{org} (%)	$\delta^{13}C_{carb}$ (‰)	$\delta^{18}O_{carb}$ (‰)
GZ66	Pago.	Sand.	N.grac.	carb.	306.45	-26.07	0.02	2.14	-9.23
GZ67	Pago.	Sand.	?	carb.	309.10	-25.72	0.03	2.04	9.05
GZ68	Pago.	Sand.	?	carb.	313.44	-28.12	0.07	1.61	-9.15
GZ69	Pago.	Sand.	?	carb.	317.00	-29.81	0.11	1.55	-9.05
GZ70	Pago.	Sand.	?	carb.	321.00	-26.94	0.04	1.50	-9.02
GZ71	Pago.	Sand.	?	carb.	324.55	-26.99	0.02	1.56	-9.31
GZ72	Pago.	Sand.	?	carb.	328.66	-27.40	0.12	2.74	-9.19
GZ73	Pago.	Sand.	?	carb.	333.43	-29.02	0.10	1.99	-9.16
GZ74	Pago.	Sand.	?	carb.	337.35	-28.98	0.10	1.95	-9.22
GZ75	Linhsi.	Katian	D. ca.	carb.	338.55	-28.76	0.07	0.46	-9.65
GZ76	Linhsi.	Katian	D. ca.	carb.	339.05	-26.07	0.06	1.19	-9.37
GZ77	Linhsi.	Katian	D. ca.	carb.	341.65	-28.97	0.06	1.32	-9.31
GZ78	Linhsi.	Katian	D. ca.	carb.	342.15	-27.70	0.03	0.77	-9.48
GZ79	Wufe.	Katian	D. ce.	shale	342.32	-30.39	5.12		
GZ80	Wufe.	Katian	D. ce.	shale	342.40	-30.48	5.25		
GZ81	Wufe.	Katian	D. ce.	shale	342.49	-30.52	5.48		
GZ82	Wufe.	Katian	D. ce.	shale	342.83	-30.15	5.75		
GZ83	Wufe.	Katian	D. ce.	shale	343.17	-30.39	5.86		
GZ84	Wufe.	Katian	D. ce.	shale	343.67	-30.45	5.00		
GZ85	Wufe.	Katian	D. ce.	shale	344.18	-30.36	5.25		
GZ86	Wufe.	Katian	D. ce.	shale	344.69	-30.28	4.84		
GZ87	Wufe.	Katian	D. ce.	shale	345.03	-30.26	5.00		
GZ88	Wufe.	Katian	D. ce.	shale	345.53	-30.29	3.63		
GZ89	Wufe.	Katian	P. paci.	shale	346.55	-30.33	3.98		
GZ90	Wufe.	Katian	P. paci.	shale	347.06	-30.35	5.00		
GZ91	Wufe.	Katian	P. paci.	shale	347.73	-30.30	4.68		
GZ92	Wufe.	Katian	P. paci.	shale	348.58	-30.31	4.16		
GZ93	Wufe.	Katian	P. paci.	shale	348.92	-30.26	3.68		
GZ94	Wufe.	Katian	P. paci.	shale	349.43	-30.32	4.27		

Table I-1 continued

Sample	Fm.	Stage	Grapt.	Litho.	H (m)	$\delta^{13}C_{org}$ (‰)	C_{org} (%)	$\delta^{13}C_{carb}$ (‰)	$\delta^{18}O_{carb}$ (‰)
GZ95	Wufe.	Katian	P. paci.	shale	349.59	-30.23	4.81		
GZ96	Wuf	Katian	P. paci.	shale	349.93	-30.26	4.78		
GZ97	Wufe.	Hirnan.	N.extra	shale	350.19	-30.30	4.47		
GZ98	Wufe.	Hirnan.	N.extra	shale	350.36	-30.33	4.46		
GZ99	Wufe.	Hirnan.	N.extra	shale	350.61	-30.32	4.18		
GZ100	Wufe.	Hirnan.	N.extra	shale	350.95	-29.97	4.69		
GZ101	Wufe.	Hirnan.	N.extra	shale	351.20	-29.95	4.87		
GZ102	Wufe.	Hirnan.	N.extra	shale	351.37	-29.84	4.47		
GZ103	Wufe.	Hirnan.	N.extra	shale	351.54	-29.97	5.04		
GZ104	Wufe.	Hirnan.	N.extra	shale	351.71	-30.00	5.41		
GZ105	Kuany.	Hirnan.	N.extra	mud.	351.86	-28.83	8.87	1.153	-8.77
GZ106	Kuany.	Hirnan.	N.extra	mud.	352.01	-28.91	8.95		
GZ107	Kuany.	Hirnan.	N.extra	mud.	352.11	-28.73	7.48	2.509	-8.70
GZ108	Kuany.	Hirnan.	N.extra	mud.	352.21	-28.72	7.30	2.386	-9.42
GZ109	Kuany.	Hirnan.	N.extra	mud.	352.31	-28.73	5.87	3.513	-9.42
GZ110	Kuany.	Hirnan.	N.extra	mud.	352.41	-28.65	4.62	3.751	-9.51
GZ111	Kuany.	Hirnan.	N.extra	mud.	352.51	-28.73	4.73	1.677	-9.54
GZ112	Kuany.	Hirnan.	N.extra	mud.	352.61	-28.83	3.47	1.247	-9.32
GZ113	Kuany.	Hirnan.	N.extra	mud.	352.71	-28.76	2.54	1.359	-9.11
GZ114	Kuany.	Hirnan.	N.extra	mud.	352.81	-28.90	2.04	1.526	-8.84
GZ115	Kuany.	Hirnan.	N.extra	mud.	352.91	-28.85	1.46	1.362	-9.01
GZ116	Kuany.	Hirnan.	N.extra	mud.	353.01	-28.73	1.32	0.896	-9.01
GZ117	Kuany.	Hirnan.	N.extra	mud.	353.08	-28.49	2.16	0.8	-9.20
GZ118	Kuany.	Hirnan.	N.extra	carb.	353.16	-28.99	2.28	1.598	-9.20
GZ119	Kuany.	Hirnan.	N.extra	carb.	353.25	-28.96	2.75	2.197	-8.81
GZ120	Kuany.	Hirnan.	N.extra	carb.	353.33	-28.97	2.90	2.255	-9.19
GZ121	Kuany.	Hirnan.	N.extra	carb.	353.42	-28.93	3.22	2.496	-9.26
GZ122	Kuany.	Hirnan.	N.extra	mud.	353.51	-28.92	3.15	2.358	-9.34
GZ123	Kuany.	Hirnan.	N.extra	mud.	353.59	-28.91	3.11	2.284	-9.18

Table I-1 continued

Sample	Fm.	Stage	Grapt.	Litho.	H (m)	$\delta^{13}C_{org}$ (‰)	C_{org} (%)	$\delta^{13}C_{carb}$ (‰)	$\delta^{18}O_{carb}$ (‰)
GZ124	Kuany.	Hirnan.	N.extra	mud.	353.68	-28.95	3.68	2.576	-9.23
GZ125	Kuany.	Hirnan.	N.extra	mud.	353.76	-28.90	4.17	2.236	-9.23
GZ126	Kuany.	Hirnan.	N.extra	mud.	353.85	-28.94	3.42	2.072	-9.29
GZ127	Kuany.	Hirnan.	N.extra	mud.	353.93	-28.95	3.26	2.161	-7.90
GZ128	Kuany.	Hirnan.	N.extra	mud.	354.02	-28.92	3.26	2.506	-7.95
GZ129	Kuany.	Hirnan.	N.extra	mud.	354.10	-28.94	3.35	2.754	-8.61
GZ130	Kuany.	Hirnan.	N.extra	mud.	354.19	-28.93	1.88	1.88	-9.03
GZ131	Kuany.	Hirnan.	N.extra	mud.	354.27	-28.90	1.79	2.25	-9.09
GZ132	Kuany.	Hirnan.	N.extra	carb.	354.35	-28.89	1.64	2.313	-9.34
GZ133	Kuany.	Hirnan.	N. per.	carb.	354.46	-28.52	0.63	2.272	-9.32
GZ134	Kuany.	Hirnan.	N. per.	carb.	354.51	-28.39	0.77	1.765	-9.07
GZ135	Kuany.	Hirnan.	N. per.	carb.	354.61	-28.42	0.52	2.476	-8.67
GZ136	Kuany.	Hirnan.	N. per.	carb.	354.69	-28.22	0.56	1.998	-8.75
GZ137	Kuany.	Hirnan.	N. per.	mud.	354.87	-27.54	0.40	0.883	-7.98
GZ138	Kuany.	Hirnan.	N. per.	mud.	355.02	-27.35	0.39	1.183	-9.04
GZ139	Kuany.	Hirnan.	N. per.	mud.	355.22	-27.49	0.30	1.536	-9.08
GZ140	Kuany.	Hirnan.	N. per.	mud.	355.42	-27.76	0.38	1.521	-9.28
GZ141	Kuany.	Hirnan.	N. per.	mud.	355.70	-27.79	0.36	1.755	-9.31
GZ142	Kuany.	Hirnan.	N. per.	mud.	355.95	-28.05	0.45	1.295	-9.33
GZ148	Kuany.	Rhud.	A. asc.	mud.	356.65	-28.58	4.31		
GZ149	Kuany.	Rhud.	A. asc.	mud.	356.85	-28.48	2.38		
GZ150	Kuany.	Rhud.	A. asc.	mud.	357.05	-28.57	0.83		
GZ151	Kuany.	Rhud.	P. acu.	mud.	357.35	-28.51	0.51		
GZ152	Kuany.	Rhud.	P. acu.	mud.	357.55	-27.73	0.10		
GZ153	Lung.	Rhud.	P. acu.	shale	357.70	-28.58	0.70	0.484	-9.25
GZ154	Lung.	Rhud.	P. acu.	shale	357.85	-28.09	0.31	0.411	-8.96
GZ155	Lung.	Rhud.	P. acu.	shale	358.05	-27.97	0.30	-0.23	-9.00
GZ156	Lung.	Rhud.	C. ves.	shale	358.25	-27.82	0.34	0.614	-9.38
GZ157	Lung.	Rhud.	C. ves.	shale	358.45	-28.32	0.38	0.465	-9.13

Abbreviations: Fm. = formation, Grapt. = graptolite biozone, Litho =lithology,

Formation abbreviations: Hung.=Hunghuayuan, Shihtz.= Shihtzupu, Pago.=Pagoda, Linhsi.=Linhsiang, Wufe.=Wufeng, Kuany.=Kuanyinchiao, Lung.=lungmachi, Stage abbreviations: Dapin.= Dapingian, Darri.= Darriwilian, Sand.= Sandbian, Hirnan.=Hirnantian, Rhud.= Rhuddanian

Graptolite taxonomic abbreviations: A.asc. = *Akidograptus ascensus*, A.filifor.= Acrograptus filiformis, D.eodif.= Didymogratellus eodifidus, C.defl.= Corymbogr. deflexus, A.sueci.=, Azygograptus suecicus, C.ves. = *Cystograptus vesiculosus*, D. c.a. = *Dicellograptus complanatus*, D. c.e. = *Dicellograptus complexus*, E.cla. = *Exigraptus clavus*, E. Hiru.= Expansograptus Hirundo, N. extra. = *Normalograptus extraordinarius*, N. per. = *Normalograptus persculptus*, P. paci. = *Paraorthograptus pacificus*, P.acu. = *Parakidograptus acuminatus*, U.aust. = *Undulograptus austrodentatus*, U.inte. = *Undulograptus intersitus*.

Lithology abbreviations: carb. = carbonate, mud. =mudstone

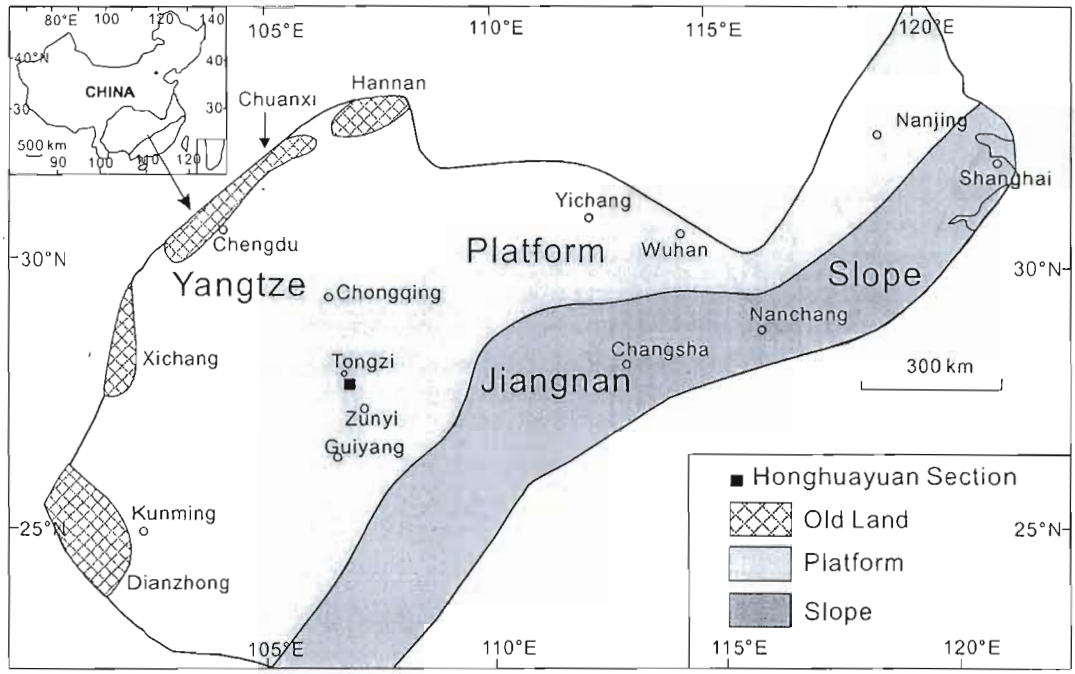
CHINA
500 km
105°E
110°E
115°E
120°E
30°N
25°N
Chuanxi
Hannan
Chengdu
Yangtze
Chongqing
Platform
Yichang
Wuhan
Nanjing
Shanghai
Slope
Nanchang
Changsha
Xichang
Tongzi
Zunyi
Guiyang
Jiangnan
300 km
Kunming
Dianzhong
Honghuayuan Section
Old Land
Platform
Slope

Fig.I-1

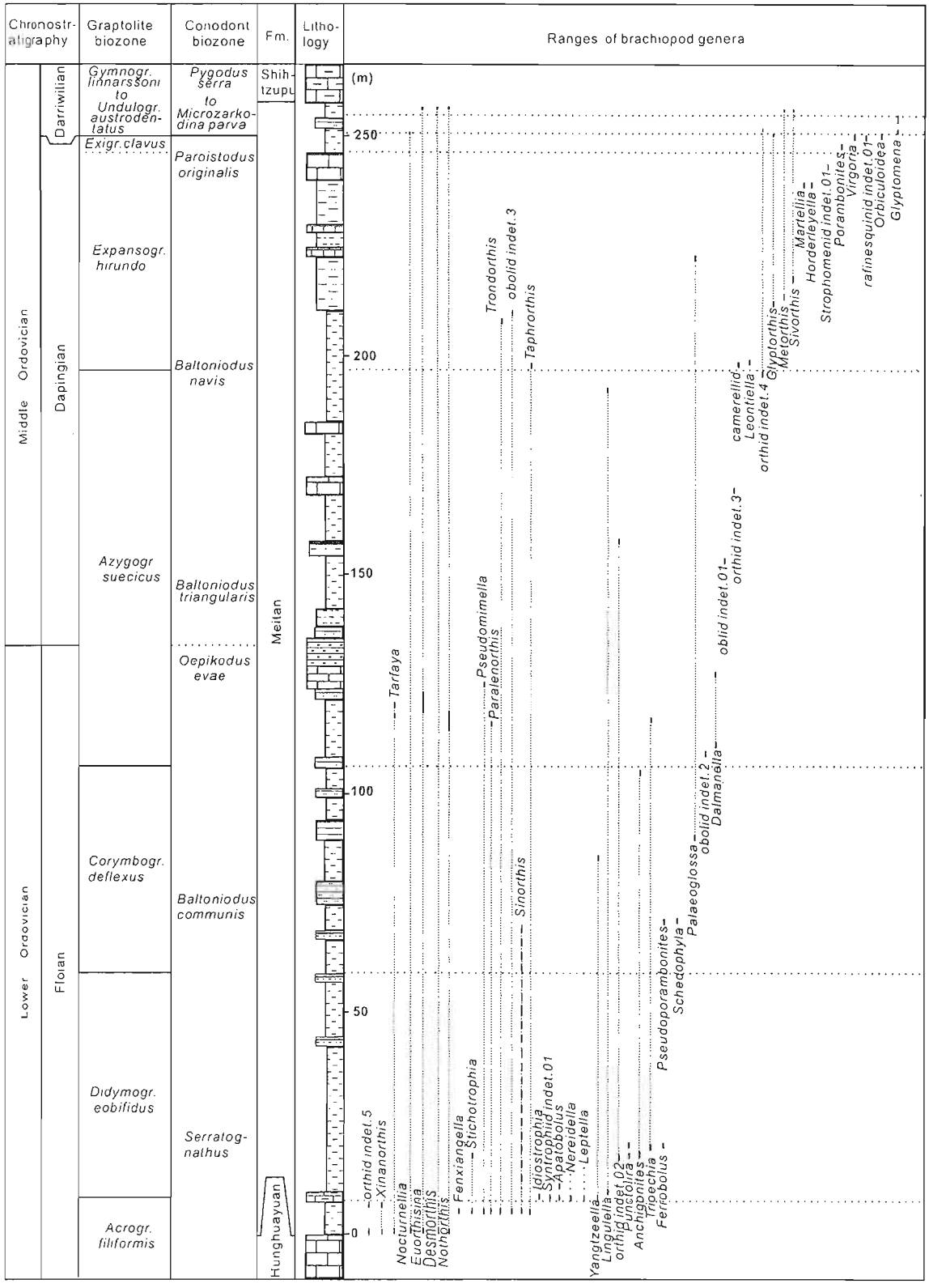
Chronostr-atigraphy
Graptolite biozone
Conodont biozone
Fm.
Litho-logy
Ranges of brachiopod genera
Middle Ordovician
Lower Ordovician
Darriwilian
Dapingian
Floian
Gymnogr. linnarssoni to Undulogr. austrodentatus
Exigr. clavus
Expansogr. hirundo
Azygogr. suecicus
Corymbogr. deflexus
Didymogr. eobifidus
Acrogr. filiformis
Pygodus serra to Microzarkodina parva
Paroistodus originalis
Baltoniodus navis
Baltoniodus triangularis
Oepikodus evae
Baltoniodus communis
Serratognathus
Shih-tzupu
Meitan
Hunghuayuan
(m)
250
200
150
100
50
0
orthid indet.5
Xinanorthis
Nocturnellia
Euorthisina
Desmorthis
Nothorthis
Tarfaya
Fenxiangella
Stichotrophia
Pseudomimella
Paralenorthis
Trondorthis
obolid indet.3
Taphrorthis
Sinorthis
Igiostrophia
Syntrophiid indet.01
Apatobolus
Nereidella
Leptella
Yangtzeella
Linguiella
orthid indet.02
Punctifira
Anchigonites
Tripechia
Ferrobolus
Pseudoporambonites
Schedophyla
Palaeoglossa
obolid indet.2
Dalmanella
oblid indet.01
orthid indet.3
camerellid
Leontiella
orthid indet.4
Glyptorthis
Meteorthis
Sivorthis
Martelilia
Horderleyella
Strophomenid indet.01
Porambonites
Virgoria
rafinesquinid indet.01
Orbiculoidea
Glyptomena
1

Fig. I-2.

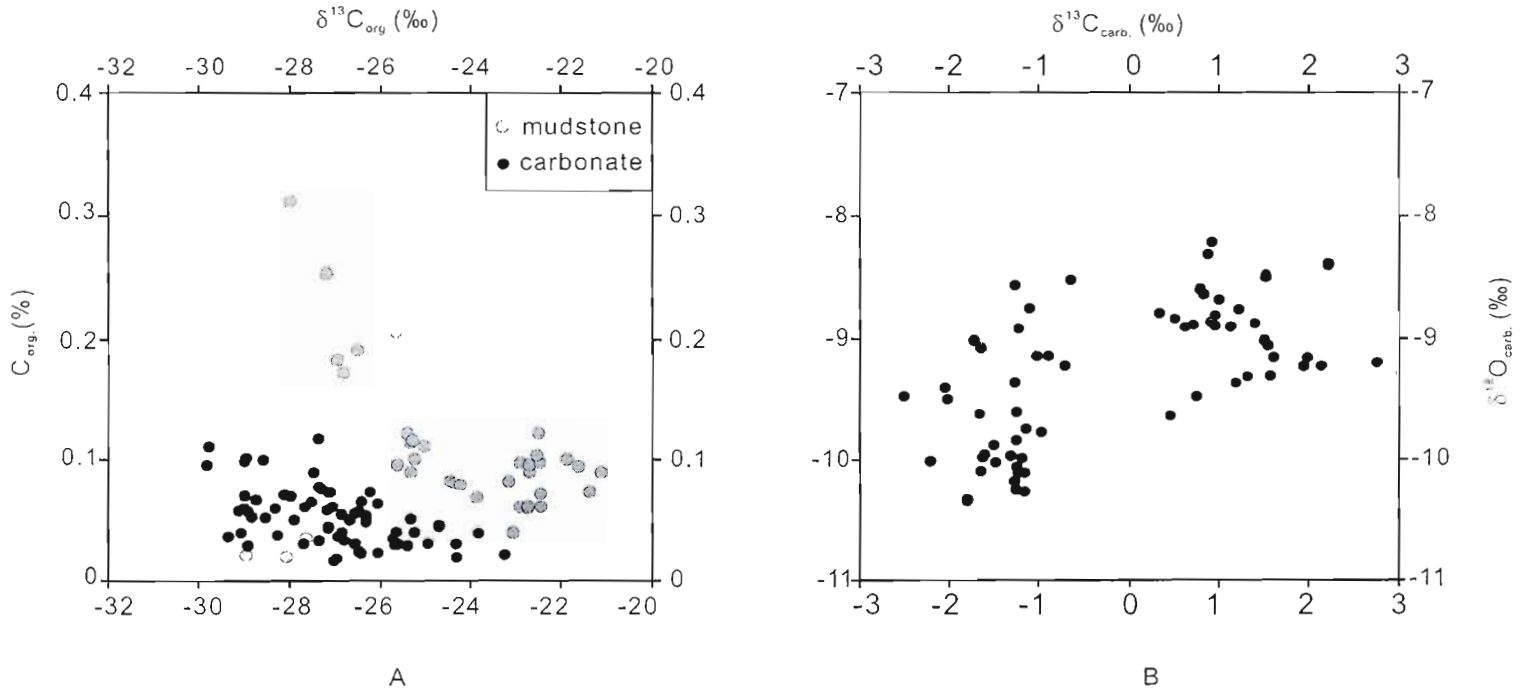
δ13Corg (‰)
-32 -30 -28 -26 -24 -22 -20
0.4 0.3 0.2 0.1 0
Corg.(%)
mudstone
carbonate
A
δ13Ccarb. (‰)
-3 -2 -1 0 1 2 3
-7 -8 -9 -10 -11
δ18Ocarb. (‰)
B

Fig. I-3

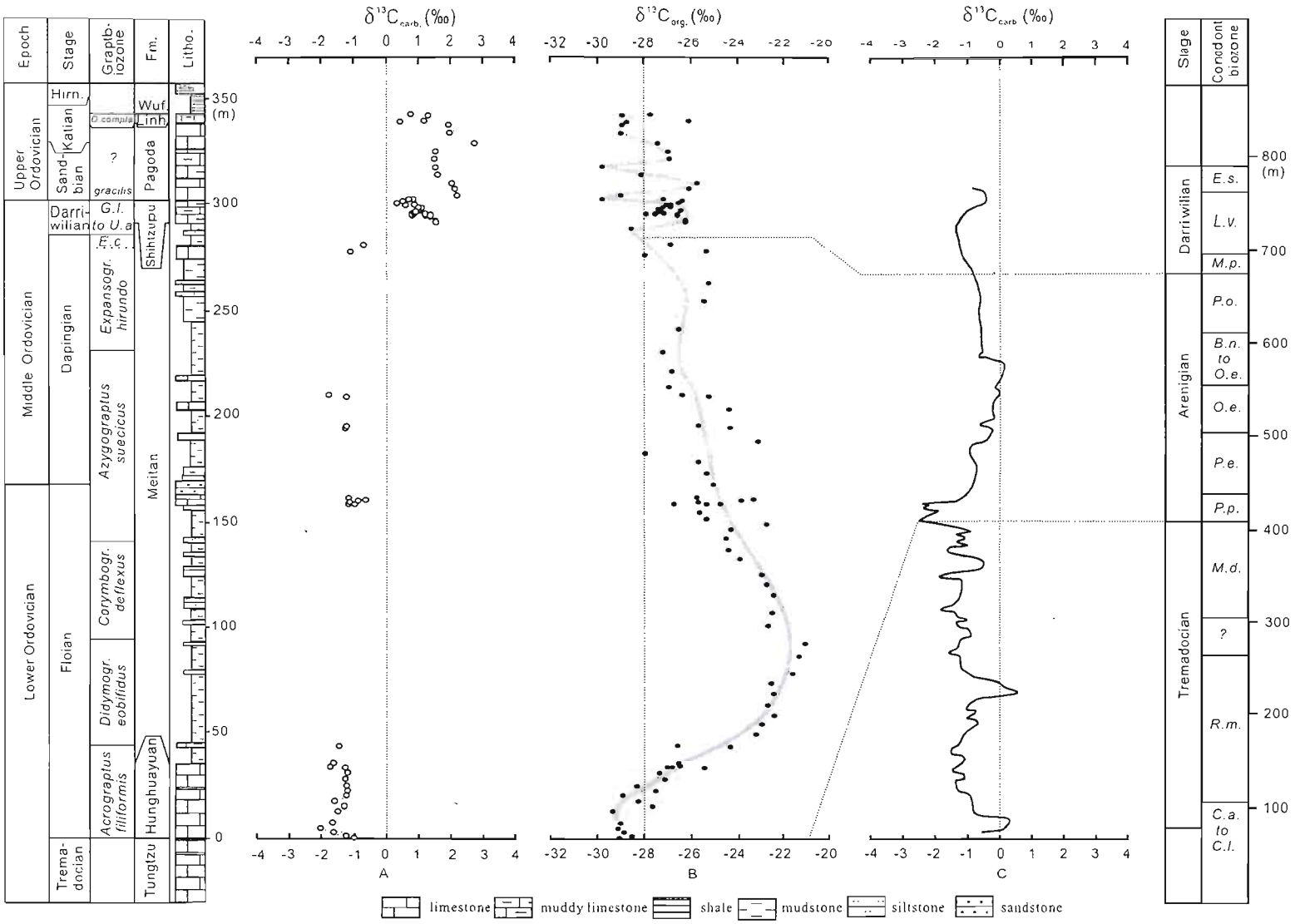
Epoch
Stage
Graptb-iozone
Fm.
Litho.
Upper Ordovician
Middle Ordovician
Lower Ordovician
Hirn.
Katian
Sand-bian
Darri-wilian
Dapingian
Floian
Trema-docian
Wuf.
Inh.
Pagoda
Shihtzupu
Meitan
Hunghuayuan
Tungtzu
O. compta
gracilis
G.l. to U.a
E.c.
Expansogr. hirundo
Azygograptus suecicus
Corymbogr. deflexus
Didymogr. eobifidus
Acrograptus filiformis
0
50
100
150
200
250
300
350
(m)
δ13Ccarb. (‰)
δ13Corg. (‰)
δ13Ccarb (‰)
-4 -3 -2 -1 0 1 2 3 4
-32 -30 -28 -26 -24 -22 -20
A
B
C
limestone
muddy limestone
shale
mudstone
siltstone
sandstone
Stage
Conodont biozone
Darriwilian
Arenigian
Tremadocian
E.s.
L.v.
M.p.
P.o.
B.n. to O.e.
O.e.
P.e.
P.p.
M.d.
?
R.m.
C.a. to C.l.
800
700
600
500
400
300
200
100
(m)

Fig. I-4

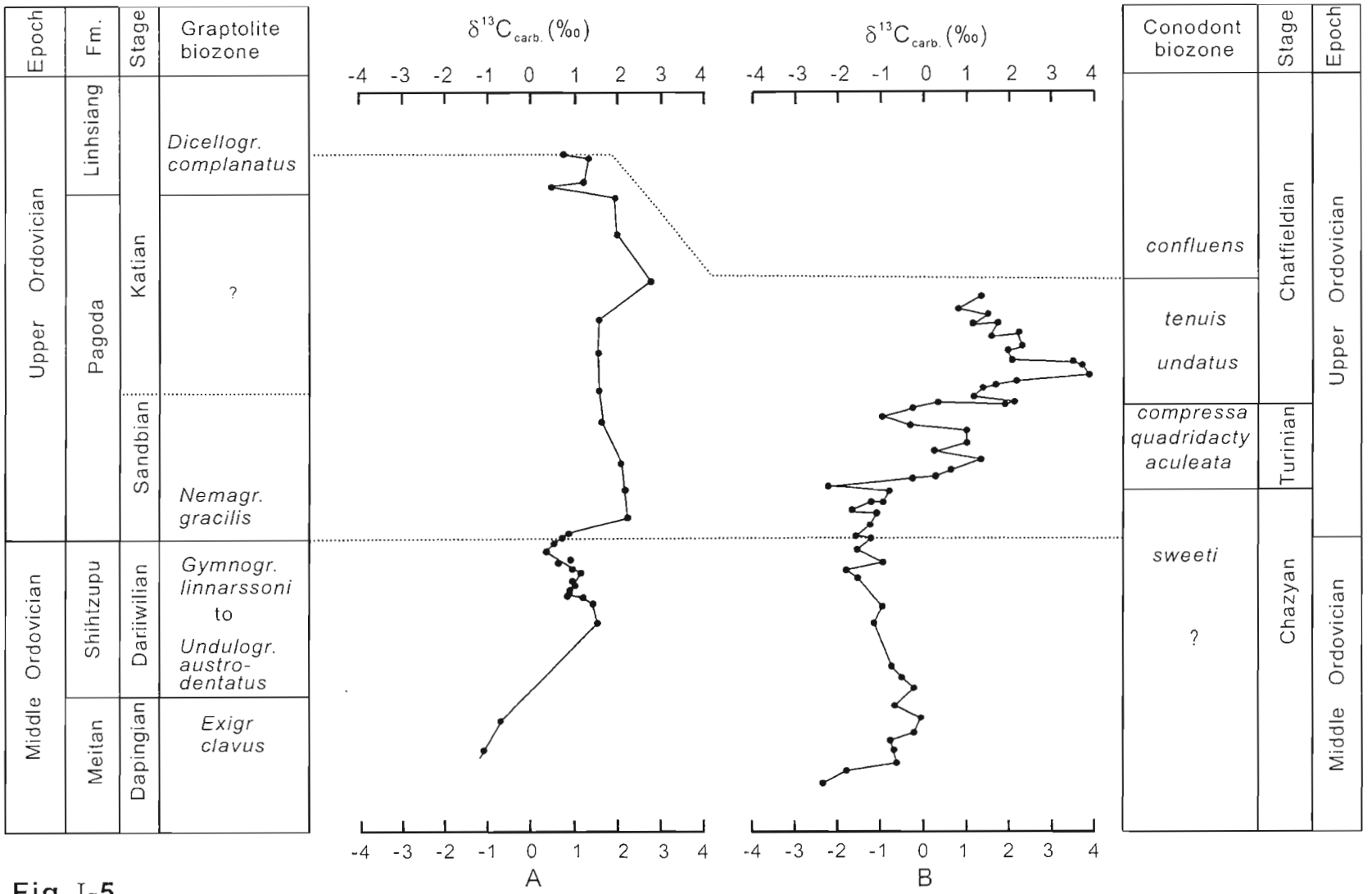
Epoch
Fm.
Stage
Graptolite biozone
Upper Ordovician
Middle Ordovician
Linhsiang
Pagoda
Meitan
Katian
Sandbian
Dariiwilian
Dapingian
Shihtzupu
Dicellogr. complanatus
?
Nemagr. gracilis
Gymnogr. linnarssoni
to
Undulogr. austro-dentatus
Exigr clavus
δ13Ccarb. (‰)
-4 -3 -2 -1 0 1 2 3 4
A
B
Conodont biozone
Stage
Epoch
confluens
tenuis
undatus
compressa
quadridacty
aculeata
sweeti
?
Chatfieldian
Turinian
Chazyan
Upper Ordovician
Middle Ordovician

Fig. I-5

CHAPTER II

Large perturbations of the carbon and sulfur cycle associated with the Late Ordovician mass extinctions in South China

Tonggang Zhang, Yanan Shen, Renbin Zhan, Shuzhong Shen, Xu Chen

Published in *Geology* (2009), vol.37, pp. 299-302.

Abstract

High-resolution $\delta^{13}C$ data of organic carbon from a continuous section of the Late Ordovician – Early Silurian reveal two positive $\delta^{13}C$ excursions that are associated with the mass extinction in South China. The first stratigraphic $\delta^{34}S$ measurements on pyrite tied to well-established biostratigraphy indicate a large perturbation of the sulfur cycle, consistent with major sea-level changes related to the glaciation. The elevated $\delta^{34}S$ values of pyrites and a large, short-lived negative $\delta^{34}S$ excursion of ~20‰ associated with the decay of the glaciation suggest deep-water anoxia during the Hirnantian Stage, in contrast to the conventional view that the global oceans were oxygenated. We suggest that deep-water anoxia may have contributed to the Late Ordovician mass extinction in South China and possibly elsewhere.

Keywords: the Late Ordovician mass extinction, $^{13}C/^{12}C$, $^{34}S/^{32}S$, chemostratigraphy, redox chemistry

II-1. Introduction

The Late Ordovician m extinction took place in the Hirnantian Stage (445.6–443.7 Ma), the latest of Ordovician (Sheenhan, 2001). In this biological crisis, it is estimated that 26% of all lies or 49% of all genera became extinct (Sepkoski, 1996), representing one of the est of all great Phanerozoic extinction events, second only to the end-Permian extinc (Sepkoski, 1996). The fossil record indicates that the Late Ordovician extinction wa tepwise and episodic, with two major pulses (e.g., Sheehan, 2001; Chen et al., 200 The two pulses of extinction appear to have coincided with the Late Ordovician glaciat that developed in high-latitude Gondwanaland. This has led many to propose that the glaciation and extinction were causally linked (Brenchley et al., 1994, 2003; Sheehan, 2001 and references therein).

Carbon isotope chemostratigraphy has been instrumental in global correlations of the Late Ordovician stratigraphy and in understanding evolution of atmospheric CO_2 (Brenchley et al., 1994, 2003; Kump et al., 1999; Saltzman and Young, 2005; Saltzman, 2005). The $\delta^{13}C$ data of both carbonate and organic carbon from numerous sections worldwide reveal a positive $\delta^{13}C$ excursion shortly after the first pulse of the extinction (e.g., Brenchley et al., 2003). This positive $\delta^{13}C$ excursion is interpreted to have resulted from high primary productivity (Brenchley et al., 1994; Marshall et al., 1997) or from the weathering of carbonate platforms that were exposed when sea level fell during the glaciation (Kump et al., 1999). However, the temporal relationship between the second major pulse of the extinction and the preceding $\delta^{13}C$ excursion is unclear (Brenchley et al., 2003), and the debates about the Late Ordovician climate changes mostly center on the multiple interpretations of C-isotopic data alone. In addition, there is little constraint on the possible influence of changes in redox chemistry of the Hirnantian glacial oceans on the extinctions, in part because the Hirnantian global ocean was thought to have been oxygenated (e.g., Brenchley et al., 1995).

Here we report high-resolution $\delta^{13}C$ data of organic carbon ($\delta^{13}C_{org}$) and $\delta^{34}S$ of pyrite from an excellent exposed and continuous section at Honghuayuan in South China (Fig. I-1). We show the temporal relationships between the major pulses of the mass extinction and the $\delta^{13}C$ excursions. The stratigraphic $\delta^{34}S$ measurements tied to well-established biostratigraphy shed new light on changes in the Late Ordovician glacial ocean chemistry and their probable influence on the mass extinction.

II-2. Geological setting and stratigraphy

In South China, there are numerous well-developed and richly fossiliferous successions of the Late Ordovician – Silurian covering a series of lithofacies and biofacies (Chen et al., 2004). Over the last 30 years, these superbly exposed sections have been examined in great detail, and the biostratigraphy that recorded the stepwise mass extinction has been well characterized (e.g., Mu, 1988; Rong et al., 2002; Chen et al., 2005). The global stratotype sections and point (GSSP) for the Hirnantian Stage has been established at Wangjiawan, Yichang (Fig. I-1). There, the rich fossil records, in particular of graptolites and conodonts, are of great utility for global correlations (Chen et al., 2006). The Hirnantian Stage at Wangjiawan consists of two graptolitic biozones: the lower *Normalograptus extraordinarius* biozone and the upper *Normalograptus persculptus* biozone (Fig. II-1, Chen et al., 2006).

Our high-resolution samples were collected from the Honghuayuan section, located in Tongzi County, Guizhou Province, South China (Fig. I-1). Lithostratigraphically, the Honghuayuan section that we measured consists of the Wufeng, Kuanyinchiao, and Lungmachi Formations (Fig. II-1, II-2). The Wufeng Formation, representing the middle-upper Katian Stage, is composed of organic-rich black shales with organic carbon content (C_{org}) of 4.77% (Table II-1) on average, which are widely distributed in South China (Mu, 1980; Chen et al., 2004). The Kuanyinchiao Formation consists of relatively thick-bedded mudstone, and, in a few areas, it is interbeded with thin carbonates of a few centimeters in thickness (Chen et al., 2004). The Kuanyinchiao Formation spans the middle *N. extraordinarius* biozone to middle *Parakidograptus acuminatus* biozone (Rong et al., 2002) (Fig. II-1). It has been well documented that the first major pulse of the Late Ordovician extinction at Honghuayuan corresponds to the lower *N. extraordinarius* biozone, the beginning of the Hirnantian Stage (Fig. II-1). The second major pulse of the extinction occurred at the base of *N. persculptus* biozone (Fig. II-1). (More detailed description of the section can be found in Chen et al. [2000] and Zhan and Jin [2007]).

There are several major advantages to studies on the Honghuayuan section in South China. Firstly, fossil graptolite and shelly fauna have been scrutinized over the last decades, and biostratigraphy at Honghuayuan has been well established (Chen et al., 2000; Rong et al., 2002; Zhan and Jin, 2007; Fig. II-1). This allows us to compare biostratigraphy with our documented isotopic record. Second, at Honghuayuan, the stepwise and episodic mass extinctions with double major pulses of biotic crisis from the *P. pacificus* biozone to the *N. persculptus* biozone are correlative to those in the GSSP

section at Wangjiawan in Yichang (Chen et al., 2006). Our study is therefore of broad significance.

II-3. Results and discussion

II-3.1. C-isotopic chemostratigraphy of Honghuayuan section and global correlation

Two step-like increases in the $\delta^{13}C_{org}$ record at Honghuayuan reveal large perturbations of the carbon cycle through the Late Ordovician (Fig. II-2). The $\delta^{13}C_{org}$ remain between -30.5‰ and -30.2‰ through the *Dicellograptus complexus* and *Paraorthograptus pacificus* biozones of the Katian Stage. We observe a positive $\delta^{13}C$ increase of ~2.0‰ in the lower *N. extraordinarius* biozone, shortly after the first major pulse of the extinction (C1 in Fig. II-2). The $\delta^{13}C_{org}$ profile is stable, with values from -28.5‰ to -29.0‰ in the middle-upper *N. extraordinarius* biozone. Shortly after the second major pulse of the extinction, a stepwise increase of ~1.5‰ is exhibited towards the lower *N. persculptus* biozone (C2 in Fig. II-2). The $\delta^{13}C_{org}$ values decrease from the upper *N. persculptus* biozone and reach a low value of -28.6‰ in the Earliest Silurian. The $\delta^{13}C_{org}$ values for the earliest Silurian sediments are between -27.7‰ to -28.6‰ (Fig. II-2).

Wang et al. (1993, 1997) demonstrated that thermal maturity of Late Ordovician sedimentary rocks in South China was low, suggesting that primary $\delta^{13}C_{org}$ values are well preserved. This suggestion is supported by the apparent stratigraphic $\delta^{13}C_{org}$ trends at Honghuayuan (Fig. II-2), which are difficult to explain by thermal maturation. Also, no systematic correlation between $\delta^{13}C_{org}$ and organic carbon content (C_{org}) is observed at either biozone or formation level (Table II-1). The lack of systematic correlation between $\delta^{13}C_{org}$ and C_{org} indicates that C-isotopic excursions from Honghuayuan section were not controlled by differential alteration of organic matter in the sediments (e.g., Kump et al., 1999). Moreover, previously reported $\delta^{13}C_{org}$ excursions worldwide provided little evidence that the primary $\delta^{13}C_{org}$ values from the Late Ordovician sediments have been significantly altered (Wang et al., 1993, 1997; Underwood et al., 1997; Kump et al., 1999). These observations strongly suggest that the primary signal of $\delta^{13}C_{org}$ variations (Fig. II-2) is well preserved at Honghuayuan.

The $\delta^{13}C_{org}$ data at Honghuayuan show several remarkable temporal relationships among the carbon cycle, glaciation, and the mass extinction. As noted above, the first positive $\delta^{13}C_{org}$ increase of ~2‰ in the lower *N. extraodinarius* biozone occurs shortly

after the first major pulse of the extinction (C1 in Fig. II-2). This positive $\delta^{13}C_{org}$ increase is consistent with a change of sedimentary facies from the deep-water Wufeng to the shallow-water Kuanyinchiao Formation, which marks sea-level fall at the start of the glaciation (Chen et al., 2005; Fig. II-2). The similar temporal relationship between the positive $\delta^{13}C$ excursion and the first major pulse of the extinction has been reported elsewhere in South China (Wang et al., 1993) and in other basins (e.g., Brenchly et al., 1994, 2003; Long, 1993; Kaljo et al., 2001; Finney et al., 1999; Melchin and Holmden, 2006) (Fig. II-3).

It is also evident that C-isotopic values decrease through the upper *N. persculptus* biozone and reach a low $\delta^{13}C$ value in the earliest Silurian at Honghuayuan, as well as in many sedimentary successions worldwide (Fig. II-3). These correlative $\delta^{13}C$ patterns in the lower *N. extraordinarius* biozone and the upper *N. perscultus* biozone among different basins suggest that these global effects were associated with the onset and demise of Gondwanan glaciation (Kump et al., 1999; Brenchly et al., 2003; Sheehan, 2001). However, the difference in the timing and magnitude of the $\delta^{13}C$ variations, as well as the second positive shift (C2) in the Hirnantian Stage between Honghuayuan and other regions (Fig. II-3) could reflect effects of carbon cycling in the epicontinental sea of South China. These $\delta^{13}C$ variations, when integrated with the S-isotopic record, allow us to explore redox ocean chemistry changes and their implications for the Late Ordovician mass extinction in South China.

II-3.2. S-isotope chemistry of pyrite at Honghuayuan and ocean chemistry

S-isotopic measurements of pyrite in Phanerozoic sedimentary rocks have been instrumental in reconstructing ocean and atmospheric chemistry (e.g., Strauss, 1997). However, there are few environmental constraints associated with the Late Ordovician mass extinction from application of $\delta^{34}S$ measurement of pyrite. To the best of our knowledge, this is the first stratigraphic $\delta^{34}S$ study of pyrite from a continuous section tied to well-established biostratigraphy, and this allows us to evaluate influence of ocean chemistry on the Late Ordovician extinction.

Figure II-2 shows that most of the $\delta^{34}S$ values for pyrite in the *D. complexus* and *P. pacificus* biozones display a narrow range of +8‰–+9‰. The $\delta^{34}S$ values increase ~6.4‰ from the topmost of the *P. pacificus* biozone to the lower *N. extraodinarius* biozone, which is coincident with facies change from the Wufeng to the shallow-water

Kuanyinchiao Formation (Fig. II-2). It is observed that the $\delta^{34}S$ increase in the lower *N. extraodinarius* biozone is coupled to the positive $\delta^{13}C_{org}$ increase in the same interval (Fig. II-2). Upwardly, the $\delta^{34}S$ values of pyrite spanning the middle-upper *N. extraordinarius* and the *N. persculptus* biozones vary between +14.3‰ and +20.4‰ (Fig. II-2). However, it appears that $\delta^{34}S$ values of pyrite experience a transient increase coupled to the $\delta^{13}C_{org}$ increase (C2 in Fig. II-2) in the lower *N. persculptus* biozone. A pronounced and short-lived negative $\delta^{34}S$ excursion occurs from +20.4‰ to +0.6‰ in the upper Kuanyinchiao Formation (Fig. II-2). The $\delta^{34}S$ values of pyrite then return to +7‰–+9‰. following the negative $\delta^{34}S$ shift of ~20‰ (Fig. II-2).

The organic-rich black shales of the Wufeng Formation were deposited across nearly the entire Yangtze Platform and Jiangnan Slope (Fig. I-1). Paleogeographic reconstruction and sedimentological studies indicate that the Wufeng black shales were deposited under anoxic oceans (e.g., Chen et al., 2004). The narrow range of $\delta^{34}S$ values for the Wufeng pyrites is consistent with oceanic anoxia, suggesting that most of the pyrites must have been formed in anoxic water columns. In anoxic water columns, the ready availabilities of sulfate and reactive Fe produce a more consistent fractionation, such that the pyrites can have more consistent $\delta^{34}S$ values than diagenetic pyrites formed within the sediments, which usually characterize a greater range of $\delta^{34}S$ values (e.g., Jørgensen, 1979). When integrated with the nearly constant $\delta^{13}C_{org}$ values through the *D. complexus* and *P pacificus* biozones, the narrow range of $\delta^{34}S$ values also suggest that the relative sizes of the reduced and oxidized reservoirs of carbon and sulfur were essentially stable.

In contrast, the coupled $\delta^{34}S$ and $\delta^{13}C_{org}$ increase in the lower *N. extraordinarius* biozone suggests enhanced burial rates of organic matter (Fig. II-2). This coupled increase is approximately coeval with the facies change from the Wufeng Formation to the shallow-water Kuanyinchiao Formation (Fig. II-2). The lower-middle Kuanyinchiao Formation is characterized by heavy $\delta^{34}S$ values (Fig. II-2). These heavy $\delta^{34}S$ values of Kuanyinchiao pyrites may have resulted from early diagenesis under oxic bottom-water conditions. The oxic bottom-water condition is evidenced by in situ occurrence of benthic shelly fauna fossils in the Kuanyinchiao sediments (Rong et al., 2002) that required oxygenated bottom waters to live. However, the Kuanyinchiao pyrites are statistically ~10‰ heavier than the Wufeng pyrites (Fig. II-2). We suggest that the isotopic differences between the two groups of pyrites may reflect facies differences between an anoxic Wufeng Formation and an oxic shallow-water Kuanyinchiao Formation, and that

the deep-water may have been predominantly anoxic when the Kuanyinchiao sediments were deposited. Under this scenario, deep water anoxia would have sequestered isotopically light sulfur of ^{32}S and light carbon of ^{12}C into deep anoxic parts. As a result, seawater sulfate in the oxic shallow would probably have been enriched in ^{34}S in particular when oceanic sulfate input is restricted, producing pyrites with heavy $\delta^{34}S$ values as seen in the Kuanyinchiao sediments (Fig. II-2). Thus, the coupled $\delta^{34}S$ and $\delta^{13}C_{org}$ increase in the lower *N. persculptus* biozone could reflect episodic increased burial rates of organic matter in the Hirnantian Stage at Honghuayuan.

Deep water anoxia at Honghuayuan is strongly supported by the short-lived, large negative $\delta^{34}S$ excursion of ~20‰ in the upper Kuanyinchiao Formation accompanying the decay of the glaciation (Fig. II-2). During rapid transgressions triggered by the decay of the Late Ordovician ice sheets, ^{32}S would have been transported from anoxic deep water into oxic shallow water, producing a transient chemical event that briefly perturbed the sulfur cycle, as observed at Honghuayuan (Fig. II-2). It is difficult to explain such a large and short-lived negative $\delta^{34}S$ shift of ~20‰ without invoking predominant deep-water anoxia. We note, however, that our hypothesis could be tested by $\delta^{34}S$ measurement of evaporitic sulfate or carbonate-associated sulfate. The sequestration of ^{32}S in anoxic basins possibly coupled with restricted input of sulfate would have driven enrichment of ^{34}S for sea-water sulfate in the Hirnantian oceans.

The deep-water anoxia beneath oxic shallow water at Honghuayuan proposed here is in contrast to the conventional view that the global oceans were oxygenated during the Hirnantian Stage. Restricted basins such as that at Honghuayuan may have been formed due to sudden sea-level fall at the onset of the Late Ordovician glaciation. So deep-water anoxia in South China might be only of regional significance. However, pyrites in the Late Ordovician glacial sediments from the Selwyn Basin, Canada, also show positive $\delta^{34}S$ values ranging from +14.6‰ to +16.8‰ (n=8) (Goodfellow and Jonasson, 1984), which are comparable with our Honghuayuan data. It was demonstrated that these positive $\delta^{34}S$ values may have resulted from stratified seas, where light sulfur was deposited into anoxic deep water (Goodfellow and Jonasson, 1984). Thus, the data from both basins suggest that deep-water anoxia in the Late Ordovician glacial oceans may have been widespread and that the redox chemistry may have been more complicated than previously thought.

II-4. Implications for the Late Ordovician Extinction

Isotopic data from South China reveal large perturbations in the sulfur and carbon cycle accompanying the onset and decay of the Late Ordovician glaciation, redox chemistry, and the mass extinction. Oceanic anoxia has been shown to have played a significant role in triggering some of the Phanerozoic mass extinctions (e.g., Hallam and Wignall, 1997; Knoll et al., 2007). Deep-water anoxia in South China, and probably also in the Selwyn Basin, Canada, would have reduced habitable zones for marine animals and would also have been deleterious to shallow-water organisms had anoxic water been delivered to the oxygenated shelf region. We suggest that deep-water anoxia in both regions may have contributed to the episodic and stepwise extinction in the Hirnantian Stage, in concert with harsh climate and temperature changes related to the glaciation (Sheehan, 2001). The deep-water anoxia advocated in this study contrasts with the conventional view that the Late Ordovician glacial oceans were oxygenated on a global scale. However, the wider or perhaps global significance of deep-water anoxia remains to be tested. We conclude that the new approach of integrating S- and C-isotope measurements with well-established biostratigraphy and sedimentary facies can be applied to investigate other basins and to elucidate the detailed history interlocking glaciation, ocean and atmospheric chemistry, and the Late Ordovician mass extinction.

Acknowledgments

We thank P.F. Hoffman for advice on the Late Ordovician ice age, and basin evolution, and T.J. Algeo, D. Johnston, A.H. Knoll, and A. S. Turchyn for comments that have greatly improved the manuscript. This study was supported by the Canada Research Chairs Program, the Natural Sciences and Engineering Research Council of Canada, and the National Natural Science Foundation of China (40503002, 40528004).

References

Brenchley, P.J., Marshall, J.D., Carden, G.A.F., Robertson, D.B.R., Long, D.G.F., Meidla, T., Hints, L., and Anderson, T.F., 1994, Bathymetric and isotopic evidence for a short-lived Late Ordovician glaciation in a greenhouse period: Geology, v. 22, p. 295-298.

Brenchley P.J., Carden G.A.F., Marshall, J.D., 1995, Environmental changes associated with the "first strike" of the late Ordovician mass extinction: Modern Geology, v. 20, p. 69–82.

Brenchley, P.J., Carden, G.A, Hints, L., Kaljo, D., Marshall, J.D., Martma, T., Meidla, T., and Nolvak, J., 2003, High-resolution stable isotope stratigraphy of Upper Ordovician sequences: Constraints on the timing of bioevents and environmental changes associated with mass extinction and glaciation: Geological Society of America Bulletin, v. 115, p. 89-104.

Chen, X., Rong, J., Mitchell, C.E., Harper, D.A.T., Fan, J., Zhan, R., Zhang, Y., Li, R., and Wang, Y., 2000, Late Ordovician to earliest Silurian graptolite and branchiopod zonation from Yangtze Region, South China with global correlation: Geological Magazine, v. 137, p. 623-650.

Chen, X., Rong, J., Li, Y., and Boucot, A. J., 2004, Facies patterns and geography of the Yangtze region, South China, through the Ordovician and Silurian transition: Palaeogeography, Palaeoclimatology, Palaeoecology, v. 204, p. 353-372.

Chen, X., Melchin, M.J., Sheets, H.D., Mitchell, C.E., and Fan, J., 2005, Patterns and processes of latest Ordovician graptolite extinction and recovery based on data from south China: Journal of Palaeontology, v. 79, p. 842-861.

Chen, X., Rong, J., Fan, J., Zhan, R., Mitchell, C., Harper, D.A.T, Melchin, M.J., Peng, P., Finney, S.C., and Wang, X., 2006, The global boundary stratotype section and point for the base of the Hirnantian Stage (the uppermost of the Ordovician System): Episode, v. 29, p. 183-196.

Finney, S.C., Berry, W.B.N., Cooper, J.D., Ripperdan, R.L., and Sweet, W.C., 1999, Late Ordovician mass extinction: a new perspective from stratigraphic sections in central Nevada: Geology, v. 27, p. 215-218.

Goodfellow, W.D., and Jonasson, I.R., 1984, Ocean stagnation and ventilation defined by secular trends in pyrite and barite, Selwyn Basin, Yukon: Geology, v. 12, p. 583-586.

Hallam, A., and Wignall, P., 1997, Mass extinctions and their aftermath: Oxford, Oxford University Press, p. 328.

Kaljo, D., Hints, L., Martma, T., and Nolvak, J., 2001, Carbon isotope stratigraphy in the latest Ordovician of Estonia: Chemical Geology, v. 175, p. 49-59.

Knoll, A.H., Bambach, R.K., Payne, J.L., Pruss, S., Fischer, W.W., 2007, Paleophysiology and end-Permian mass extinction: Earth and Planetary Science Letters, v. 256, p. 295–313.

Kump, L.R., Arthur, M.A., Patzkowsky, M.E., Gibbs, M.T., Pinkus, D.S., Sheehan, P.M.,

1999, A weathering hypothesis for glaciation at high atmospheric pCO_2 during the Late Ordovician: Palaeogeography, Palaeoclimatology, Palaeoecology, v. 152, p.173–187.

Long, D.G.F., 1993, Oxygen and carbon isotopes and event stratigraphy near the Ordovician-Silurian boundary, Anticosti Island, Quebec: Palaeogeography, Palaeoclimatology, Palaeoecology, v. 104, p. 49-59.

Marshall, J.D., Brenchley, P.J., Mason, P., Wolff, G.A., Astini, R.A., Hints, L., and Meidla, T., 1997, Global carbon isotopic events associated with mass extinction and glaciation in the Late Ordovician: Palaeogeography, Palaeoclimatology, Palaeoecology, v. 132, p. 195-210.

Melchin, M.J., and Holmden, C., 2006, Carbon isotope chemostratigraphy in Arctic Canada: Sea-level forcing of carbonate platform weathering and implications for Hirnantian global correlation: Palaeogeography, Palaeoclimatology, Palaeoecology, v. 234, p.186-200.

Mu, E., 1980, Research on the graptolithina of China: Acta Palaeontologica Sinica, v. 19, p. 143-151 (in Chinese with English abstract).

Mu, E., Li, J., Ge, M., Chen, X., Ni, Y., and Lin, Y., 1981, Late Ordovician paleogeography of South China: Acta Stratigraphy Sinica, v. 5, p.165-170 (in Chinese with English abstract).

Mu, E., 1988, The Ordovician-Silurian boundary in China: Bulletin of British Museum of Natural History (Geology), v. 43, p. 117-131.

Rong, J., Chen X., and Harper, D.A.T., 2002, The latest Ordovician Hirnantia Fauna (Brachiopoda) in time and space: Lethaia, v. 35, p. 231-249.

Saltzman, M. R., and Young, S.A., 2005, Long-lived glaciation in the Late Ordovician? Isotopic and sequence-stratigraphic evidence from western Laurentia: Geology, v. 33, p. 109-112.

Saltzman, M.R., 2005, Phosphorus, nitrogen, and the redox evolution of the Paleozoic oceans: Geology, v. 33, p. 573-576.

Sepkoski, J.J., 1996, Patterns of Phanerozoic extinction: a perspective from global data bases: *in* Walliser, O.H., ed., Global Event and Event Stratigraphy in the Phanerozoic, Berlin, Springer, p. 35-51.

Sheehan, P.M., 2001, The Late Ordovician mass extinction: Annual Review of Earth and Planetary Sciences, v. 29, p. 331-364.

Strauss, H., 199 .he isotopic composition of sedimentary sulfur through time: Palaeogeography, l aeoclimatology, Palaeoecology, v. 132, p. 97-118.

Underwood, C.J (rowley, S.F., Marshall, J.D., and Brenchley, P.J., 1997, High-resolution c.. n isotope stratigraphy of the basal Silurian stratotype (Dob's Linn, Scotland) and its . bal correlation: Journal of Geological Society London, v. 154, p. 709-718.

Wang, K., Orth, C.J Attrep, M., Chatterton, B.D.E., Wang, X., and Li, J., 1993, The great latest Ordovician extinction on the South China Plate: Chemostratigraphic studies of the Ordovician-Silurian boundary interval on the Yangtze platform: Palaeogeography, Palaeoclimatology, Palaeoecology, v. 104, p. 61-79.

Wang, K., Chatterton, B.D.E., and Wang, Y., 1997, An organic carbon isotope record of Late Ordovician to Early Silurian marine sedimentary rocks, Yangtze Sea, South China: Implications for CO_2 changes during the Hirnantian glaciation: Palaeogeography, Palaeoclimatology, Palaeoecology, v. 132, p. 147-158.

Zhan, R., and Jin, J. (eds.), 2007, Ordovician-Early Silurian (Llandovery) Stratigraphy and Palaeontology of the Upper Yangtze Platform, South China: Beijing, Science Press, p.1-169.

Figure captions

Figure II-1. Biostratigraphy of Honghuayuan section (from Chen et al., 2000, 2005; Rong et al., 2002; Zhan and Jin, 2007).

Figure II-2. Integrated C- and S-isotopic chemostratigraphy and biostratigraphy of the Late Ordovician – Early Silurian at Honghuayuan, South China

Figure II-3. C-isotopic chemostratigraphic correlation of Honghuayuan section (A) with sections in Copenhagen Canyon, Nevada (B) (Finney et al., 1999; Kump et al., 1999), East Baltic (C) (Brenchley et al., 2003), and Arctic Canada(D) (Melchin and Holmden, 2006).

Table II-1 C- and S-isotope data of Late Ordovican samples at Honghuayuan in South China.

Sample No.	Formation	Stage	Graptolite zone	Height (m)	$\delta^{13}C_{org}$ (‰)	$\delta^{34}S$ (‰)	C_{org} (%)
GZ157	Lungmachi	Rhuddanian	C. vesiculosus	16.30	-28.32	9.74	0.38
GZ156	Lungmachi	Rhuddanian	C. vesiculosus	16.10	-27.82	9.96	0.34
GZ155	Lungmachi	Rhuddanian	P. acuminatus	15.90	-27.97	8.73	0.30
GZ154	Lungmachi	Rhuddanian	P. acuminatus	15.70	-28.09	7.71	0.31
GZ153	Lungmachi	Rhuddanian	P. acuminatus	15.55	-28.58	0.57	0.70
GZ152	Kuanyichiao	Rhuddanian	P. acuminatus	15.40	-27.73	9.15	0.10
GZ151	Kuanyichiao	Rhuddanian	P. acuminatus	15.20	-28.51	4.98	0.51
GZ150	Kuanyichiao	Rhuddanian	A. ascensus	14.90	-28.57	9.58	0.83
GZ149	Kuanyichiao	Rhuddanian	A. ascensus	14.70	-28.48	14.76	2.38
GZ148	Kuanyichiao	Rhuddanian	A. ascensus	14.50	-28.58	15.94	4.31
GZ142	Kuanyichiao	Hirnantian	N. persculptus	13.80	-28.05	20.41	0.45
GZ141	Kuanyichiao	Hirnantian	N. persculptus	13.55	-27.79	19.78	0.36
GZ140	Kuanyichiao	Hirnantian	N. persculptus	13.27	-27.76	18.97	0.38
GZ139	Kuanyichiao	Hirnantian	N. persculptus	13.07	-27.49	19.15	0.30
GZ138	Kuanyichiao	Hirnantian	N. persculptus	12.87	-27.35	19.70	0.39
GZ137	Kuanyichiao	Hirnantian	N. persculptus	12.72	-27.54	19.84	0.40
GZ136	Kuanyichiao	Hirnantian	N. persculptus	12.54	-28.22	17.47	0.56
GZ135	Kuanyichiao	Hirnantian	N. persculptus	12.46	-28.42	14.33	0.52
GZ134	Kuanyichiao	Hirnantian	N. persculptus	12.36	-28.39	16.38	0.77
GZ133	Kuanyichiao	Hirnantian	N. persculptus	12.31	-28.52	15.71	0.63
GZ132	Kuanyichiao	Hirnantian	N. extraordiarius	12.20	-28.89	18.59	1.64
GZ131	Kuanyichiao	Hirnantian	N. extraordiarius	12.12	-28.90	18.61	1.79
GZ130	Kuanyichiao	Hirnantian	N. extraordiarius	12.04	-28.93	17.85	1.88
GZ129	Kuanyichiao	Hirnantian	N. extraordiarius	11.95	-28.94	18.25	3.35
GZ128	Kuanyichiao	Hirnantian	N. extraordiarius	11.87	-28.92	18.78	3.26
GZ127	Kuanyichiao	Hirnantian	N. extraordiarius	11.78	-28.95	18.96	3.26
GZ126	Kuanyichiao	Hirnantian	N. extraordiarius	11.70	-28.94	16.53	3.42
GZ125	Kuanyichiao	Hirnantian	N. extraordiarius	11.61	-28.90	18.73	4.17
GZ124	Kuanyichiao	Hirnantian	N. extraordiarius	11.53	-28.95	18.84	3.68
GZ123	Kuanyichiao	Hirnantian	N. extraordiarius	11.44	-28.91	18.97	3.11
GZ122	Kuanyichiao	Hirnantian	N. extraordiarius	11.36	-28.92	18.92	3.15
GZ121	Kuanyichiao	Hirnantian	N. extraordiarius	11.27	-28.93	18.94	3.22
GZ120	Kuanyichiao	Hirnantian	N. extraordiarius	11.18	-28.97	18.78	2.90
GZ119	Kuanyichiao	Hirnantian	N. extraordiarius	11.10	-28.96	19.08	2.75
GZ118	Kuanyichiao	Hirnantian	N. extraordiarius	11.01	-28.99	16.81	2.28
GZ117	Kuanyichiao	Hirnantian	N. extraordiarius	10.93	-28.49	18.46	2.16

GZ116	Kuanyichiao	Hirnantian	N. extraordiarius	10.86	-28.73	18.39	1.32
GZ115	Kuanyichiao	Hirnantian	N. extraordiarius	10.76	-28.85	16.97	1.46
GZ114	Kuanyichiao	Hirnantian	N. extraordiarius	10.66	-28.90	16.48	2.04
GZ113	Kuanyichiao	Hirnantian	N. extraordiarius	10.56	-28.76	18.85	2.54
GZ112	Kuanyichiao	Hirnantian	N. extraordiarius	10.46	-28.83	18.77	3.47
GZ111	Kuanyichiao	Hirnantian	N. extraordiarius	10.36	-28.73	18.45	4.73
GZ110	Kuanyichiao	Hirnantian	N. extraordiarius	10.26	-28.65	18.65	4.62
GZ109	Kuanyichiao	Hirnantian	N. extraordiarius	10.16	-28.73	18.21	5.87
GZ108	Kuanyichiao	Hirnantian	N. extraordiarius	10.06	-28.72	17.26	7.30
GZ107	Kuanyichiao	Hirnantian	N. extraordiarius	9.96	-28.73	18.01	7.48
GZ106	Kuanyichiao	Hirnantian	N. extraordiarius	9.86	-28.91	18.16	8.95
GZ105	Kuanyichiao	Hirnantian	N. extraordiarius	9.71	-28.83	17.97	8.87
GZ104	Wufeng	Hirnantian	N. extraordiarius	9.56	-30.00	15.72	5.41
GZ103	Wufeng	Hirnantian	N. extraordiarius	9.39	-29.97	12.53	5.04
GZ102	Wufeng	Hirnantian	N. extraordiarius	9.22	-29.84	12.27	4.47
GZ101	Wufeng	Hirnantian	N. extraordiarius	9.05	-29.95	13.42	4.87
GZ100	Wufeng	Hirnantian	N. extraordiarius	8.80	-29.97	11.88	4.69
GZ99	Wufeng	Hirnantian	N. extraordiarius	8.46	-30.32	11.37	4.18
GZ98	Wufeng	Hirnantian	N. extraordiarius	8.21	-30.33	11.60	4.46
GZ97	Wufeng	Hirnantian	N. extraordiarius	8.04	-30.30	10.85	4.47
GZ96	Wufeng	Katian	P. pacificus	7.78	-30.26	11.59	4.78
GZ95	Wufeng	Katian	P. pacificus	7.44	-30.23	9.55	4.81
GZ94	Wufeng	Katian	P. pacificus	7.28	-30.32	8.85	4.27
GZ93	Wufeng	Katian	P. pacificus	6.77	-30.26	8.34	3.68
GZ92	Wufeng	Katian	P. pacificus	6.43	-30.31	7.40	4.16
GZ91	Wufeng	Katian	P. pacificus	5.58	-30.30	8.27	4.68
GZ90	Wufeng	Katian	P. pacificus	4.91	-30.35	9.22	5.00
GZ89	Wufeng	Katian	P. pacificus	4.40	-30.33	9.07	3.98
GZ88	Wufeng	Katian	D. complexus	3.38	-30.29	9.39	3.63
GZ87	Wufeng	Katian	D. complexus	2.88	-30.26	9.04	5.00
GZ86	Wufeng	Katian	D. complexus	2.54	-30.28	8.15	4.84
GZ85	Wufeng	Katian	D. complexus	2.03	-30.36	9.59	5.25
GZ84	Wufeng	Katian	D. complexus	1.52	-30.45	9.45	5.00
GZ83	Wufeng	Katian	D. complexus	1.02	-30.39	9.36	5.86
GZ82	Wufeng	Katian	D. complexus	0.68	-30.15	6.64	5.75
GZ81	Wufeng	Katian	D. complexus	0.34	-30.52	8.62	5.48
GZ80	Wufeng	Katian	D. complexus	0.25	-30.48	8.72	5.25
GZ79	Wufeng	Katian	D. complexus	0.17	-30.39	9.61	5.12

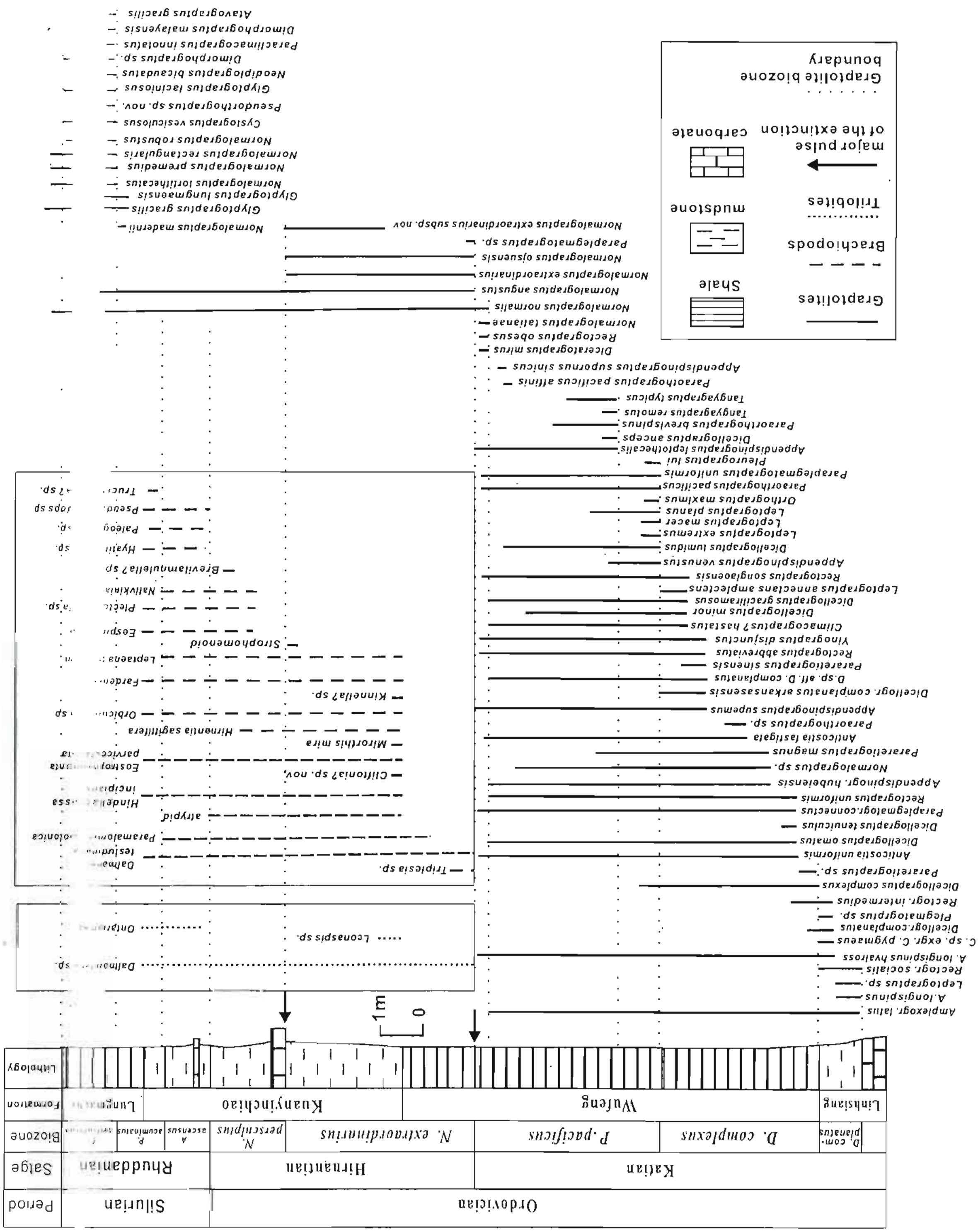
Graptolites
Brachiopods
Trilobites
major pulse of the extinction
Graptolite biozone boundary
Shale
mudstone
carbonate
1m
0
Lithology
Formation
Biozone
Salge
Period
Linhsiang
Wufeng
Kuanyinchiao
Lungmachi
D. complanatus
D. complexus
P. pacificus
N. extraordinarius
N. persculptus
A. ascensus
P. acuminatus
Katian
Hirnantian
Rhuddanian
Ordovician
Silurian

Fig.II-1

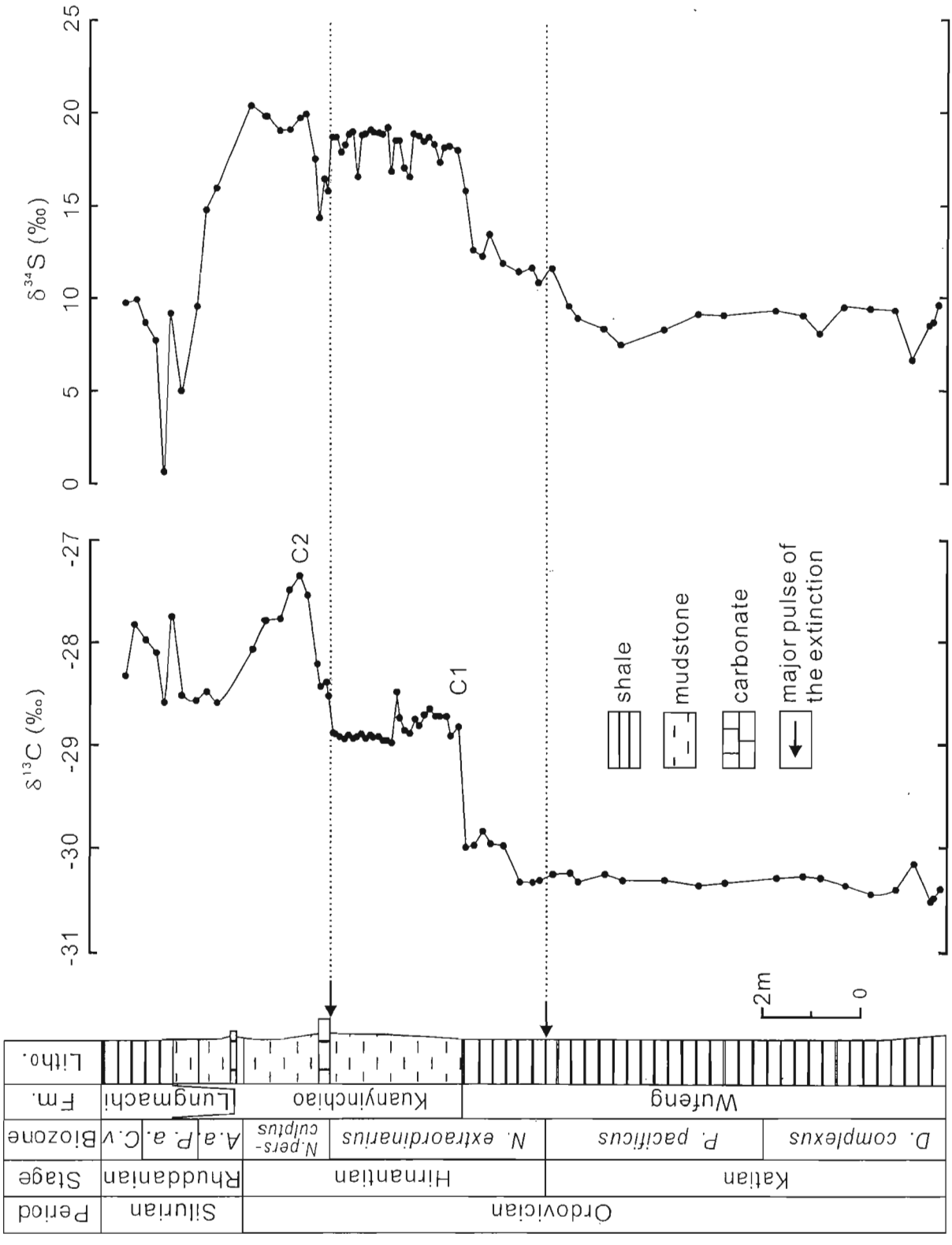
δ34S (‰)
0
5
10
15
20
25
δ13C (‰)
-31
-30
-29
-28
-27
C2
C1
shale
mudstone
carbonate
major pulse of the extinction
2m
0
Litho.
Fm.
Lungmachi
Kuanyinchiao
Wufeng
Biozone
A. a.
P. a.
C. v
N. pers-culptus
N. extraordinarius
P. pacificus
D. complexus
Stage
Rhuddanian
Hirnantian
Katian
Period
Silurian
Ordovician

Fig.II-2

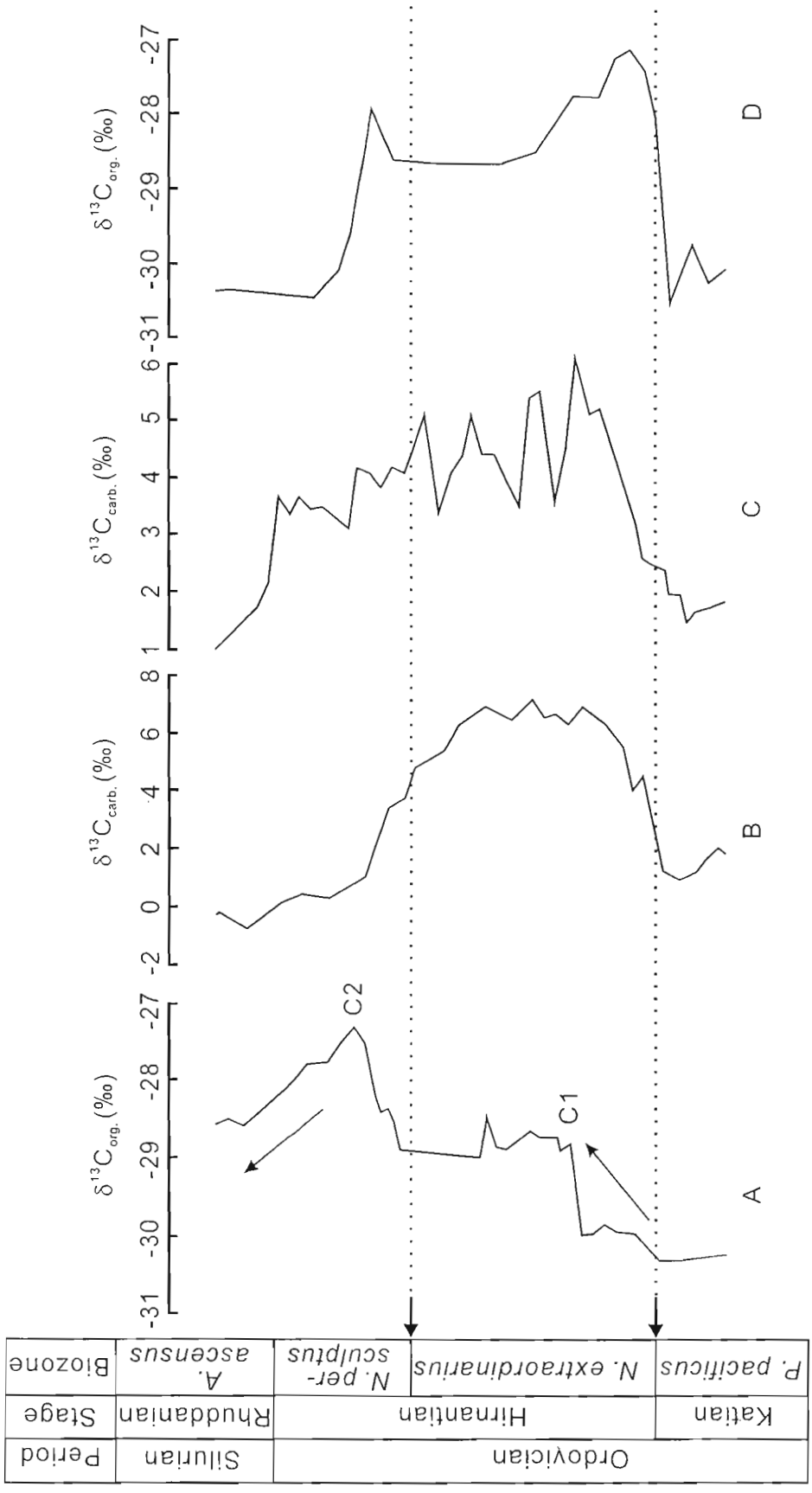
Period
Stage
Biozone
Ordovician
Silurian
Hirnantian
Rhuddanian
Katian
P. pacificus
N. extraordinarius
N. per-sculptus
A. ascensus
δ13Corg. (‰)
δ13Ccarb. (‰)
A
B
C
D
C1
C2

Fig.II-3

CHAPTER III

On the coevolution of Ediacaran oceans and animals

Yanan Shen, Tonggang Zhang, Paul F. Hoffman

Published in *Proc. Natl. Acad. Sci. USA* (2008), vol. 105, pp. 7376-7381

Abstract

Fe speciation and S-isotope of pyrite data from the terminal Proterozoic Sheepbed Formation in Canada and Doushantuo Formation in China reveal that ocean deep waters were anoxic after the global glaciations (snowball Earth) ending 635 million years ago, but that marine sulfate concentrations and inferentially atmospheric oxygen levels were higher than before the glaciations. This supports a long-postulated link between oxygen levels and the emergence of eumetazoa. Subsequent ventilation of the deep ocean, inferred from shifts in Fe speciation in Newfoundland (previously published data) and western Canada (this report), paved the way for Ediacaran macrobiota to colonize the deep-sea floors.

Keywords: atmospheric oxygen, iron speciation, sulfur isotopes, Sheepbed Formation, Doushantuo Fornation, Ediacaran biota

III-1. Introduction

A pair of global glaciations (Hoffman and Schrag, 2002) between 725 and 635 million years ago (Cryogenian Period) was followed by the appearance and diversification of (mainly non-skeletal) multicellular animals in the Ediacaran Period from 635 to 541 million years ago (Harland and Rudwick, 1964; Gehling and Rigby, 1996; Fedonkin and Waggoner, 1997; Xiao et al., 1998; Knoll and Caroll, 1999; Fedonkin, 2003). The oldest animal fossils include diapause egg and embryo cysts (*Tianzhushania spinosa*) from the lower Doushantuo Formation (~632 Ma) in South China (Yin et al., 2007) and lipid biomarkers (24-isopropyl-cholestane) diagnostic of marine demosponges in late Cryogenian and early Ediacaran strata of Oman (Love et al., 2006). In contrast, colonization of the deep-sea floor (below the euphotic zone) by large soft-bodied organisms was delayed until mid-Ediacaran time around 579 Ma (Narbonne and Gehling, 2003; Bowring et al., 2003; Wood et al., 2003; Narbonne 2005; Bottjer and Clapham, 2006). The delayed appearance of large animals in the fossil record, ~600 million years after multicellularity arose in algae (Butterfield 2000), inspired the hypothesis that an increase in atmospheric oxygen catalyzed early animal evolution (Knoll and Caroll, 1999; Nursall 1959; Berkner and Marshall, 1965; Towe 1970; Cloud 1972; Runnegar 1982; Graham 1988; Knoll et al., 1986).

Recent chemostratigraphic studies provide some evidence for progressive oxygenation of the Ediacaran ocean (Fike et al., 2006), including mid-Ediacaran (ca. 580 Ma) deep waters (Canfield et al., 2007). The first study based its inference mainly on increasing sulfur isotope fractionation between coexisting sulfides and carbonate-associated sulfate (Fike et al., 2006); the second was based on the low ratios between highly reactive Fe and total Fe (FeHR/FeT) (Canfield et al., 2007). These data purport to "see" through the veil of diagenesis under the influence of anoxic pore-waters to the redox state of ancient seawater. Here, we present Fe speciation and S-isotope of pyrite data from deep-water ocean-margin settings in northwestern Canada and in South China that point to an extended early Ediacaran interval of sulfate-rich oceans with sulfidic deep waters, implying an oxygen-rich atmosphere, followed by the ventilation of deep waters in mid-Ediacaran time.

III-2. Geological Setting

III-2.1. Northwest Canada.

Ediacaran strata of the Windermere Supergroup (Narbonne and Aitken, 1995) are exposed for > 500 km along the concave-to-southwest arc of the Mackenzie Mountains, topographic expression of the early Cenozoic foreland thrust-fold belt of the northern Canadian Cordillera. Because of a low-angle unconformity with overlying Cambrian strata, the Ediacaran is mainly limited to the Plateau Thrust system, an outcrop belt less than ≈30 km wide. Fortuitously, it preserves the shelf-to-slope transition of an Ediacaran passive continental margin (Narbonne and Aitken, 1995; Dalrymple and Narbonne, 1996; James et al, 2001). To the northeast (landward), Ediacaran strata were removed by sub-Cambrian erosion and to the southwest (seaward), they are mostly buried by younger rocks. Southwest of the Plateau Thrust system, a single transverse structural culmination exposes three separate inliers of Ediacaran strata, the most easterly of which (Sekwi Brook) contains a moderately diverse assemblage of mostly disc-shaped macrofossils, apparently representing the bases of sessile, polypoid and frond-like, soft-bodied organisms, as well as rare ovate segmented fossils, and abundant simple or irregularly meandering burrows (Aitken 1989; Narbonne and Aitken 1990; Narbonne 1994). The oldest fossils (five genera of disk-shaped forms) occur in the middle Sheepbed Formation (Fig. III-1), a 1050-m-thick sequence of black shales, turbiditic siltstones and contour-current sands, deposited at estimated water depths of 1-1.5 km on an open-marine continental slope subject to geostrophic currents (Dalrymple and Narbonne, 1996). They are much larger and more diverse than the simple discs found between the two Cryogenian glacial horizons in the same area (Hofmann et al, 1990).

The shelf-slope transition is best exposed on Stelfox Mountain (Fig. III-1), 25 km northeast of Sekwi Brook, where a major down-to-southwest breakaway paleoscarp (Aitken 1991) marks the outer edge of the Keele Formation, a mixed carbonate-clastic shelf sequence beneath the end-Cryogenian glacial horizon (Day et al., 2004). The submarine landslide responsible for the paleoscarp generated an enormous megabreccia, the Durkan Formation (Aitken 1991), carrying house-size blocks of Keele shelf lithologies. The landslide is thought to be unrelated to the subsequent glaciation (Aitken 1991), the retreat of which left a blanket (Stelfox Member) of non-stratified diamictite (marine till) and ice-rafted debris on both the hanging wall and footwall of the paleoscarp (Fig. III-1). Stelfox diamictite is overlain by a well-developed syn-deglacial "cap"

dolostone (Ravensthroat Formation) with giant wave ripples and corrugate stromatolites, overlain discontinuously by limestone (Hayhook Formation) with sea-floor cements (James et al, 2001). At Stelfox Mountain, the dolostone-limestone couplet tapers downslope because of slump-related truncation (Fig. III-1). The Ravensthroat Formation is widely assumed to be correlative with the Nuccaleena cap dolostone at the global stratotype section and point (GSSP) in South Australia, which defines the base of the Ediacaran Period (Knoll et al., 2006; Halverson 2006).

The basal Ediacaran cap-carbonate couplet is overlain everywhere by a thick black shale, the Sheepbed Formation, which grades into flaggy dark limestones of the overlying Gametrail Formation on Stelfox Mountain (Fig. III-1). The shale is associated with long-term flooding of the shelf after the end-Cryogenian ("Marinoan") glaciation. A stratigraphically and lithologically homologous section of Sheepbed Formation occurs at Shale Lake, 130 km to the northwest. Like Stelfox Mountain, the Shale Lake section is situated on the extreme edge of the Keele shelf (Dalrymple and Narbonne, 1996; Aitken 1989). The Gametrail at Shale Lake is a cliff-forming crystalline dolostone. We elected to measure and sample the Sheepbed Formation at two locations at Shale Lake. The first (64°31′40″N, 129°30′15″W) exposes the basal 60 m of the Sheepbed Formation above the Hayhook limestone; the second (64°30′15″N, 129°27′15″W) begins 33 m above the Hayhook and continues to the base of the Gametrail at a height of 559 m (Table III-1). Together, the two sections provide complete coverage of the Sheepbed Formation at Shale Lake (Fig. III-1). Although stratigraphic correlations within the Sheepbed Formation between Shale Lake and Sekwi Brook are unknown, the repeated occurrence of sandy contourites (Fig. III-1) at paleowater depths (1-1.5 km) estimated for the middle Sheepbed indicates that the continental slope was open to the world ocean in a gulf >100 km wide (Dalrymple and Narbonne, 1996). The uniform direction of contour-current flow (toward the northwest) implies a northern hemisphere location because a right-turning Coriolis force is "usually required to keep a current in contact with a right-hand margin (as viewed looking downcurrent)" (Dalrymple and Narbonne, 1996). In this situation, Ekman transport would have tended to push ocean waters onto the shelf. The shelf-edge section at Shale Lake should therefore reliably record the chemistry of the open ocean, with fewer problems related to faulting and submarine landsliding with the slope section at Sekwi Brook (Dalrymple and Narbonne, 1996).

III-2.2. South China

The fossiliferous Doushantuo Formation in south China accumulated slowly (3.45 m yr^{-6} average rate) from 635 Ma, the end of the Nantuo glaciation, until 551 Ma (Condon et al., 2005). In the shelf succession, the Doushantuo Formation consists mostly of flaggy carbonate and phosphorite overlain by the Dengying Formation, a cliff-forming sequence of carbonates that has yielded Ediacaran fossils (Sun 1986; Xiao et al., 2005). Putative bilaterian animal fossils and remarkable phosphatized embryos occur in Doushantuo shallow shelf phosphorite (Xiao et al., 1998; Li et al., 1998; Yuan and Hofmann 1998; Xiao et al., 2000; Xiao and Knoll, 2000; Chen et al., 2004).

In the Lantian area of Anhui Province, black shales of the Lantian Formation (Fig. III-2; Table III-2) are the deep-water basinal equivalents of the Doushantuo Formation (e.g., Zhu et al., 2007). The black shales overlie deposits of the Leigongwei glaciation, correlative with the Nantuo on the shelf, and underlie carbonates of the Piyuancun Formation that may be correlative to the Dengying Formation (Chen et al, 1994; Yan et al., 1992). Organic-rich black shales of the Lantian Formation were sampled from a basinal section where disseminated and small nodular pyrites are common throughout the whole succession (Fig. III-2). The section (Fig. III-2) is ≈136 m thick and may represent the thickest basinal succession in the region. It thus records a relatively complete history of deep-water ocean chemistry.

III-3. Results and Discussion

III-3.1. Fe Speciation and Oceanic Redox Chemistry

To reconstruct the redox chemistry of the Ediacaran oceans, various Fe species were measured including dithionite-extractable Fe (FeD), pyrite Fe (FeP), and total Fe (FeT). A paleo-redox proxy (FeHR/FeT), the ratio between highly reactive Fe (FeHR=FeD + FeP) and total Fe (FeT) has been developed to distinguish shales deposited under sulfidic bottom waters from those formed under oxygenated bottom waters. In modern marine sediments, the former have FeHR/FeT ratios typically exceeding 0.38 (Raiswell and Canfield 1998; Lyons and Severmann, 2006). In contrast, sediments deposited under oxic bottom waters have FeHR/FeT ratios of <0.38 (Raiswell and Canfield 1998; Lyons and Severmann, 2006). The Fe speciation criterion has been successfully tested in ancient (Mesozoic) fine-grained sediments where oxic bottom waters are independently indicated by the presence and diversity of oxygen-requiring benthic fauna, and by the disruption of

sedimentary layering (bioturbation) resulting from their feeding activities (Raiswell et al., 2001). Fe speciation analyses are most useful in Precambrian sediments deposited before animals had evolved (Canfield et al., 2007; Shen et al., 2002; Shen et al., 2003; Poulton et al, 2004). The elevated FeHR/FeT ratios of sediments deposited in anoxic basins may result from the formation of pyrite in sulfidic water columns in addition to that formed during diagenesis. The source of water-column Fe is probably either the reduction of Fe oxides in basin margin sediments impinged on by the anoxic water column or Fe oxide-containing particles falling through the water column (Raiswell and Canfield 1998; Lyons and Severmann, 2006; 5 Shen et al., 2002; Wijsman et al., 2001).

III-3.1.1. Fe Speciation in the Sheepbed Formation.

In the first 140 m of the Sheepbed Formation at Shale Lake, 56% (18 of 32) of the measured FeHR/FeT ratios are >0.38, with an average value of 0.43 (Fig. III-1, Table III-1). Above this level, no value exceeds 0.25 and the average (n=27) is only 0.11. This striking shift of FeHR/FeT ratio indicates prevalent bottom-water anoxia at <140 m and persistent oxic conditions at >160 m. There is no corresponding change in the physical conditions of sedimentation between 140 and 160 m at Shale Lake (Fig. III-1). The first 420 m consists of organic-rich black shale, broken only by silty turbidite beds at 83 and 129 m. The first evidence of bottom traction currents appears between 420 and 462 m, where calcareous concretions are localized on starved contour-current ripples with crestal azimuths of ≈70°. Only at >488 m does evidence of wave action appear, well above the shift in Fe speciation (Fig. III-1). We therefore regard the shift in FeHR/FeT ratio to reflect a secular change in the redox state of ocean deep waters, not in the depth of water. Although we found no benthic macrofossils in the section at Shale Lake, their first appearance in the middle Sheepbed Formation at Sekwi Brook (Narbonne and Aitken, 1995; Dalrymple and Narbonne, 1996), at a stratigraphic height of ≈500 m (Fig. III-1), strongly suggests that they postdate the shift in FeHR/FeT ratio, consistent with a vital requirement for persistently oxygenated bottom waters.

III-3.1.2. Fe Speciation in the Lantian Formation.

Organic-rich black shales of the Lantian Formation are dominated by FeHR/FeT values of >0.38 (Fig. III- 2, Table III-2), providing compelling evidence for sulfidic conditions in the deep basinal waters adjacent to the Doushantuo shelf on which the oldest known animal fossils are found (Yin et al., 2007). A few Lantian shales (n=9) have FeHR/FeT

ratios of <0.38 (Fig. III-2), similar to values that have been reported from the lower sulfidic Sheepbed Formation (Fig. III- 1) and modern as well as ancient sulfidic marine sediments (Raiswell and Canfield 1998; Shen et al., 2002, Shen et al., 2003). The low FeHR/FeT values could result from a decreased transfer of reactive Fe mobilized from shelf sediments or a high flux of terrigenous clastics that could overwhelm Fe scavenging in the anoxic water columns (Raiswell and Canfield 1998; Lyons and Severmann, 2006; Shen et al., 2002; Wijsman et al., 2001).

III-3.2. Redox Chemistry of the Ediacaran Oceans.

The middle and upper Sheepbed Formation at Sekwi Brook (Fig. III-1) is generally considered to be younger than ≈580 Ma (Bowring et al, 2003; Knoll et al., 2006), based on correlation with the radiometrically dated fossil assemblages on the Avalon Peninsula of eastern Newfoundland (Fig. III-3). We attempted to test this correlation with C-isotope data from the Gametrail Formation (Table SIII-4), a unit sparsely sampled in previous studies (Narbonne et al., 1994, Kaufman et al., 1997). In the dolomitized and top-truncated Gametrail section at Shale Lake, C-isotopic values hover close to 4‰ (Fig. III-1). This is most similar to the Khufai Formation (Nafun Group) in Oman (Fike et al., 2006; Burns and Matter 1993). Because uncertainty over the age of the overlying Shuram C-isotope anomaly, the Khufai Formation could be younger (Condon et al., 2005) or older (Fike et al., 2006; Le Guerroué et al., 2006) than 580 Ma. The Gametrail values are also similar (with less scatter) to the upper Hüttenberg Formation (Otavi Group) in Namibia (Halverson et al., 2005) and the lower-middle Doushantuo Formation in South China (Zhu et al., 2007; Zhou and Xiao, 2007), both of which are tentatively interpreted to predate 580 Ma. If the Gametrail Formation predates 580 Ma (Fig. III-3, column A), then the macrofossils in the middle Sheepbed Formation (Narbonne and Aitken, 1990) and the FeHR/FeT shift (Fig. III-1) must be older than their counterparts in eastern Newfoundland (Narbonne and Gehling, 2003; Canfield et al., 2007). Alternatively, if the Gametrail Formation is younger than 580 Ma (Knoll et al., 2006; Condon et al., 2005), the FeHR/FeT shift and benthic macrofossils in both areas might be correlative (Fig. III-3, column B). In this case, our Fe speciation data from the Doushantuo and Sheepbed formations provide evidence for global deep-water anoxia for ≈ 55 million years after the end-Cryogenian glacial termination in 635 Ma (Condon et al., 2005).

III-3 S-isotope and Oceanic Sulfate Concentration.

Sulfate concentrations inferred from S-isotopic records are an excellent tracer of atmospheric oxygen levels (*e.g.*, Hayes et al., 1992; Canfield 1998; Strauss, 2002; Shen and Li, 2004; Halverson and Hurtgen, 2007). To reconstruct their concentrations in late Neoproterozoic oceans, S-isotopic compositions of pyrites in sedimentary rocks of the Sheepbed and Lantian formations were measured. S-isotopic compositions of pyrite in the lower Sheepbed Formation range from -23.1 to +27.3‰ (see also Hayes *et al.*, 1992 with S-isotopic analyses ranging from -12.6 to +22.6‰) (Fig. III-1). Pyrites in the oxic sediments of the upper Sheepbed Formation show a similar wide range of $\delta^{34}S$ values from -22.5 to +44.8‰ (Fig. III-1). Likewise, pyrites in the Lantian black shales are characterized by $\delta^{34}S$ values from –21.9 to +20.9‰ (Fig III-2).

The S-isotopic data of pyrites from both the lower Sheepbed and Lantian formations show significant ^{34}S-depleted values relative to coeval seawater sulfate with a probable isotopic value of +30–35‰ (Goldberg et al., 2005) (Figs. III-1, III-2). These isotopic records are consistent with sulfidic depositional environments where pyrite formation in the water columns and sediments are often not limited by sulfate availability and are therefore ^{34}S-depleted. However, the S-isotopic data of pyrites from oxic upper Sheepbed Formation also show ^{34}S-depleted values comparable to those from the lower sulfidic sediments and the basinal Lantian Formation (Fig. III-1, III-2). The same pattern is seen when we compare S-isotopic data from the sulfidic Lantian Formation in China ranging from -21.9 to +20.9‰ and the correlative Pertatataka Formation deposited under oxic normal marine conditions in Australia with $\delta^{34}S$ values from -22.0 to +34.1‰ (Gorjan et al., 2000). Thus, intra- and interbasinal correlations suggest that the late Ediacaran S-isotopic records of pyrites are not sensitive to changes in water-column redox chemistry.

S-isotopic patterns of pyrites that are independent of water-column redox chemistry have been observed from numerous Phanerozoic anoxic marine basins, arguably as a result of high oceanic sulfate concentrations in an oxygen-rich Phanerozoic world (Hayes et al., 1992, Logan et al., 1995). Under sulfate-rich conditions, most diagenetic pyrites in oxic sediments are formed near the redox boundary within the sediments where sulfate depletions are minimal. Therefore, $\delta^{34}S$ value of seawater sulfate is inherited in near-surface pore waters, producing a wide range of ^{34}S-depleted isotopic values as observed in many Phanerozoic rocks (*e.g.*, Logan et al., 1995).

Pyrites in the oxic upper Sheepbed Formation exhibit comparable ^{34}S-depleted isotopic values (down to -22.5‰) to those in the sulfidic Lantian and lower Sheepbed formations (down to -23.1‰) (Figs. III-1, III-2). A few pyrites (n=4) in the oxic upper Sheepbed with exceptionally positive values of heavier than seawater sulfate (+30-35‰) could have resulted from rare sulfate depletion in the sediments and/or methane-driven sulfate reduction (Jørgensen et al., 2004). Regardless, the Sheepbed and Lantian formations display Phanerozoic-type S-isotopic fractionations. Therefore, they provide strong evidence for sulfate-rich conditions in the Ediacaran oceans and, by implication, elevated atmospheric oxygen. However, the early Ediacaran ocean was sulfidic, evidenced by our Fe speciation data, suggesting that sulfate concentrations had not yet reached the levels of modern oceans (≈28 mM) and that atmospheric oxygen was below present levels.

III-4. Conclusions

Low oceanic sulfate concentrations during the Proterozoic have been documented by S-isotopic records of pyrite (Shen et al., 2002, 2003; Poulton et al., 2004; Hayes et al., 1992; Canfield 1998), trace sulfate (Kah et al., 2004, Gellatly and Lyons, 2005 Hurtgen et al, 2005, 2006), calculations of the Proterozoic hydrothermal fluid compositions (Kump and Seyfried 2005), and measurements of multiple S-isotopes on trace sulfate in Proterozoic carbonate (Johnston et al., 2005). The low sulfate concentrations persisted until the end-Cryogenian (635 Ma) snowball glaciation (Gorjan et al., 2000, Hurtgen et al., 2003). The S-isotopic records from the Lantian and Sheepbed formations indicate a rise in sulfate and therefore atmospheric oxygen concentrations to levels intermediate between the earlier Proterozoic and the present day. This is consistent with the findings of Halverson and Hurtgen (2007) and with the metabolic and collagen-synthesis requirements of eumetazoa in oxic surface waters of the Doushantuo shelf. Early Ediacaran oxygen levels were insufficient, however, to oxidize the deep oceans. Deep-sea ventilation, recorded by the shift in FeHR/FeT ratios in Newfoundland (Canfield et al., 2007) and western Canada (Fig. III-1), occurred later, ≈580 Ma in Newfoundland, allowing large organisms to flourish for the first time on the deep seafloor.

Acknowledgments.

We thank Boswell Wing and Shuhai Xiao for constructive comments and Robert Dalrymple for discussions on the Sheepbed sedimentology. This work was supported by

Canada Research Chairs Program, NSERC, and in part by the NASA Astrobiology Institute (Y.S.). Fieldwork in Canada was supported by NSF Grant EAR-9905495 (to P.F.H.). P.F.H. was also supported by the Canadian Institute for Advanced Research and from Harvard University. The Gametrail C-isotopes were measured by Francis A. Macdonald and Greg Eischeid from micro-drilled samples in the Harvard University Laboratory for Geochemical Oceanography according to methods described in Halverson *et al.* (2005).

References

Aitken JD, 1989. Uppermost Proterozoic formations in central Mackenzie Mountains, Northwest Territories. *Geol Surv Can Bull* 368:1-26.

Aitken JD, 1991. The Ice Brook Formation and post-Rapitan, Late Proterozoic glaciation, Mackenzie Mountains, Northwest Territories. *Geol Surv Can Bull* 404:1-43.

Berkner LV, Marshall J, 1965. On origin and rise of oxygen concentration in Earth's atmosphere. *J Atmos Sci* 22:225-261.

Bottjer DJ, Clapham ME, 2006. in: *Neoproterozoic Geobiology and Paleobiology,* eds Xiao S, Kaufman AJ (Springer, Dordrecht, Netherlands), pp 91-114.

Bowring SA, Myrow P, Landing E, Ramenzani J, 2003. Geochronological constraints on terminal Neoproterozoic events and the rise of Metazoans. *NASA Astrobiol Inst (NAI Gen Mtg Abstr)*:113-114.

Butterfield NJ, 2000. *Bangiomorpha pubescens* n. gen., n. sp.: implications for the evolution of sex, multicellularity, and the Mesoproterozoic/Neoproterozoic radiation of eukaryotes. *Paleobiology* 26:386-404.

Burns SJ, Matter A, 1993. Carbon isotopic record of the latest Proterozoic from Oman. *Eclogae Geol Helv* 86:595-607.

Canfield DE, 1998. A new model for Proterozoic ocean chemistry. *Nature* 396:450-453.

Canfield DE, Poulton SW, Narbonne GM, 2007. Late-Neoproterozoic deep-ocean oxygenation and the rise of animal life. *Science* 315:92-95.

Chen M, Lu G, Xiao Z, 1994. Preliminary study on the algal macrofossils -- Lantian Flora from the Lantian Formation of Upper Sinian in southern Anhui. *Bull Inst of Geology, Academia Sinica* 7: 252-267.

Chen JY, *et al.*, 2004. Small bilaterian fossils from 40 to 55 million years before the Cambrian. *Science* 305:218-222.

Cloud P, 1972. Working model of primitive Earth. *Am J Sci* 272:537-548.

Condon D, *et al.*, 2005. U-Pb ages from the Neoproterozoic Doushantuo Formation, China. *Science* 308:95-98.

Dalrymple RW, Narbonne GM 1996. Continental slope sedimentation in the Sheepbed Formation (Neoproterozoic, Windermere Supergroup), Mackenzie Mountains, N.W.T. *Can J Earth Sci* 33:848-862.

Day ES, James NP, Narbonne GM, Dalrymple RW, 2004. A sedimentary prelude to marinoan glaciation, Cryogenian (Middle Neoproterozoic) Keele Formation, Mackenzie Mountains, northwestern Canada. *Precambrian Res* 133:223-247.

Fedonkin MA, Waggoner BM. 1997. The Late Precambrian fossil *Kimberella* is a mollusc-like bilaterian organism. *Nature* 388:868-871.

Fedonkin MA, 2003. The origin of the Metazoa in the light of the Proterozoic fossil record. *Paleont Res* 7:9-41.

Fike DA, Grotzinger JP, Pratt LM, Summons RE, 2006. Oxidation of the Ediacaran Ocean. *Nature* 444:744-747.

Gehling JG, Rigby KJ, 1996.Long expected sponges from the Neoproterozoic Ediacara fauna of South Australia. *J Paleont* 70:185-195.

Gellatly AM, Lyons TW, 2005. Trace sulfate in mid-Proterozoic carbonates and the sulfur isotope record of biospheric evolution. *Geochim Cosmochim Acta* 69:3813-3829

Goldberg T, Poulton SW, Strauss H, 2005. Sulphur and oxygen isotope signatures of late Neoproterozoic to early Cambrian sulphate, Yangtze Platform, China: Diagenetic constraints and seawater evolution. *Precambrian Res.* 137:223–241

Gorjan P, Veevers JJ, Walter MR, 2000. Neoproterozoic sulfur-isotope variation in Australia and global implications. *Precambrian Res* 100:151-179.

Graham JB, 1988. Ecological and evolutionary aspects of integumentary respiration: Body size, diffusion, and the Invertebrata. *Am Zool* 28:1031-1045.

Halverson GP, Hoffman PF, Schrag DP, Maloof AC, Rice AHN, 2005. Toward a Neoproterozoic composite carbon-isotope record. *Geol Soc Am Bull* 117:1181-1207.

Halverson, GP, 2006. in *Neoproterozoic Geobiology and Paleobiology,* eds Xiao S, Kaufman, AJ (Springer, Dordrecht, Netherlands), pp 231-271.

Halverson GP, Hurtgen MT, 2007. Ediacaran growth of the marine sulfate reservoir. *Earth Planet Sci Lett* 263:32-44.

Harland WB, Rudwick MJS, 1964. The great infra-Cambrian ice age. *Sci Am* 211:28-36.

Hayes JM, Lambert IB, Strauss H, 1992. in *The Proterozoic Biosphere: A Multidisciplinary Study,* eds Schopf JW, Klein C (Cambridge University Press, Cambridge), pp 129-132.

Hofmann HJ, Narbonne GM, Aitken JD, 1990. Ediacaran remains from intertillite beds in Northwestern Canada. *Geology* 18:1199-1202.

Hoffman PF, Schrag DP, 2002. The snowball Earth hypothesis: testing the limits of global change. *Terra Nova* 14:129-155.

Hurtgen MT, Arthur MA, Suits NS, Kaufman AJ, 2003. The sulfur isotopic composition of Neoproterozoic seawater sulfate: implications for a snowball Earth? *Earth Planet Sci Lett* 203:413-429.

Hurtgen MT, Arthur MA, Halverson GP, 2005. Neoproterozoic sulfur isotopes, the evolution of microbial sulfur species, and the burial efficiency of sulfide as sedimentary pyrite. *Geology* 33:41-44.

Hurtgen MT, Halverson GP, Arthur MA, Hoffman PF, 2006. Sulfur cycling in the aftermath of a 635-Ma snowball glaciation: Evidence for a syn-glacial sulfidic deep ocean. *Earth Planet Sci Lett* 245:551-570.

James NP, Narbonne GM, Kyser TK, 2001. Late Neoproterozoic cap carbonates: Mackenzie Mountains, northwestern Canada: precipitation and global glacial meltdown. *Can J Earth Sci* 38:1229-1262.

Johnston DT, *et al.*, 2005. Active microbial sulfur disproportionation in the Mesoproterozoic. *Science* 310:1477-1479.

Jørgensen BB, Böttcher ME, Lüschen H, Neretin LN, Volkov II, 2004. Anaerobic methane oxidation and a deep H_2S sink generate isotopically heavy sulfides in Black Sea sediments. *Geochim Cosmochim Acta* 68:2095-2118

Kah LC, Lyons TW, Frank TD, 2004. Low marine sulphate and protracted oxygenation of the Proterozoic biosphere. *Nature* 431:834-838.

Kaufman AJ, Knoll AH, Narbonne GM, 1997. Isotopes, ice ages, and terminal Proterozoic earth history. *Proc Natl Acad Sci USA* 94:6600-6605.

Knoll AH, Hayes JM, Kaufman AJ, Swett K, Lambert IB, 1986. Secular variation in carbon isotope ratios from Upper Proterozoic successions of Svalbard and East Greenland. *Nature* 321:832-838.

Knoll AH, Caroll SB, 1999. The early evolution of animals: emerging views from comparative biology and geology. *Science* 284:2129-2137.

Knoll AH, Walter MR, Narbonne GM, Christie-Blick N, 2006. The Ediacaran Period: a new addition to the geologic time scale. *Lethaia* 39:13-30.

Kump LR, Seyfried WE, 2005. Hydrothermal Fe fluxes during the Precambrian: effect of low oceanic sulfate concentrations and low hydrostatic pressure on the composition of black smokers. *Earth Planet Sci Lett* 235:654-662.

Le Guerroué E, Allen PA, Cozzi A, Etienne JL, Fanning M, 2006. 50 Myr recovery from the largest negative $\delta^{13}C$ excursion in the Ediacaran ocean. *Terra Nova* 18:147-153.

Li C, Chen JY, Hua T, 1998. Precambrian sponges with cellular structures. *Science* 279:879-882.

Logan GA, Hayes JM, Hieshima GB, Summons R, 1995. Terminal Proterozoic reorganization of biogeochemical cycles. *Nature* 376:53-56.

Love GD, *et al.*, 2006. Constraining the timing of basal metazoan radiation using molecular biomarkers and U-Pb isotope dating. *Geochim Cosmochim Acta (Goldschmidt Conf Abstr Suppl)* 70:A371.

Lyons TW, Severmann S, 2006. A critical look at iron paleoredox proxies based on new insights from modern euxinic marine basins. *Geochim Cosmochim Acta* 70:5698-5722.

Narbonne GM, Aitken JD, 1990. Ediacaran fossils from the Sekwi Brook area, Mackenzie Mountains, Northwestern Canada. *Palaeontology* 33:945-980.

Narbonne GM, 1994. New Ediacaran fossils from the MacKenzie Mountains, Northwestern Canada. *J Paleont* 68:411-416.

Narbonne GM, Kaufman AJ, Knoll AH, 1994. Integrated chemostratigraphy and biostratigraphy of the Windermere Supergroup, Northwestern Canada – Implications for Neoproterozoic correlations and the early evolution of animals. *Geol Soc Am Bull* 106:1281-1292.

Narbonne GM, Aitken JD, 1995. Neoproterozoic of the Mackenzie Mountains, northwestern Canada. *Precambrian Res* 73:101-121.

Narbonne GM, Gehling JG, 2003. Life after snowball: The oldest complex Ediacaran fossils. *Geology* 31:27-30.

Narbonne GM, 2005. The Ediacara biota: Neoproterozoic origin of animals and their ecosystems. *Annu Rev Earth Planet Sci* 33:421-442.

Nursall JR, 1959. Oxygen as a prerequisite to the origin of the Metazoa. *Nature* 183:1170-1172.

Poulton SW, Fralick PW, Canfield DE, 2004. The transition to a sulfidic ocean ~1.84 billion years ago. *Nature* 431:173-177.

Raiswell R, Canfield DE, 1998. Sources of iron for pyrite formation in marine sediments. *Am J Sci* 298:219-245.

Raiswell R, Newton R, Wignall PB, 2001. An indicator of water-column anoxia: Resolution of biofacies variations in the Kimmeridge Clay (Upper Jurassic, UK). *J Sediment Res* 71:286-294.

Runnegar B, 1982. Oxygen requirements, biology and phylogenetic significance of the late Precambrian worm Dickinsonia, and the evolution of the burrowing habit. *Alcheringa* 6:223-239.

Shen Y, Canfield DE, Knoll AH, 2002. Middle Proterozoic ocean chemistry: Evidence from the McArthur Basin, northern Australia. *Am J Sci* 302:81-109.

Shen Y, Knoll AH, Walter MR, 2003. Evidence for low sulphate and anoxia in a mid Proterozoic marine basin. *Nature* 423:632-635.

Shen Y, Buick R, 2004. The antiquity of microbial sulfate reduction *Earth-Sci Rev* 64:243-272.

Strauss H, 2002. in *Precambrian Sedimentary Environments: A Modern Approach to Ancient Depositional Systems,* eds Altermann W, Corcoran PL (Blackwell Science, Oxford), pp 67-105.

Sun WG, 1986. Late Precambrian pennatulids (sea pens) from the eastern Yangtze Gorge, China: *Paracharnia* gen. nov. *Precambrian Res* 31:361-375.

Towe KM, 1970. Oxygen-collagen priority and early metazoan fossil record. *Proc Natl Acad Sci USA* 65:781-788.

Wijsman JWM, Middleburg JJ, Herman PMJ, Böttcher ME, Heip CHR, 2001. Sulfur and iron speciation in surface sediments along the northwestern margin of the Black Sea. *Marine Chem* 74:261-278.

Wood DA, Dalrymple RW, Narbonne GM, Gehling JG, Clapham ME, 2003. Paleoenvironmental analysis of the late Neoproterozoic Mistaken Point and Trepassey formations, southeastern Newfoundland. *Can J Earth Sci* 40:1375-1391.

Xiao S, Zhang Y, Knoll AH, 1998. Three-dimensional preservation of algae and animal embryos in a Neoproterozoic phosphorite. *Nature* 391:553-558.

Xiao S, Yuan X, Knoll AH, 2000. Eumetazoan fossils in terminal Proterozoic phosphorites? *Proc Natl Acad Sci USA* 97:13684-13689.

Xiao S, Knoll AH, 2000. Phosphatized animal embryos from the Neoproterozoic Doushantuo Formation at Weng'An, Guizhou, South China. *J Paleont* 74:767-788.

Xiao S, Shen B, Zhou C, Yuan X, 2005. A uniquely preserved Ediacaran fossil with direct evidence for a quilted bodyplan. *Proc Natl Acad Sci USA* 102:10227-10232.

Yan Y, Jiang C, Zhang S, Du S, Bi Z, 1992. Research of the Sinian System in the region of western Zhejiang, northern Jiangxi, and southern Anhui provinces. *Bull of the Nanjing Inst of Geol and Mineral Resources, Chinese Acad. Geol Sci* 12:1-105.

Yin L, *et al.*, 2007. Doushantuo embryos preserved inside diapause egg cysts. *Nature* 446:661-663.

Yuan X, Hofmann HJ, 1998. New microfossils from the Neoproterozoic (Sinian) Doushantuo Formation, Wengan, Guizhou Province, southwestern China. *Alcheringa* 22:189-222.

Zhou C, Xiao S, 2007. Ediacaran $\delta^{13}C$ chemostratigraphy of South China. *Chem Geol* 237:89-108.

Zhu M, Zhang J, Yang A, 2007. Integrated Ediacaran (Sinian) chronostratigraphy of South China. *Palaeogeogr Palaeoclimatol Palaeoecol* 254:7-61.

Figure captions:

Fig. III-1. Fe speciation and S-isotopic data from the Sheepbed Formation and C-isotope data from the Gametrail Formation in the Shale Lake section, Northwest Territories, Canada. Correlative sections at Stelfox Mountain (Aitken 1991) and Sekwi Brook (Dalrymple and Naronne, 1996) are shown for reference. Note the shift in FeHR/FeT ratio between 138 and 160 m at Shale Lake. The dashed line separates anoxic deep water at >0.38 from oxic deep water at <0.38 (Raiswell and Canfield, 1998). Fe speciation data of filled circles were measured by using the method in (Raiswell and Canfield, 1998) and the data of open circles were measured by using the method in (Poulton et al., 2004).

Fig. III-2. Fe speciation and S-isotopic data from the Lantian Formation, South China. The radiometric age (Condon et al., 2005) and early animal fossils occur in the correlative Doushantuo and Dengying formations in the oxic shelf succession. Fe speciation data of filled circles were measured by using the method in (Raiswell and Canfield, 1998) and the data of open circles were measured by using the method in (Poulton et al., 2004).

Fig. III-3. Correlation chart for Ediacaran strata in the Mackenzie Mountains (northwestern Canada), Avalon Peninsula (eastern Newfoundland) and Yangtze platform (South China), showing U-Pb zircon age control, early animal fossils, and changes in FeHR/FeT ratios (sources cited in the text). Alternative correlations (discussed in the text) for the Mackenzie Mountains assume the Gametrail Formation is older (A) or younger (B) than the Gaskiers glaciation in Newfoundland.

TABLE CAPTIONS:

Table III-1. FeHR/FeT and $\delta^{34}S_{py}$ in Sheepbed Formation, at Section 1(64°34′40"N, 129°30′15"W) and Section 2 (64°30′15"N, 129°27′15"W) (datum base of Sheepbed Fm) Shale Lake, Northwest Canada.

Table III-2 FeHR/FeT and $\delta^{34}S_{py}$ in Lantian Formation, Anhui Province in South China (datum base of Lantian Fm)

Table III-3 Carbon isotope in Gametrail Formation, Shale Lake, NWT (datum base of Gametrail Fm)

Table III-1. FeHR/FeT and $\delta^{34}S_{py}$ in Sheepbed Formation, Shale Lake, NWT, at section 1 and section 2 (datum base of Sheepbed Fm)

Section 1 (64°34'40"N, 129°30'15"W)			Section 2 (64°30'15"N, 129°27'15"W)		
H (m)	FeHR/FeT	$\delta^{34}S$ (‰)	H (m)	FeHR/FeT	$\delta^{34}S$ (‰)
60	0.59	-12.7	520	0.19	2.8
57	0.20	9.4	511	0.15	34.8
54	0.60	-14.4	476	0.1	17.8
50	0.21	13.9	456	0.08	7.1
47	0.41	10.4	446	0.25	20.8
44.5	0.50	17.3	417	0.19	-22.5
43	0.37	17.7	373	0.2	15.1
39	0.29	-23.1	362	0.04	2.8
37.5	0.65	19.8	345	0.12	-15.9
35.5	0.41	-18.3	340	0.17	9.0
33	0.64	10.1	331	0.19	21.2
29	0.63	11.6	322	0.02	23.5
27	0.26	5.1	313	0.03	-3.1
23	0.56	10.8	307	0.13	-11.9
18	0.37	2.9	304	0.04	28.1
16	0.45	-16.5	292	0.05	44.8
14	0.70	0.6	276	0.03	-4.9
12	0.39	-4.3	266	0.15	-0.8
10	0.54	-2.7	244	0.07	-12.5
8	0.78	-2.3	226	0.04	6.7
7	0.31	-1.5	209	0.17	-20.0
5.5	0.32	0.8	200	0.07	5.7
5	0.40	0.1	195	0.07	
4	0.45	-0.6	192	0.15	-2.1
			186	0.08	34.7
			171	0.12	8.4
			157	0.12	25.9
			138	0.42	27.3
			118	0.45	22.5
			90	0.16	25.4
			74	0.41	8.2
			57.5	0.25	19.3
			39	0.45	20.6
			35.5	0.3	-7.8
			34	0.32	-19.9

Table III-2 FeHR/FeT and $\delta^{34}S_{py}$ in Lantian Formation, Anhui Province (datum base of Lantian Fm)

H (m)	FeHR/FeT	$\delta^{34}S$ (‰)
136.2	0.41	-5.6
133.8	0.43	3.7
127.4	0.41	-1.8
124.5	0.27	-2.9
121	0.19	8.0
118	0.67	1.0
114	0.22	-21.9
112	0.7	1.0
108	0.51	-9.5
105	0.45	-11.3
98	0.21	11.4
95	0.56	-4.4
92	0.21	11.0
90	0.25	-2.0
87.8	0.51	13.6
85.3	0.51	-5.1
81	0.77	6.4
77.3	0.76	-1.1
73.3	0.51	-12.7
70	0.78	-3.8
66.7	0.2	-1.5
63.5	0.56	9.2
58.5	0.46	14.0
53.5	0.42	12.6
50	0.21	7.5
45.7	0.78	3.6
40.9	0.63	6.8
25	0.64	-6.3
20	0.82	-4.0
17	0.75	-18.3
12.6	0.56	-19.6
10	0.38	-1.5
5.4	0.45	-2.5
0	0.24	20.9

Table III-3 Carbon isotope in Gametrail Formation, Shale Lake, NWT (datum base of Gametrail Fm)

H (m)	$\delta^{13}C$(‰)	$\delta^{18}O$(‰)
100	4.46	-3.78
96	4.23	-4.03
93	4.08	-3.93
90	3.76	-4.48
87	3.53	-6.09
85	3.12	-4.48
81	3.07	-5.24
77	4.12	-3.96
75	4.08	-4.41
71	3.97	-5.19
68	4.02	-4.09
64	3.37	-4.66
60	3.37	-3.67
56	3.87	-5.57
53	3.42	-6.38
50	3.99	-4.84
45	3.24	-5.66
42	3.24	-4.22
41	4.27	-4.09
38	3.42	-6.14
35	4.35	-4.84
32	3.83	-5.35
29	4.07	-4.66
26	4.24	-5.12
25	3.73	-4.92
20	3.79	-4.14
17	4.33	-6.67
14	3.66	-6.22
11	3.56	-6.74
8	3.46	-6.69
5	4.40	-6.57
2	3.91	-6.61
0.5	3.62	-4.79

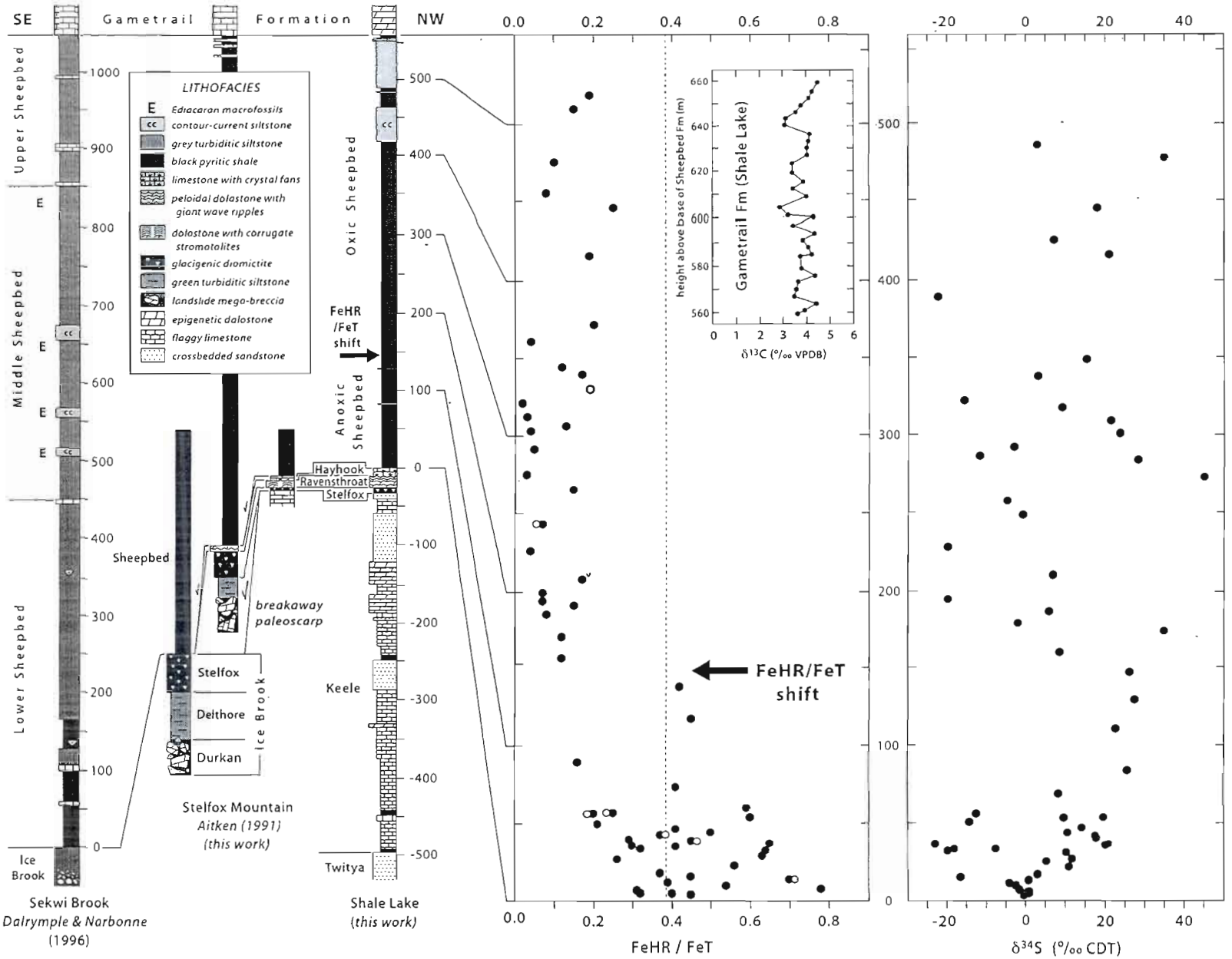
SE
Gametrail
Formation
NW
LITHOFACIES
Ediacaran macrofossils
contour-current siltstone
grey turbiditic siltstone
black pyritic shale
limestone with crystal fans
peloidal dolastone with giant wave ripples
dolostone with corrugate stromatolites
glacigenic diomictite
green turbiditic siltstone
landslide mega-breccia
epigenetic dalostone
flaggy limestone
crossbedded sandstone
Upper Sheepbed
Middle Sheepbed
Lower Sheepbed
Oxic Sheepbed
Anoxic Sheepbed
FeHR /FeT shift
Hayhook
Ravensthroat
Stelfox
Sheepbed
breakaway paleoscarp
Stelfox
Delthore
Durkan
Ice Brook
Keele
Twitya
Ice Brook
Sekwi Brook
Dalrymple & Narbonne (1996)
Stelfox Mountain
Aitken (1991)
(this work)
Shale Lake
(this work)
height above base of Sheepbed Fm (m)
Gametrail Fm (Shale Lake)
δ13C (‰ VPDB)
FeHR/FeT shift
FeHR / FeT
δ34S (‰ CDT)

Fig. III-1

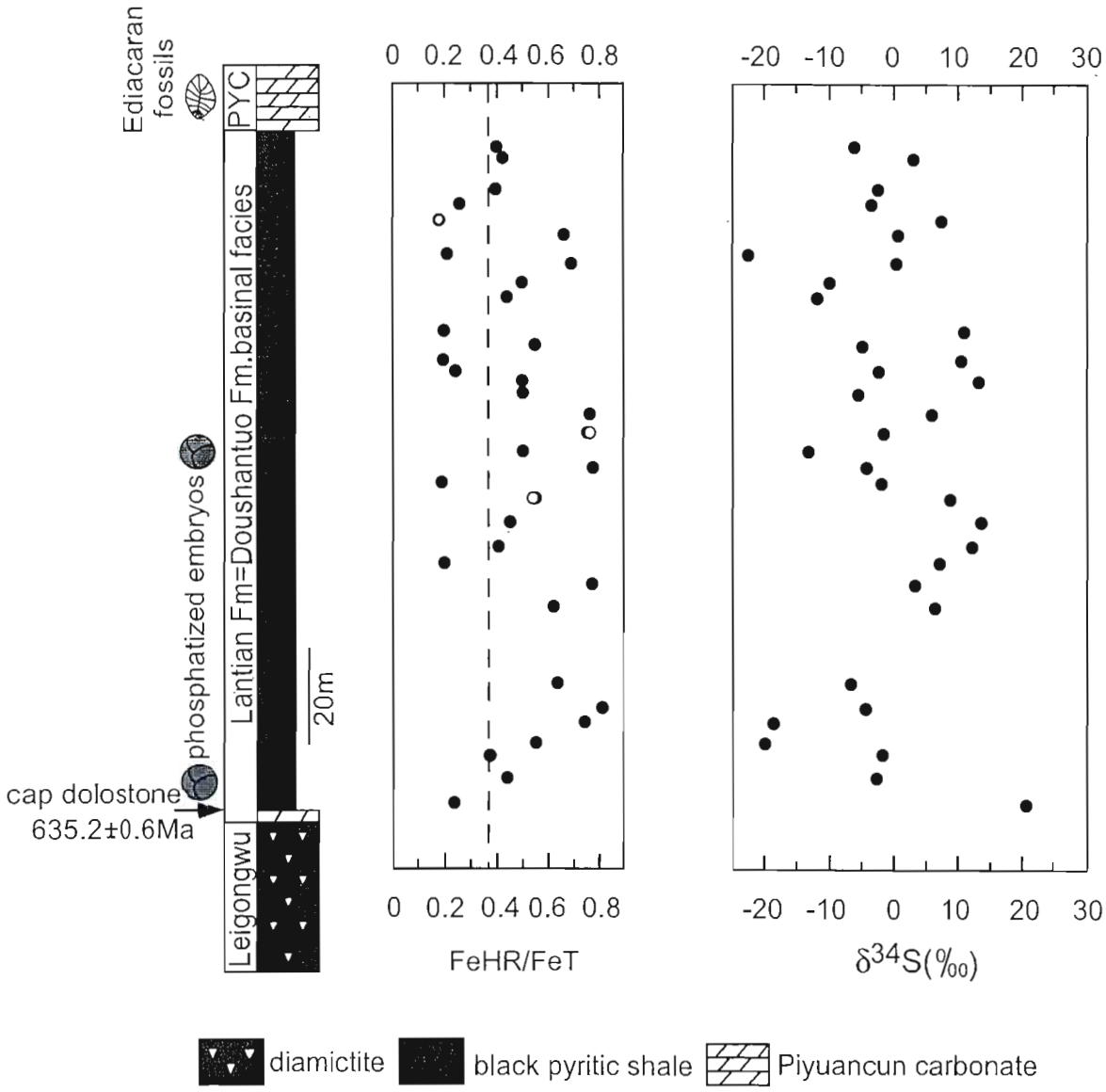
Ediacaran fossils
PYC
Lantian Fm=Doushantuo Fm.basinal facies
phosphatized embryos
20m
cap dolostone
635.2±0.6Ma
Leigongwu
0 0.2 0.4 0.6 0.8
FeHR/FeT
-20 -10 0 10 20 30
δ34S(‰)
diamictite
black pyritic shale
Piyuancun carbonate

Fig. III-2

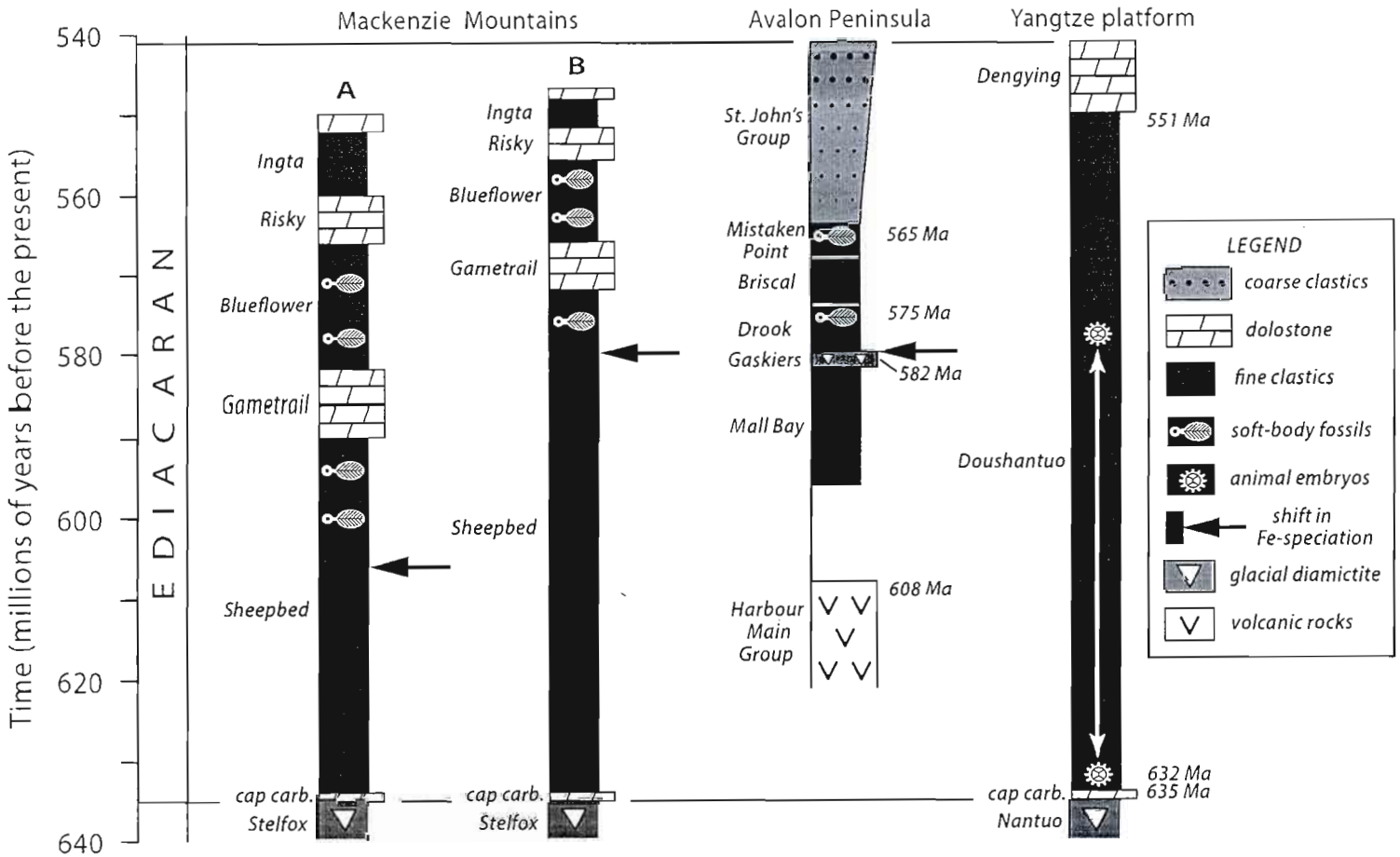
Mackenzie Mountains
Avalon Peninsula
Yangtze platform
Time (millions of years before the present)
540
560
580
600
620
640
EDIACARAN
A
B
Ingta
Risky
Blueflower
Gametrail
Sheepbed
cap carb.
Stelfox
St. John's Group
Mistaken Point
Briscal
Drook
Gaskiers
Mall Bay
Harbour Main Group
565 Ma
575 Ma
582 Ma
608 Ma
Dengying
Doushantuo
Nantuo
551 Ma
632 Ma
635 Ma
LEGEND
coarse clastics
dolostone
fine clastics
soft-body fossils
animal embryos
shift in Fe-speciation
glacial diamictite
volcanic rocks

Fig. III-3

CHAPTER IV

Association of ^{34}S-depleted pyrite layers with negative carbonate $\delta^{13}C$ excursions at the Permian-Triassic boundary: Evidence for upwelling of sulfidic deep-ocean water masses

Thomas Algeo, Yanan Shen, Tonggang Zhang, Timothy Lyons, Steven Bates, Harry Rowe, T. K. T. Nguyen

Published in *Geochem. Geophys. Geosyst.* (2008), vol. 9, Q04025, doi:10.1029/2007GC001823.

Abstract

A marine Permian-Triassic boundary (PTB) section at Nhi Tao, Vietnam, contains a series of at least 9 pyritic horizons characterized by concurrent decreases in pyrite S- ($\delta^{34}S_{py}$) and carbonate C-isotopic compositions ($\delta^{13}C_{carb}$). The first and largest of the events that precipitated these pyritic horizons was coincident with the Late Permian mass extinction, while subsequent events were generally smaller and occurred at quasiperiodic intervals of ~20 to 30 ka. A near complete lack of organic carbon to drive bacterial sulfate reduction in sediment pore waters, among other considerations, argues against a diagenetic control for these relationships. Rather, the covariant patterns documented herein are most easily explained as the product of recurrent upwelling of anoxic deep-ocean waters containing ^{34}S-depleted hydrogen sulfide and ^{13}C-depleted dissolved inorganic carbon. The sulfide $\delta^{34}S$ record of the study section represents a mixture of a small amount of isotopically heavy authigenic pyrite (formed via in situ bacterial sulfate reduction) with a generally larger quantity of isotopically light syngenetic pyrite precipitated within the water column during upwelling episodes. Although upwelling of toxic deepwaters has been invoked in earlier studies as a mechanism for the Late Permian marine mass extinction, this is the first study to (1) document patterns of pyrite-$\delta^{13}C_{carb}$ covariation that strongly support upwelling as a major process at the PTB and (2) provide evidence of multiple, quasiperiodic upwelling events that may reflect reinvigoration of global-ocean overturn following a prolonged interval of Late Permian deep-ocean stagnation.

Keywords: P-Tr boundary; S isotopes; carbonate C isotopes; anoxia; extinction.

IV-1. Introduction

The ~252-million-year-old (Bowring et al.,1998; Mundil et al., 2004) Permian-Triassic boundary (PTB) is associated with the single largest mass extinction event in Earth history, during which ~90% of marine and ~70% of terrestrial taxa disappeared (Erwin, 1994; Retallack, 1995). The C-isotope chemostratigraphy of the PTB has been the subject of scores of published studies, most of which document a -3 to -8‰ shift commencing at the Late Permian extinction/event horizon (LPEH), a feature present not only in marine $\delta^{13}C_{carb}$ but also in marine and terrestrial $\delta^{13}C_{org}$ records (e.g., Baud et al., 1989; Krull and Retallack, 2000; Twitchett et al., 2001; de Wit et al., 2002; Sephton et al., 2002; Krull et al., 2004; Payne et al., 2004; Korte et al., 2004, 2008). This shift reflects a major perturbation to the global carbon cycle that has been variously attributed to biomass destruction, reduced organic carbon burial, oxidation of methane from seafloor clathrates or coal or of organic matter from soils, and volcanic CO_2 emissions (see Berner (2002) and Erwin et al. (2002) for reviews). Because the carbon cycle is subject to so many possible influences, C-isotope data alone do not allow for a unique interpretation of causation.

The existence of deep-ocean anoxia during the Late Permian and Early Triassic is now well established (Wignall and Twitchett, 1996, 2002; Isozaki, 1997; Hotinski et al., 2001; Kiehl and Shields, 2005), and S-isotope studies have provided insights regarding contemporaneous changes in seawater chemistry. Carbonate-associated-sulfate (CAS) $\delta^{34}S$ records from shallow-marine sections document a rapid negative excursion (-10 to -20‰) at the LPEH, followed by a larger positive shift (+20 to +40‰) during the first ~1 Ma of the Early Triassic (Kaiho et al., 2001, 2006; Newton et al., 2004; Riccardi et al., 2006), a pattern of longer-term variation also suggested by pyrite $\delta^{34}S$ records (Kajiwara et al., 1994; Nielsen and Shen, 2004; Riccardi et al., 2006). These records have been interpreted to reflect strong bacterial sulfate reduction (BSR) in the Late Permian deep ocean, with upwelling and partial oxidation of sulfide in shallow-marine environments at the PTB, and subsequent massive burial of pyrite driving seawater sulfate toward more ^{34}S-enriched values during the Early Triassic. These inferences are consistent with independent evidence of transiently anoxic conditions in shallow-marine environments at the PTB based on biomarker and Ce anomaly data (Grice et al., 2005; Xie et al., 2005; Kakuwa and Matsumoto, 2006; Hays et al., 2007; Son et al., 2007).

Paired C- and S-isotopic records have been published for only a few PTB sections to date, and relationships between these records have received only scant attention. The Italian Dolomites section studied by Newton et al. (2004) exhibits negative $\delta^{13}C_{carb}$-$\delta^{34}S_{py}$ covariation through the Upper Permian but positive covariation within the Lower Triassic, although the rather coarse sample spacing (~0.5 to 10 m) within the latter interval makes such inferences tenuous. The Chinese sections at Meishan and Shangsi studied by Riccardi et al. (2006, 2007) do not appear to exhibit any C- and S-isotopic covariation, although the possibility of such covariation was not specifically considered. In the present study of the PTB at Nhi Tao, Vietnam, we demonstrate significant positive covariation of pyritic horizons (as proxied by $[S]_{py}$ and $\delta^{34}S_{py}$) with carbonate $\delta^{13}C$ at a fine (10–20 cm) stratigraphic scale, and we consider the implications of these relationships for understanding causation of the PTB. The Nhi Tao PTB section was examined previously by Algeo et al. (2007) and, independently, by Son et al. (2007). In the present contribution, we report results of S-isotopic analyses that were generated subsequent to our earlier paper.

IV-2. Geologic Background

The PTB interval at Nhi Tao, Vietnam, comprises shallow-marine facies of the Jinxi Platform, one of several large (>50 km wide) carbonate platforms within the Nanpanjiang Basin on the southern margin of the south China craton (Figure IV-1) (Lehrmann et al., 2003; Payne et al., 2004). During the Late Permian and Early Triassic, the south China craton was located at tropical latitudes in the eastern half of the Paleotethys Ocean. The study site proved advantageous for an analysis of hydrogenous (seawater-derived) chemostratigraphic signals associated with the PTB owing to its paleogeographic location on an open shelf margin subject to influence by deep water masses and to its relative isolation from terrigenous siliciclastic influx.

The 7.5-m-thick study section ranges from the upper *changxingensis* zone (late Upper Permian) to the lower *isarcica* zone (early Lower Triassic; Figure IV-2a). The gradualness of stratigraphic variation in $\delta^{13}C_{carb}$ and magnetic susceptibility (MS) at Nhi Tao suggests that the section does not contain major hiati and that the PTB interval is stratigraphically complete (Algeo et al., 2007). The position of the PTB has been constrained on the basis of foraminiferal biostratigraphy and correlation of $\delta^{13}C_{carb}$ and MS records with

the Global Stratotype Section at Meishan, Zhejiang Province, China (Algeo et al., 2007; Son et al., 2007). The Late Permian extinction horizon (LPEH) is located ~45 cm below the PTB, at the base of a 12-cm-thick oolitic-pisolitic grainstone event bed. This horizon coincides with an abrupt change in carbonate microfacies, from cherty fossiliferous wackestones-packstones below the LPEH to *Renalcis*-type calcimicrobial framestones above the LPEH. Similar facies patterns are found in carbonate successions throughout the Nanpanjiang Basin (Kershaw et al., 2002; Lehrmann et al., 2003).

IV-3. Methods

C and S concentrations were determined at the U. of Cincinnati using an Eltra 2000 C-S analyzer. Results were calibrated using USGS standards; analytical precision (2σ) was ±2.5% of reported values for C and ±5% for S. An aliquot of each sample was digested in HCl at 50 °C for 12 hours, and the residue was analyzed for total organic carbon (TOC) and non-acid-volatile sulfur (NAVS). Carbonate $\delta^{13}C$-$\delta^{18}O$ was analyzed at the U. of Kentucky using a GasBench-II peripheral coupled to a Delta*Plus*XP isotope-ratio-mass spectrometer. Samples were equilibrated at 40 °C for 24 hours before analysis. Analytical precision (2σ) was better than 0.05‰ for both $\delta^{13}C$ and $\delta^{18}O$; results are reported relative to the V-PDB standard. S and Fe extractions were performed at the U. of California at Riverside. Pyrite S was quantitatively extracted by the chromium reduction method of Canfield et al. (1986). The extracted Ag_2S was burned with excess Cu_2O at 1050 °C, producing SO_2 gas that was purified on a high-vacuum extraction line and stored in Pyrex break-seal tubes for S-isotopic analysis. S-isotope analyses were performed at both the U. of California at Riverside and the U. of Quebec at Montreal; results have a reproducibility of better than ±0.5‰ and are reported relative to the CDT standard.

IV-4. Results

See auxiliary material Tables IV-1, IV-2, IV-3 and IV-4.

The LPEH is associated with major geochemical changes: (1) an abrupt decline in total organic carbon (TOC) to near-zero concentrations (Figure IV-2b; also seen in other south China PTB sections) (Krull et al., 2004; Riccardi et al., 2006); (2) the first of 9 pyritic horizons (Figure IV-2c); (3) the onset of a 5-m-thick interval characterized by locally lower $\delta^{34}S_{py}$ values (Figure IV-2d); and (4) the onset of a sustained -3‰ shift in $\delta^{13}C_{carb}$ (Figure IV-

The first pyritic horizon (P1) is the most pyrite rich, and stratigraphically higher horizons exhibit a trend toward lower pyrite S concentrations (Figure IV-2c). Pyrite $\delta^{34}S$ values range from -37.8‰ to +10.0‰ CDT with the most ^{34}S-depleted values clustered in a 5-m-thick interval immediately above the LPEH (Figure IV-2d). The negative $\delta^{13}C_{carb}$ shift commencing at the LPEH is initially rapid and reaches a local minimum of ~-0.5‰ PDB about 1.3 m above the LPEH. Over the next four meters, the $\delta^{13}C_{carb}$ record exhibits a series of small-scale (~1-m) fluctuations with amplitudes of ~1‰, defining at least four C-isotope cycles (or more, if smaller inflections within cycles C1 and C2 are counted; Figure IV-2e).

Close examination of the Nhi Tao $[S]_{py}$, $\delta^{34}S_{py}$, and $\delta^{13}C_{carb}$ records reveals significant covariant relationships among them. Each pyritic horizon is associated with a local decrease in $\delta^{34}S_{py}$ values ranging from ~-5‰ to -40‰ in magnitude, whereas pyrite-poor "background" intervals exhibit relatively heavier S-isotopic compositions (Figures IV-2c and IV-2d). Negative covariation between $[S]_{py}$ and $\delta^{34}S_{py}$ is highly statistically significant ($r = -0.74$, $p(\alpha) < 0.001$ for a 2nd-order polynomial fit; Figure IV-3). Each pyritic horizon is also associated with an interval of decreasing $\delta^{13}C_{carb}$ values, with peak pyrite concentrations located mostly at or close to the onset of negative C-isotope excursions (Figures IV-2c and IV-2e). This relationship is most obvious for the P1 and P2 horizons, which are associated with the -3‰ $\delta^{13}C_{carb}$ shift just above the LPEH, but it exists for all of the other pyritic horizons in the study section as well. P3 and P4 are associated with a negative $\delta^{13}C_{carb}$ excursion at the top of cycle C1, P5 and P6 with the onset of negative excursions in cycle C2, P7 with the onset of a negative excursion in cycle C3, and P8 and P9 with the onset and culmination of a negative excursion in cycle C4 (Figure IV-2e). Covariation between the $\delta^{34}S_{py}$ and $\delta^{13}C_{carb}$ records is more subtle, but samples with more ^{34}S-enriched values tend to be clustered at the contacts between C-isotopic cycles (i.e., at local $\delta^{13}C_{carb}$ maxima), reflecting generally positive covariation at a fine (sub-meter) scale (Figures IV-2d and IV-2e).

IV-5. Discussion

A diagenetic explanation for patterns of covariation among $[S]_{py}$, $\delta^{34}S_{py}$, and $\delta^{13}C_{carb}$ is unlikely for several reasons. First, TOC data do not support BSR as the source of sulfide in the Nhi Tao section: no pyritic horizons formed below the LPEH despite TOC values as high as ~1%, whereas multiple pyritic horizons are found above the LPEH despite a lack of

organic matter (<0.1% TOC) to drive bacterial reduction of pore water sulfate (Figures IV-2b and IV-2c). Second, Rayleigh distillation of pore water sulfate would yield positive covariation between $[S]_{py}$ and $\delta^{34}S_{py}$, (Goldhaber and Kaplan, 1974), inconsistent with the pattern of negative covariation observed in this study (Figure IV-3). Third, if $[S]_{py}$-$\delta^{13}C_{carb}$ covariation were due to oxidation of organic matter and precipitation of diagenetic carbonate within the sediment, then pyritic horizons would correlate with $\delta^{13}C$ minima (peak organic matter oxidation) and possibly be associated with carbonate nodule layers (due to associated alkalinity increases). In fact, pyritic horizons show a clear association with the onset of negative $\delta^{13}C_{carb}$ excursions, and carbonate nodules are absent (Figures IV-2c and IV-2e). Fourth, the -3‰ C-isotopic excursion just above the LPEH, which is associated with ^{34}S-depleted pyritic horizons P1 and P2 (Figures IV-2c and IV-2e), is known to represent a global environmental signal. If this feature has a (global) environmental origin, then the other, smaller negative C-isotope excursions (C2–C4), which show the same relationships to $[S]_{py}$ and $\delta^{34}S_{py}$ as C1, can also be inferred to represent responses to an environmental forcing. Finally, if Fe limitation were the primary control on pyrite formation, then [Fe] would covary positively with $[S]_{py}$ and $\delta^{34}S_{py}$, and degree-of-pyritization (DOP) values would be high. In fact, [Fe] exhibits statistically insignificant ($p(\alpha) > 0.05$) relationships with $[S]_{py}$ and $\delta^{34}S_{py}$, and DOP values above the LPEH are low to intermediate (0.35 ± 0.21). Collectively, these observations favor a primary (environmental) origin for the chemostratigraphic patterns observed at Nhi Tao.

The relationships discussed above, i.e., the association of pyritic horizons with lower $\delta^{34}S_{py}$ and $\delta^{13}C_{carb}$ values, limit the range of viable models for the Nhi Tao depositional system. The tight coupling among these proxies implies control by a common environmental process. The most likely mechanisms are upwelling of anoxic deep-ocean water masses (Kajiwara et al., 1994) or chemocline upward excursions (Kump et al., 2005), in either case introducing ^{13}C-depleted dissolved inorganic carbon and ^{34}S-depleted hydrogen sulfide into the ocean surface layer. The nonlinear covariant relationship between $[S]_{py}$ and $\delta^{34}S_{py}$ was probably the product of a two-component mixing system, in which a relatively fixed quantity (~0.02%) of authigenic pyrite having a ^{34}S-enriched composition (~0 to +10‰; derived via near-quantitative BSR of Late Permian seawater sulfate (Strauss, 1997)) was diluted by

variable amounts of ^{34}S-depleted (~-45‰) syngenetic pyrite formed during upwelling events (Figure IV-3). The strongly ^{34}S-depleted composition of the latter end-member was due to the generation of H_2S under open-system (non-sulfate-limited) conditions in the anoxic Late Permian deep ocean (Wignall and Twitchett, 1996, 2002; Isozaki, 1997). Although Nhi Tao samples were too small to allow petrographic analysis, study of thin sections from another PTB section in the Nanpanjiang Basin has revealed numerous clusters of small (~3–6μ) pyrite framboids of probable syngenetic origin distributed throughout the sample matrix (cf. Wilkin et al., 1996; Wignall and Newton, 1998; Nielsen and Shen, 2004; Wignall et al., 2005).

Although upwelling of sulfidic deep-ocean waters has been proposed in earlier studies (Kajiwara et al., 1994; Knoll et al., 1996; Wignall and Twitchett, 1996, 2002; Isozaki, 1997), the present study provides important new insights in demonstrating the occurrence of multiple episodes of upwelling along the margin of the south China craton at quasiperiodic intervals of ~20–30 ka. Peri-equatorial upwelling in the eastern Paleotethys is consistent with Permian oceanic modeling results (Kutzbach et al., 1990; Winguth et al., 2002). Algeo et al. (2007) hypothesized that these episodes occurred in response to reinvigoration of oceanic overturn following a prolonged interval of Late Permian deep-ocean stagnation. Stagnation of the Late Permian ocean did not require complete cessation of deepwater formation but, rather, only a reduction in the rate of vertical overturn and deepwater ventilation. Circulation in the modern ocean is thought to oscillate between several ''modes'' owing to changes in atmospheric water vapor transport, freshwater influx, and other factors, with resultant variation in rates of oceanic ventilation at both millennial and longer timescales (Broecker and Denton, 1989; Burton et al., 1997; Hillaire-Marcel et al., 2001; Elliot et al., 2002). With regard to Permian-Triassic oceans, modeling studies have implicated flatter latitudinal temperature gradients, increased freshwater discharge, higher nutrient inventories, and enhanced particle ballasting as possible factors contributing to deep-ocean anoxia (Hotinski et al., 2001; Kiehl and Shields, 2005; Winguth and Maier-Reimer, 2005). Also possible is a switch between high-latitude cold and low-latitude warm-saline deepwater formation (Wilde and Berry, 1982), as the warmer bottom-water temperatures associated with the latter mode would result in significantly lower dissolved oxygen concentrations (Hotinski et al., 2001).

An alternative to the oceanic-overturn model of Algeo et al. (2007) is the chemocline-upward-excursion model proposed by Kump et al. (2005) and tested by Riccardi et al. (2006, 2007). Although both models assume the existence of a shallow oceanic chemocline as a starting point, a key difference is the nature of the climatic trigger causing transfer of deep-ocean hydrogen sulfide to shallow-marine systems. Whereas the trigger in the oceanic-overturn model is abrupt climatic cooling due to onset of Siberian Trap volcanism (Renne et al., 1995; Korte et al., 2008), the chemocline-upward-excursion model assumes that warming and oceanic stagnation intensify until the chemocline shallows to the point of instability, causing hydrogen sulfide to erupt into the atmosphere and thence to enter surface waters. This issue cannot be resolved at present, but because these two models make diametrically opposed predictions regarding climatic forcing of sulfide-flux events, they may be testable if a suitable proxy (e.g., conodont $\delta^{18}O$) can be measured at the necessary level of stratigraphic resolution. Existing conodont $\delta^{18}O$ (Korte et al., 2004, 2008) document a ~4–6 °C warming from the Late Permian into the Early Triassic, but the level of stratigraphic resolution is much too coarse to evaluate the relationship of climate change to high-frequency sulfide-flux events.

IV-6. Conclusions

The PTB section at Nhi Tao, Vietnam, contains at least 9 pyritic horizons of probable syngenetic origin characterized by strongly ^{34}S-depleted sulfur isotopic compositions. A consistent stratigraphic relationship of these horizons to the onset of negative carbonate $\delta^{13}C$ excursions is most easily explained as the product of recurrent upwelling of anoxic deep-ocean waters that contained ^{34}S-depleted hydrogen sulfide and ^{13}C-depleted dissolved inorganic carbon. The pyritic horizons commence at the Late Permian extinction horizon and are found at quasi-regular intervals over the next ~5 meters of section, suggesting that upwelling occurred along the southern margin of the south China craton with a periodicity of ~20–30 ka, i.e., consistent with control by climate variation at orbital timescales. The broader significance of this pattern may be as a record of reinvigorated global-ocean overturn following a prolonged interval of stagnation during the Late Permian, during which the oceanic chemocline rose to relatively shallow depths. This is the first published study to document a strong relationship between pyrite horizons and carbonate

$\delta^{13}C$ trends at the Permian-Triassic boundary. The evidence from Nhi Tao offers no support for an extraterrestrial cause for the PTB (cf. Becker et al., 2001).

Acknowledgments

We thank Barry Maynard and Bob King for analytical assistance and Jesper Kresten Nielsen, Lee Kump, and Laurent Labeyrie for constructive reviews of the manuscript. This project was supported in part by grants to T.J.A. from the National Science Foundation (EAR-0310072 and EAR- 0618003) and the University of Cincinnati Research Council.

References

Algeo, T. J., B. B. Ellwood, T. K. T. Nguyen, H. Rowe, and J. B. Maynard (2007), The Permian-Triassic boundary at Nhi Tao, Vietnam: Evidence for recurrent influx of sulfidic watermasses to a shallow-marine carbonate platform, Palaeogeogr. Palaeoclimatol. Palaeoecol., 252, 304–327, doi:10.1016/j.palaeo.2006.11.055.

Baud, A., W. T. Holser, and M. Magaritz (1989), Permian-Triassic of the Tethys: Carbon isotope studies, Geol. Rundsch., 78, 649–677.

Becker, L., R. J. Poreda, A. G. Hunt, T. E. Bunch, and M. Rampino (2001), Impact event at the Permian-Triassic boundary: Evidence from extraterrestrial noble gases in fullerenes, Science, 291, 1530–1533.

Berner, R. A. (2002), Examination of hypotheses for the Permo-Triassic boundary extinction by carbon cycle modeling, Proc.Natl. Acad. Sci. U.S.A., 99, 4172–4177.

Bowring, S. A., D. H. Erwin, Y. G. Jin, M. W. Martin, K. Davidek, and W. Wang (1998), U/Pb zircon geochronology and tempo of the end-Permian mass extinction, Science, 280, 1039–1045.

Broecker, W. S., and G. H. Denton (1989), The role of oceanatmosphere reorganizations in glacial cycles, Geochim. Cosmochim. Acta, 53, 2465–2501.

Burton, K. W., H.-F. Ling, and R.-K. O'Nions (1997), Closure of the Central American Isthmus and its effect on deep-water formation in the North Atlantic, Nature, 386, 382–385.

Canfield, D. E., R. Raiswell, J. T. Westrich, C. M. Reaves, and R. A. Berner (1986), The use of chromium reduction in the analysis of reduced inorganic sulfur in sediments and shales, Chem. Geol., 54, 149–155.

de Wit, M. J., J. G. Ghosh, S. de Villiers, N. Rakotosolofo, J. Alexander, A. Tripathi, and C. Looy (2002), Multiple organic carbon isotope reversals across the Permo-Triassic boundary

of terrestrial Gondwana sequences: Clues to extinction patterns and delayed ecosystem recovery, J. Geol., 110, 227–240.

Elliot, M., L. Labeyrie, and J. C. Duplessy (2002), Changes in North Atlantic deep-water formation associated with the Dansgaard-Oeschger temperature oscillations (60–10 ka), Quat. Sci. Rev., 21, 1153–1165.

Erwin, D. H. (1994), The Permo-Triassic extinction, Nature, 367, 231–236.

Erwin, D. H., S. A. Bowring, Y.-G. Jin (2002), End-Permian mass-extinctions: A review, in Catastrophic Events and Mass Extinctions: Impacts and Beyond, edited by C. Koeberl and K. G. MacLeod, Spec. Pap. Geol. Soc. Am., 356, 353–383.

Goldhaber, M. B., and I. R. Kaplan (1974). The sulfur cycle, in The Sea, vol. 5, Marine Chemistry, edited by E. D. Goldberg, pp. 569–655, John Wiley, New York.

Grice, K., C. Cao, G. D. Love, M. E. Böttcher, R. J. Twitchett, E. Grosjean, R. E. Summons, S. C. Turgeon, W. Dunning, and Y. Jin (2005), Photic zone euxinia during the Permian-Triassic superanoxic event, Science, 307, 706–709.

Hays, L. E., T. Beatty, C. M. Henderson, G. D. Love, and R. E. Summons (2007), Evidence for photic zone euxinia through the end-Permian mass extinction in the Panthalassic Ocean (Peace River Basin, Western Canada), Palaeoworld, 16, 39–50.

Hillaire-Marcel, C., A. de Vernal, G. Bilodeau, and A. J. Weaver (2001), Absence of deep-water formation in the Labrador Sea during the last interglacial period, Nature, 410, 1073–1077.

Hotinski, R. M., K. L. Bice, L. R. Kump, R. G. Najjar, and M. A. Arthur (2001), Ocean stagnation and end-Permian anoxia, Geology, 29, 7–10.

Isozaki, Y. (1997), Permo-Triassic boundary superanoxia and stratified superocean: Records from lost deep sea, Science, 276, 235–238.

Kaiho, K., T. Kajiwara, T. Nakano, Y. Muira, H. Kawahata, K. Tazaki, M. Ueshima, Z. Chen, and G. R. Shi (2001), End-Permian catastrophe by a bolide impact: Evidence of a gigantic release of sulfur from the mantle, Geology, 29, 815–818.

Kaiho, K., Z.-Q. Chen, H. Kawahata, Y. Kajiwara, and H. Sato (2006), Close-up of the end-Permian mass extinction horizon recorded in the Meishan section, south China: Sedimentary, elemental, and biotic characterization and a negative shift of sulphate sulfur isotope ratio, Palaeogeogr. Palaeoclimatol. Palaeoecol., 239, 396–405.

Kajiwara, Y., S. Yamakita, K. Ishida, H. Ishiga, and A. Imai (1994), Development of a largely anoxic stratified ocean and its temporary massive mixing at the Permian-Triassic

boundary supported by the sulfur isotope record, Palaeogeogr. Palaeoclimatol. Palaeoecol., 111, 367–379.

Kakuwa, Y., and R. Matsumoto (2006), Cerium negative anomaly just before the Permian and Triassic boundary event: The upward expansion of anoxia in the water column, Palaeogeogr. Palaeoclimatol. Palaeoecol., 229, 335–344.

Kershaw, S., L. Guo, A. Swift, and J.-S. Fan (2002), Microbialites in the Permian-Triassic boundary interval in central China: Structure, age and distribution, Facies, 47, 83–90.

Kiehl, J. T., and C. A. Shields (2005), Climate simulation of the latest Permian: Implications for mass extinction, Geology, 33, 757–760.

Knoll, A. H., R. K. Bambach, D. E. Canfield, and J. P. Grotzinger (1996), Comparative Earth history and Late Permian mass extinction, Science, 273, 452–457.

Korte, C., H. W. Kozur, M. M. Joachimski, H. Strauss, J. Veizer, and L. Schwark (2004), Carbon, sulfur, oxygen and strontium isotope records, organic geochemistry and biostratigraphy across the Permian/Triassic boundary in Abadeh, Iran, Int. J. Earth Sci., 93, 565–581.

Korte, C., P. Pande, P. Kalia, H. W. Kozur, M. M. Joachimski, and H. Oberha¨nsli (2008), Massive volcanism at the Permian- Triassic boundary and its impact on the isotopic composition of the ocean and atmosphere, J. Asian Earth Sci.37, 293-311.

Krull, E. S., and G. J. Retallack (2000), d13Corg depth profiles from paleosols across the Permian-Triassic boundary: Evidence for methane release, Geol. Soc. Am. Bull., 112, 1459–1472.

Krull, E. S., D. J. Lehrmann, D. Druke, B. Kessel, Y. Yu, and R. Li (2004), Stable carbon isotope stratigraphy across the Permian-Triassic boundary in shallow marine carbonate platforms, Nanpanjiang Basin, south China, Palaeogeogr. Palaeoclimatol. Palaeoecol., 204, 297–315.

Kump, L. R., A. Pavlov, and M. A. Arthur (2005), Massive release of hydrogen sulfide to the surface ocean and atmosphere during intervals of oceanic anoxia, Geology, 33, 397–400.

Kutzbach, J. E., P. J. Guetter, and W. M. Washington (1990), Simulated circulation of an idealized ocean for Pangaean time, Paleoceanography, 5, 299–317.

Lehrmann, D. J., J. L. Payne, S. V. Felix, P. M. Dillett, H.Wang, Y. Yu, and J.Wei (2003), Permian-Triassic boundary sections from shallow-marine carbonate platforms of the Nanpanjiang Basin, south China: Implications for oceanic conditions associated with the end-Permian extinction and its aftermath, Palaios, 18, 138–152.

Mundil, R., K. R. Ludwig, I. Metcalfe, and P. R. Renne (2004), Age and timing of the Permian mass extinctions: U/Pb dating of closed-system zircons, Science, 305, 1760–1763.

Newton, R. J., E. L. Pevitt, P. B. Wignall, and S. H. Bottrell (2004), Large shifts in the isotopic composition of seawater sulphate across the Permo-Triassic boundary in northern Italy, Earth Planet. Sci. Lett., 218, 331–345.

Nielsen, J. K., and Y. Shen (2004), Evidence for sulfidic deep water during the Late Permian in the East Greenland Basin, Geology, 32, 1037–1040.

Payne, J. L., D. J. Lehrmann, J. Wei, M. J. Orchard, D. P. Schrag, and A. H. Knoll (2004), Large perturbations of the carbon cycle during recovery from the end-Permian extinction, Science, 305, 506–509.

Payne, J. L., D. J. Lehrmann, D. Follett, M. Seibel, L. R. Kump, A. Riccardi, D. Altiner, H. Sano, and J. Wei (2007), Erosional truncation of uppermost Permian shallow-marine carbonates and implications for Permian-Triassic boundary events, Geol. Soc. Am. Bull., 119, 771–784.

Renne, P. R., Z. C. Zheng, M. A. Richards, M. T. Black, and A. R. Basu (1995), Synchrony and causal relations between Permian-Triassic boundary crisis and Siberian flood volcanism, Science, 269, 1413–1416.

Retallack, G. J. (1995), Permian-Triassic extinction on land, Science, 267, 77–80.

Riccardi, A. L., M. A. Arthur, and L. R. Kump (2006), Sulfur isotopic evidence for chemocline upward excursions during the end-Permian mass extinction, Geochim. Cosmochim. Acta, 70, 5740–5752.

Riccardi, A., L. R. Kump, M. A. Arthur, and S. D'Hondt (2007), Carbon isotopic evidence for chemocline upward excursions during the end-Permian event, Palaeogeogr. Palaeoclimatol. Palaeoecol., 248, 73–81.

Sephton, M. A., H. Brinkhuis, C. V. Looy, R. J. Veefkind, H. Visscher, and J. W. de Leeuw (2002), Synchronous record of d13C shifts in the oceans and atmosphere at the end of the Permian, in Catastrophic Events and Mass Extinctions: Impacts and Beyond, edited by C. Koeberl and K. G. MacLeod, Spec. Pap., Geol. Soc. Am., 356, 455-462.

Son, T. H., C. Koeberl, N. L. Ngoc, and D. T. Huyen (2007), The Permian-Triassic boundary sections in northern Vietnam (Nhi Tao and Lung Cam sections): Carbon-isotope excursion and elemental variations indicate major anoxic event, Palaeoworld, 16, 51–66.

Strauss, H. (1997), The isotopic composition of sedimentary sulfur through time, Paleogeogr. Palaeoclimatol. Paleoecol., 132, 97–118.

Twitchett, R. J., C. V. Looy, R. Morante, H. Visscher, and P. B. Wignall (2001), Rapid and synchronous collapse of marine and terrestrial ecosystems during the end- Permian biotic crisis, Geology, 29, 351–354.

Wignall, P. B., and R. Newton (1998), Pyrite framboid diameter as a measure of oxygen deficiency in ancient mudrocks, Am. J. Sci., 298, 537–552.

Wignall, P. B., and R. J. Twitchett (1996), Oceanic anoxia and the end Permian mass extinction, Science, 272, 1155–1158.

Wignall, P. B., R. J. Twitchett, (2002), Extent, duration and nature of the Permian-Triassic superanoxic event, in Catastrophic Events and Mass Extinctions: Impacts and Beyond, edited by C. Koeberl and K. G. MacLeod, Spec. Pap. Geol. Soc. Am. 356, 395-413.

Wignall, P. B., R. Newton, and M. E. Brookfield (2005), Pyrite framboid evidence for oxygen-poor deposition during the Permian-Triassic crisis in Kashmir, Palaeogeogr. Palaeoclimatol. Palaeoecol., 216, 183–188.

Wilde, P., W. B. N. Berry (1982), Progressive ventilation of the oceans–Potential for return to anoxic conditions in the post- Paleozoic, in Nature and Origin of Cretaceous Carbon-Rich Facies, edited by S. O. Schlanger and M. B. Cita, pp. 209–224, Academic, New York.

Wilkin, R. T., H. L. Barnes, and S. L. Brantley (1996), The size distribution of ramboidal pyrite in modern sediments: An indicator of redox conditions, Geochem. Cosmochim. Acta, 60, 3897–3912.

Winguth, A. M. E., and E. Maier-Reimer (2005), Causes of marine productivity and oxygen changes associated with the Permian-Triassic boundary: A reevalution with ocean general circulation models, Mar. Geol., 217, 283–304.

Winguth, A. M. E., C. Heinze, J. E. Kutzbach, E. Maier- Reimer, U. Mikolajewicz, D. Rowley, A. Rees, and A. M. Ziegler (2002), Simulated warm polar currents during the middle Permian, Paleoceanography, 17(4), 1057, doi:10.1029/2001PA000646.

Xie, S., R. D. Pancost, H. Yin, H. Wang, and R. P. Evershed (2005), Two episodes of microbial change coupled with Permo/Triassic faunal mass extinction, Nature, 434, 494–497.

Figure Captions

Figure IV-1. (A) Paleogeography and location map for Nhi Tao. GBG = Great Bank of Guizhou; NB, Nanpanjiang Basin. Modified from Lehrmann et al. (2003). (B) Paleogeography of Tethyan Ocean region at the PTB (251 Ma). ANG = Angara, CM = Cimmeria, GND =Gondwana, NC = North China, PAN = Panthalassic Ocean, and SC = South China. Base map courtesy of Ron Blakey (http://jan.ucc.nau.edu/~rcb7/).

Figure IV-2. The Nhi Tao section: (A) stratigraphy, (B) TOC, (C) total [S] and pyrite [S], (D) pyrite $\delta^{34}S$, and (E) carbonate $\delta^{13}C$. LPEH = Late Permian event horizon; PTB = Permian/Triassic boundary. l.-m. = *latidentatus-meishanensis* zone; parv. = *parvus* zone; P1-P9 = pyritic horizons; C1-C4 = carbon isotope cycles.

Figure IV-3. Pyrite $\delta^{34}S$ versus pyrite [S]. Black lines connect stratigraphically adjacent samples. The red curve represents a two-component mixing model with low-S and high-S endmembers having $\delta^{34}S$ = +10‰ and -45‰ and representing authigenic and syngenetic pyrite fractions, respectively; also shown are syngenetic:authigenic pyrite mixing ratios of 1:1, 4:1, and 9:1.

Table captions

Table IV-1. TOC, S and S-, C-, and O-isotopic data of Pr-T samples from Nhi Tao, Vietnam

Table IV-2. Major elements data of Pr-T samples from Nhi Tao, Vietnam

Table IV-3. Trace elements data of Pr-T sample s from Nhi Tao, Vietnam

Table IV-4. Sulfur-iron data of Pr-T samples from Nhi Tao, Vietnam

Table IV-1 TOC, S and S-, C-, and O-isotopic data of Pr-T samples from Nhi Tao, Vietnam

Sample	Height (m)	TOC (%)	TIC (%)	TS (%)	S_{py} (%)	$\delta^{34}S_{Py}$ (‰)	$\delta^{13}C_{carb}$ (‰)	$\delta^{18}O_{carb}$ (‰)
NT-001	-1.64	0.08	10.60	0.02	0.02	6.95	1.92	-9.82
NT-004	-1.45	0.21	10.69	0.02	0.03	-13.17	1.49	-10.25
NT-007	-1.30	0.26	11.55	0.03	0.03	-12.97	2.03	-8.70
NT-010	-1.21	0.24	10.97	0.03	0.02		2.03	-9.08
NT-013	-1.05	0.61	11.05	0.03	0.03	-4.37	2.60	-6.90
NT-016	-0.90	0.12	11.65	0.03	0.02	-11.82	1.28	-10.01
NT-019	-0.75	0.13	10.81	0.03	0.03	-22.48	1.65	-7.93
NT-022	-0.60	1.07	9.72	0.04	0.04	2.41	1.87	-8.12
NT-025	-0.45	0.26	10.03	0.03	0.03	-4.12	2.17	-7.71
NT-028	-0.31	0.07	11.36	0.21	0.17	-30.93	1.61	-6.41
NT-031	-0.20	0.06	10.87	0.05	0.02	-22.16	1.31	-8.55
NT-034	-0.05	0.07	10.52	0.17	0.09	-26.57	1.05	-7.46
NT-037	0.10	0.06	10.19	0.03	0.03	-18.4	0.80	-8.31
NT-040	0.30	0.08	9.58	0.02	0.03		0.11	-8.32
NT-043	0.50	0.07	10.78	0.04	0.04	-26.7	0.03	-9.86
NT-046	0.65	0.08	10.77	0.06	0.05	-30.81	0.05	-7.76
NT-049	0.80	0.05	11.02	0.05	0.04	-20.54	-0.17	-7.22
NT-052	0.95	0.11	10.81	0.13	0.11	-17.85	-0.27	-10.61
NT-055	1.13	0.07	12.49	0.03	0.03	1.87	-0.15	-5.43
NT-058	1.30	0.07	9.56	0.03	0.03		0.57	-8.92
NT-061	1.45	0.07	9.82	0.09	0.08	-37.85	0.36	-7.98
NT-064	1.55	0.06	9.92	0.13	0.12	-33.99	0.27	-7.44
NT-067	1.65	0.07	10.87	0.06	0.05	-32.33	-0.24	-8.25
NT-070	1.77	0.07	10.50	0.03	0.03		-0.17	-8.85
NT-071	1.88	0.06	9.82	0.07	0.07	-29.92	0.17	-6.25
NT-074	2.00	0.07	11.05	0.13	0.10	-30.77	-0.22	-6.89
NT-077	2.13	0.04	9.58	0.05	0.07	-27.38	-0.35	-7.98
NT-080	2.28	0.05	10.47	0.02	0.02	-1.59	-0.56	-8.75
NT-083	2.39	0.05	9.49	0.02	0.02	5.15	-0.81	-8.87
NT-086	2.50	0.05	10.72	0.02	0.02	-19.21	-0.73	-8.52
NT-089	2.65	0.09	10.65	0.02	0.03	1.79	0.20	-8.61
NT-092	2.85	0.12	9.56	0.02	0.02		0.16	-8.40
NT-095	2.97	0.08	10.25	0.05	0.03	-25.39	-0.34	-7.27
NT-098	3.06	0.09	10.55	0.03	0.02	-5.18	-0.45	-6.55
NT-101	3.23					-32.8		
NT-104	3.40	0.08	10.52	0.03	0.02	8.84	-0.35	-5.65
NT-107	3.65	0.07	10.66	0.02	0.02	13.48	-0.33	-5.98
NT-110	3.80	0.06	10.58	0.02	0.02	-8.29	0.07	-5.66
NT-113	3.95	0.06	12.21	0.02	0.03	-12.31	-0.06	-4.92
NT-116	4.15	0.06	11.36	0.02	0.02	9.97	-0.10	-4.88
NT-119	4.35	0.07	11.76	0.04	0.02	-20.74	-0.27	-9.55
NT-122	4.53	0.09	11.29	0.05	0.05	-33.63	-0.53	-7.05
NT-125	4.72	0.06	11.71	0.02	0.02	-0.90	-0.64	-8.21
NT-128	4.90	0.08	11.22	0.02	0.02	4.81	-0.57	-8.78
NT-131	5.17	0.08	10.89	0.02	0.02	6.18	-0.57	-9.64
NT-134	5.35	0.07	10.04	0.03	0.02	6.29	-0.19	-6.45
NT-137	5.48	0.08	10.82	0.03	0.02	7.17	-0.18	-5.95
NT-140	5.85	0.09	11.11	0.02	0.03		-0.19	-5.82

Table IV-2 Major elements data of Pr-T samples from Nhi Tao, Vietnam

Sample	Fe_2O_3 (%)	MnO_2 (%)	TiO_2 (%)	SiO_2 (%)	Al_2O_3 (%)	CaO (%)	K_2O (%)	P_2O_5 (%)	MgO (%)	Na_2O (%)	LOI (%)
NT-001	0.33	0.01	0.06	2.71	1.25	53.39	0.03	0.00	0.40	0.00	41.8
NT-004	0.21	0.01	0.02	7.08	1.41	51.88	0.12	0.00	0.25	0.03	40.4
NT-007	0.16	0.01	0.05	7.15	1.92	47.53	0.33	0.01	0.17	0.20	42.5
NT-010	0.40	0.01	0.08	6.64	2.45	47.97	0.61	0.01	0.21	0.01	41.6
NT-013	0.44	0.01	0.04	8.13	1.09	48.44	0.13	0.01	0.51	0.02	41.2
NT-016	0.22	0.01	0.07	5.96	1.99	48.79	0.50	0.02	0.15	0.00	42.3
NT-019	0.47	0.01	0.08	5.11	2.43	48.08	0.59	0.01	0.54	0.15	42.5
NT-022	0.51	0.02	0.06	2.79	0.80	51.79	0.09	0.00	0.69	0.04	43.2
NT-025	0.73	0.02	0.08	3.79	2.41	50.20	0.32	0.00	1.25	0.01	41.2
NT-028	0.91	0.02	0.09	4.22	1.88	48.49	0.43	0.01	0.37	0.10	43.5
NT-031	0.63	0.03	0.11	6.92	1.80	48.45	0.34	0.00	0.56	0.09	41.1
NT-034	0.69	0.02	0.09	7.21	2.06	48.49	0.45	0.01	1.14	0.09	39.8
NT-037	0.71	0.02	0.10	5.60	2.00	48.73	0.40	0.00	0.63	0.09	41.7
NT-040	0.92	0.02	0.11	6.37	1.84	49.59	0.28	0.07	1.03	0.01	39.8
NT-043	1.13	0.04	0.13	5.55	2.03	49.02	0.26	0.13	1.03	0.05	40.6
NT-046	1.49	0.05	0.16	5.63	1.96	48.03	0.30	0.03	2.45	0.01	39.9
NT-049	2.04	0.07	0.20	1.77	2.31	48.21	0.39	0.03	2.24	0.01	42.7
NT-052	1.37	0.04	0.13	1.71	1.91	50.39	0.24	0.05	0.92	0.04	43.2
NT-055	3.59	0.14	0.33	1.49	3.90	43.13	0.81	0.01	5.28	0.00	41.3
NT-058	3.05	0.08	0.29	8.99	4.04	40.10	0.99	0.02	3.17	0.01	39.2
NT-061	1.93	0.07	0.23	10.41	3.24	42.09	0.69	0.02	4.05	0.00	37.3
NT-064	1.60	0.06	0.18	9.10	2.36	44.37	0.57	0.00	3.35	0.02	38.4
NT-067	1.60	0.05	0.18	5.07	2.48	47.45	0.45	0.01	1.25	0.02	41.4
NT-070	0.95	0.03	0.13	7.15	1.99	47.74	0.43	0.00	0.94	0.03	40.6
NT-071	1.04	0.04	0.14	8.48	2.41	47.02	0.42	0.00	1.63	0.02	38.8
NT-074	1.18	0.04	0.14	6.34	2.40	47.06	0.47	0.00	1.91	0.03	40.4
NT-077	1.49	0.04	0.18	9.86	3.00	44.94	0.67	0.01	2.03	0.04	37.7
NT-080	1.43	0.04	0.17	9.30	2.87	45.67	0.52	0.01	2.07	0.03	37.9
NT-083	1.27	0.04	0.20	14.21	3.28	43.44	0.75	0.02	1.03	0.05	35.7
NT-086	1.68	0.05	0.20	8.53	3.22	46.14	0.56	0.01	1.43	0.03	38.2
NT-089	1.32	0.05	0.16	8.91	2.60	47.57	0.34	0.01	1.23	0.04	37.8
NT-092	1.49	0.05	0.19	9.72	2.91	45.42	0.47	0.02	1.68	0.04	38.0
NT-095	1.67	0.06	0.22	10.53	3.22	43.26	0.61	0.03	2.12	0.04	38.2
NT-098	1.93	0.07	0.24	8.72	3.09	43.12	0.65	0.03	2.78	0.04	39.3
NT-101											
NT-104	4.87	0.19	0.47	8.65	5.20	34.64	1.18	0.07	5.80	0.04	38.9
NT-107	4.83	0.18	0.46	4.21	4.84	38.84	1.21	0.02	5.59	0.04	39.8
NT-110	4.83	0.20	0.45	6.38	4.23	34.57	1.17	0.02	7.70	0.02	40.4
NT-113	9.14	0.36	0.75	1.49	6.11	31.25	1.29	0.08	9.60	0.01	39.9
NT-116	7.81	0.32	0.67	2.23	5.49	32.12	1.15	0.07	8.26	0.01	41.9
NT-119	2.30	0.08	0.24	8.38	3.27	44.24	0.70	0.02	2.30	0.03	38.4
NT-122	1.91	0.07	0.20	5.71	2.84	47.26	0.54	0.01	1.98	0.02	39.5
NT-125	3.83	0.15	0.34	2.46	3.53	44.12	0.79	0.03	3.80	0.01	40.9
NT-128	2.39	0.09	0.24	5.88	3.28	46.41	0.67	0.02	2.36	0.05	38.6
NT-131	1.64	0.06	0.20	9.69	2.93	44.26	0.57	0.05	1.42	0.00	39.2
NT-134	3.70	0.14	0.39	12.09	4.59	34.01	1.06	0.04	6.20	0.06	37.7
NT-137	3.00	0.12	0.33	10.39	3.82	37.83	0.92	0.04	4.19	0.03	39.3
NT-140	4.19	0.16	0.40	5.59	4.14	38.97	0.94	0.07	5.93	0.03	39.6

Table IV-3 Trace elements data of Pr-T samples from Nhi Tao, Vietnam

Sample	Mo (ppm)	U (ppm)	V (ppm)	Zn (ppm)	Cu (ppm)	Ni (ppm)	Cr (ppm)	Pb (ppm)	Sr (ppm)	Th (ppm)	Co (ppm)	Ba (ppm)
NT-001	0.90	0.09	26.6	3.6	9.0	14.6	12.9	3.80	570	1.14	0.00	8.2
NT-004	0.87	1.40	16.3	3.5	9.5	13.3	21.9	2.92	475	0.94	0.61	1.6
NT-007	0.99	0.96	24.3	3.4	8.8	15.9	19.1	2.26	515	0.30	0.12	3.7
NT-010	0.74	1.48	18.2	5.3	9.1	14.7	12.2	5.04	532	1.52	0.65	9.3
NT-013	0.27	1.52	34.3	6.2	10.3	16.0	37.0	4.75	1722	0.90	0.18	9.1
NT-016	0.90	1.24	17.7	2.6	9.0	12.6	11.7	3.94	330	0.77	0.78	6.3
NT-019	0.91	0.36	13.8	3.3	9.5	14.9	13.0	1.61	620	1.22	0.22	3.8
NT-022	0.99	1.28	12.8	3.6	9.1	14.4	30.0	5.06	1141	1.31	1.72	11.0
NT-025	0.37	1.62	1.8	4.1	9.4	17.1	11.7	6.02	667	2.91	0.24	8.2
NT-028	0.26	2.06	14.8	3.8	10.5	14.9	9.0	4.16	1901	1.45	0.72	9.6
NT-031	0.88	0.91	16.4	4.5	8.7	13.6	8.6	5.26	351	1.14	0.80	8.5
NT-034	0.43	1.13	0.8	6.0	9.8	16.3	11.5	4.28	356	1.07	1.63	14.7
NT-037	1.18	1.60	6.2	6.4	9.6	14.3	10.8	4.44	305	1.30	1.90	16.3
NT-040	0.56	1.48	31.7	10.8	11.9	17.1	13.1	2.84	313	1.68	2.86	8.9
NT-043	0.98	0.56	13.8	7.3	11.6	14.5	11.0	6.36	281	1.37	1.58	1.1
NT-046	0.30	1.16	5.5	6.8	11.4	15.5	11.5	5.48	329	1.54	2.50	11.6
NT-049	0.44	0.70	10.1	4.7	10.2	14.1	10.7	5.19	298	1.82	0.58	0.9
NT-052	0.51	0.70	2.5	3.6	10.5	12.6	9.9	4.83	276	0.93	0.70	9.1
NT-055	0.55	0.94	5.6	2.5	9.3	12.9	6.6	2.15	328	1.32	2.04	0.6
NT-058	0.62	1.21	1.8	20.5	14.4	18.0	16.8	6.99	242	2.46	3.27	49.3
NT-061	0.79	0.10	16.9	10.6	12.7	16.8	14.3	5.44	296	2.03	2.96	47.9
NT-064	1.00	0.54	0.2	6.2	11.7	15.0	11.0	2.51	307	2.22	1.30	21.7
NT-067	0.60	1.06	8.6	6.3	11.6	14.1	14.8	4.25	326	2.12	2.00	15.9
NT-070	0.77	0.46	2.4	6.4	12.2	14.7	8.9	4.51	337	1.60	0.33	13.2
NT-071	0.75	2.33	18.1	6.8	10.8	15.1	16.5	1.52	462	1.93	1.17	3.5
NT-074	0.78	0.02	0.5	6.3	10.8	13.9	8.4	2.52	317	1.12	1.08	21.6
NT-077	0.86	0.56	6.0	12.4	12.4	17.5	14.1	5.08	290	1.94	2.55	40.8
NT-080	0.42	0.98	10.3	14.0	10.5	18.1	13.4	5.99	294	1.66	1.74	7.0
NT-083	0.37	1.21	22.6	16.1	12.7	18.1	20.3	4.73	266	2.28	1.42	43.7
NT-086	0.42	1.63	17.0	11.2	12.6	18.1	13.4	5.67	275	1.48	0.81	17.5
NT-089	0.83	0.93	9.2	5.9	11.5	14.8	12.3	4.58	382	2.05	0.97	10.9
NT-092	0.67	0.77	7.81	8.2	11.8	15.8	13.9	3.29	355	2.21	1.24	11.6
NT-095	0.52	0.62	6.4	10.4	12.1	16.8	15.5	2.01	329	2.36	1.51	12.2
NT-098	0.56	0.83	2.5	9.0	13.0	16.5	19.2	5.34	331	1.95	0.85	23.6
NT-101												
NT-104	0.89	0.19	2.7	11.8	14.1	15.6	12.2	1.60	262	1.40	2.94	40.2
NT-107	1.14	1.70	27.3	7.3	12.6	15.2	12.4	4.76	246	1.77	1.54	7.2
NT-110	1.02	0.78	18.4	7.3	13.7	14.6	12.9	1.86	341	1.47	0.79	0.5
NT-113	0.71	1.46	18.0	4.0	11.2	14.0	8.9	2.16	287	1.38	2.50	10.0
NT-116	1.06	0.76	5.0	4.6	10.3	13.1	8.1	2.69	332	1.37	1.70	7.7
NT-119	0.56	1.91	10.7	9.6	16.7	16.3	11.3	4.95	248	2.09	1.04	30.7
NT-122	0.75	0.15	2.6	4.8	10.6	15.5	9.0	1.77	341	1.61	1.21	4.2
NT-125	0.73	1.13	4.0	7.7	10.4	15.5	10.2	3.78	289	0.95	1.72	13.0
NT-128	0.31	0.52	14.7	9.1	11.5	15.1	9.5	3.34	276	1.45	1.49	16.8
NT-131	0.58	0.20	1.1	12.5	11.0	14.7	13.8	4.74	245	1.79	2.02	32.9
NT-134	0.64	0.84	9.8	13.6	17.1	16.8	15.3	3.17	253	3.24	1.41	47.9
NT-137	0.62	0.41	6.5	11.1	13.1	16.0	14.7	5.05	290	2.35	0.94	10.9
NT-140	0.88	1.12	0.7	9.3	10.7	16.0	12.6	4.30	285	0.69	1.09	17.3

Table IV-4 Sulfur-iron data of Pr-T samples from Nhi Tao, Vietnam

Sample	Height (m)	S_{py} (%)	Fe_{py} (%)	Fe_{HCl} (%)	DOP
NT-010	-1.21	0.53	0.46	0.12	0.79
NT-028	-0.31	0.20	0.17	0.18	0.50
NT-034	-0.05	0.27	0.24	0.13	0.65
NT-046	0.65	0.33	0.29	0.34	0.46
NT-052	0.95	0.21	0.18	0.13	0.58
NT-058	1.30	0.08	0.07	1.09	0.06
NT-064	1.55	0.20	0.17	0.29	0.37
NT-070	1.77	0.07	0.06	0.28	0.18
NT-074	2.00	0.18	0.16	0.23	0.41
NT-140	5.85	0.06	0.05	0.45	0.10

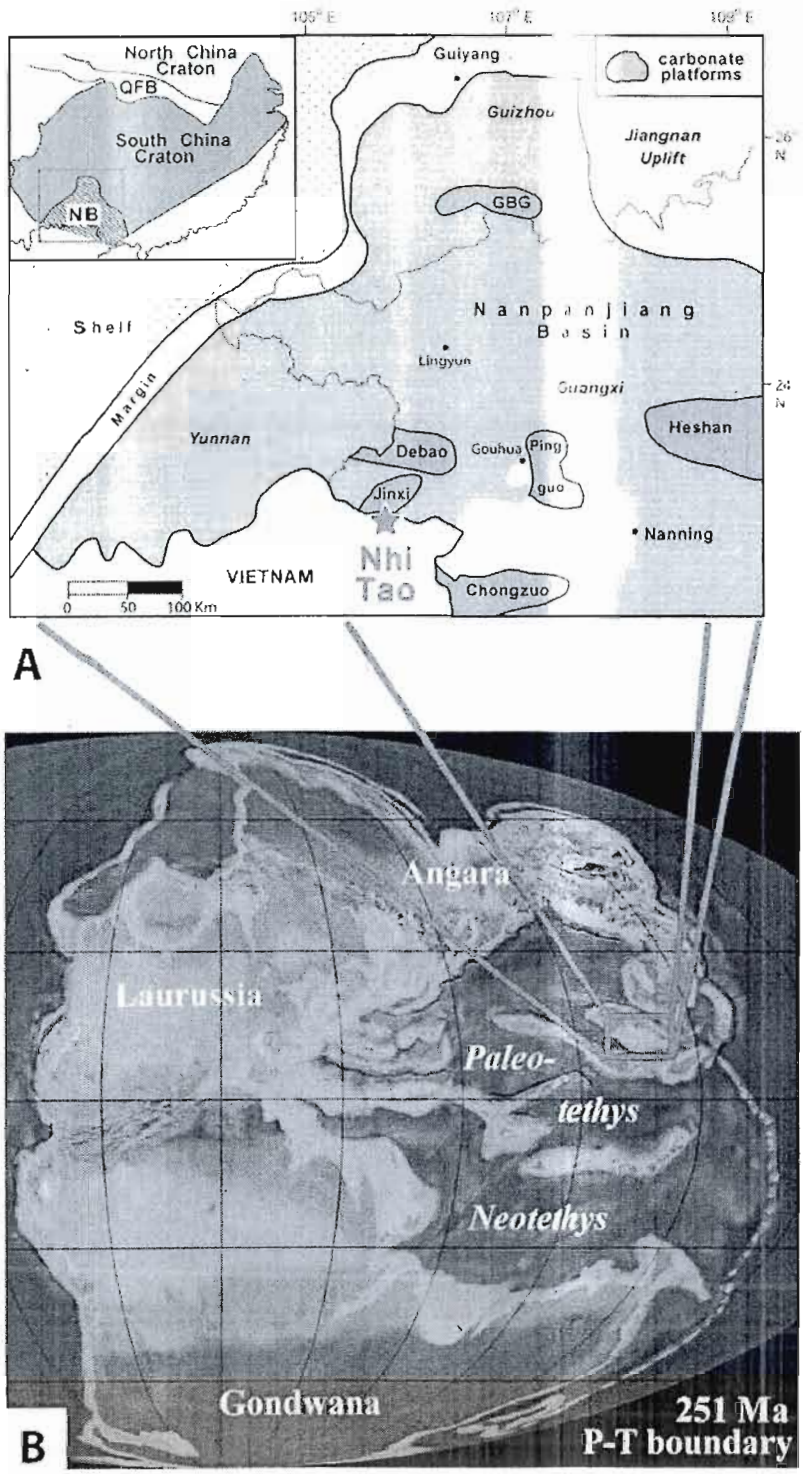
North China Craton
QFB
South China Craton
NB
Guiyang
carbonate platforms
Guizhou
Jiangnan Uplift
GBG
Nanpanjiang Basin
Shelf
Margin
Lingyun
Guangxi
Yunnan
Debao
Gouhua
Ping
guo
Heshan
Jinxi
Nanning
VIETNAM
Nhi Tao
Chongzuo
0 50 100 Km
A
Angara
Laurussia
Paleo-
tethys
Neotethys
Gondwana
251 Ma
P-T boundary
B

Fig. IV-1

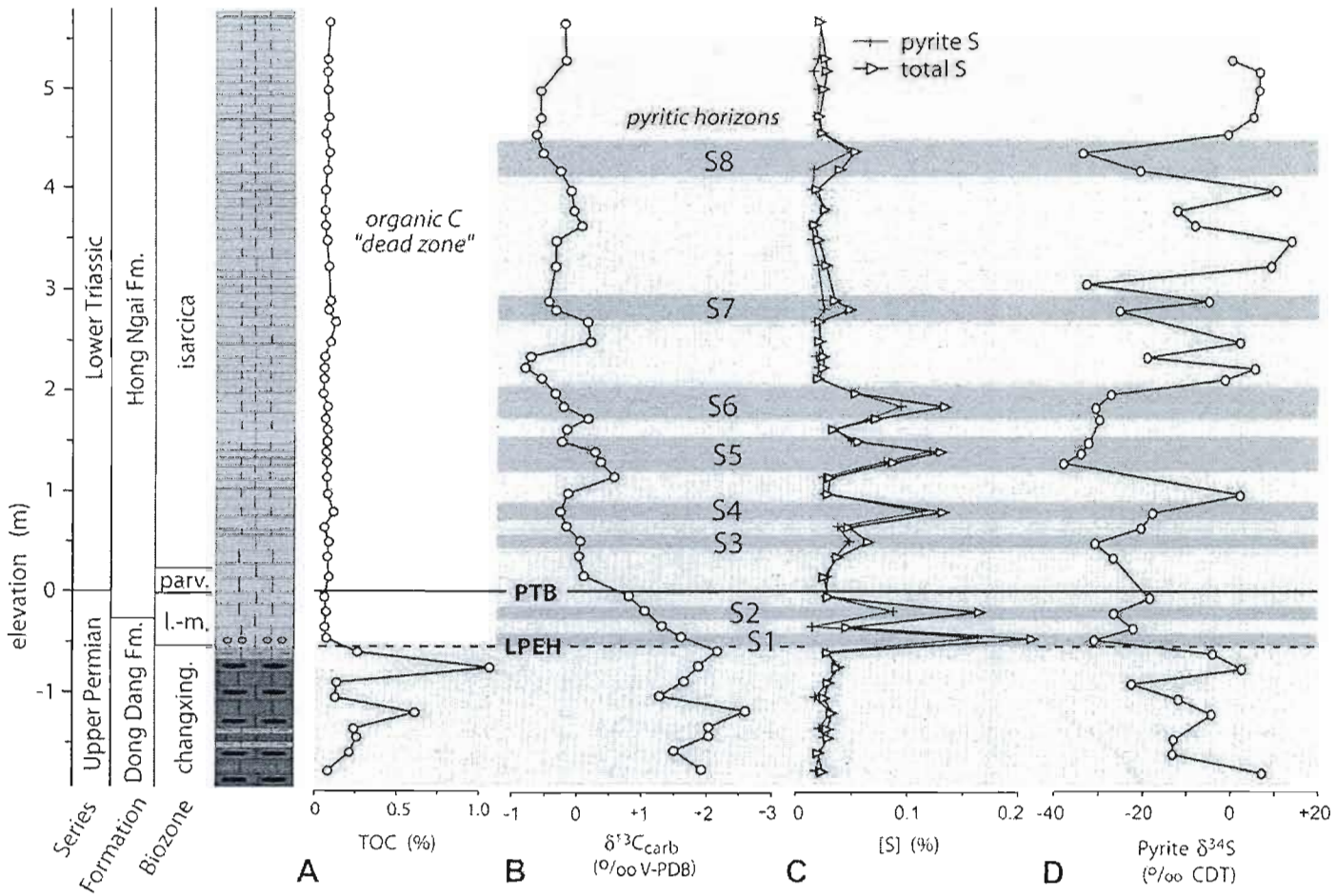
elevation (m)
5
4
3
2
1
0
-1
Series
Formation
Biozone
Upper Permian
Lower Triassic
Dong Dang Fm.
Hong Ngai Fm.
changxing.
isarcica
l.-m.
parv.
organic C
"dead zone"
pyritic horizons
S8
S7
S6
S5
S4
S3
S2
S1
PTB
LPEH
pyrite S
total S
0
0.5
1.0
TOC (%)
A
-1
0
+1
-2
-3
δ13Ccarb
(o/oo V-PDB)
B
0
0.1
0.2
[S] (%)
C
-40
-20
0
+20
Pyrite δ34S
(o/oo CDT)
D

Fig. IV-2

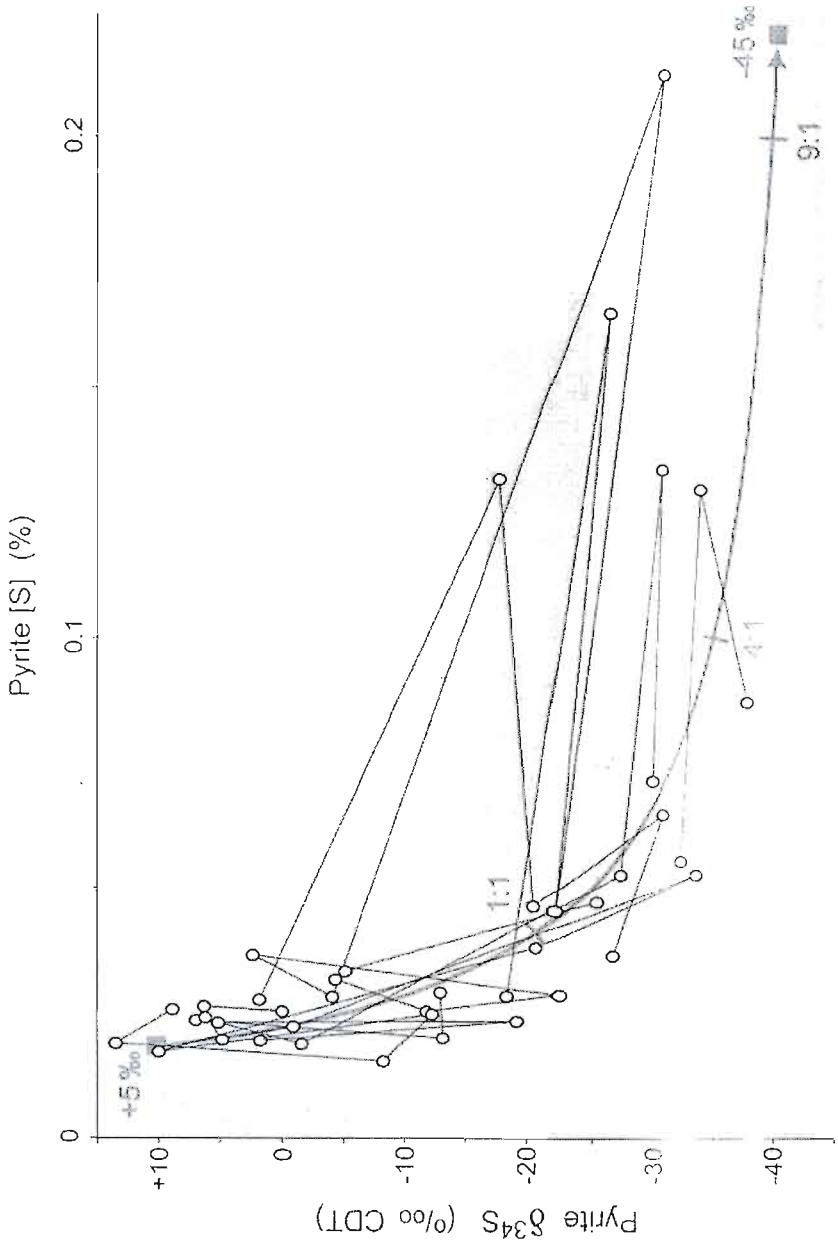

Fig. IV-3

CONCLUSIONS GÉNÉRALES ET PERSPECTIVES

En résumé, les enregistrements géochimiques des échantillons sédimentaires indiquent une série de changements importants dans le climat global et l'environnement océanique à la fin du Néoprotérozoïque, à l'Ordovicien et à la fin du Permien. Intégrés aux données paléontologiques, ces changements environnementaux correspondent, respectivement, à la diversification de la faune d'Édiacara (EBB), à l'événement de diversification de l'Ordovicien inférieur et moyen (GOBE), aux extinctions de masse de l'Ordovicien (GOME) et à la frontière P-T (PTME). Ainsi, il peut être conclu que ces changements environnementaux pourraient avoir agi de façon significative sur ces évènements biologiques majeurs. L'oxygénation progressive des eaux de fond indiquée par les compositions isotopiques de Fe et de S pourrait avoir déclenchée le EBB. Une période de refroidissement suggérées par une variation positive du $\delta^{13}C$ pourrait avoir contribué au début du GOBE. Ainsi, le climat froid et les changements des conditions redox, suggérées par les rapports isotopiques de C et S, ont pu jouer un rôle important dans le GOME. La remontée des eaux profondes anoxiques aurait pu servir comme mécanisme de déclenchement pour l'extinction de masse à la fin du Permien.

Le niveau de pCO_2 atmosphérique a un impact significatif sur les changements climatiques, la productivité du phytoplancton, le pH et les conditions redox de l'eau de mer. Berner (1990) a décrit une courbe sommaire (sur une échelle de 50 Ma) de la concentration de CO_2 atmosphérique pour le Phanérozoïque basée sur l'observation des changements de l isotope du carbone, permettant de comprendre les changements chroniques de pCO_2 atmosphérique au cours du Phanérozoïque. Toutefois, il y a très peu de données quantitatives et détaillées sur la concentration en CO_2 atmosphérique du Paléozoïque puisque le celles-ci sont difficilement mesurables. Bien que les changements de la productivité marine soient cruciaux pour le cycle du carbone et l'évolution animale, il est difficile de bien décrire les changements océaniques à la fin du Précambrien et au Paléozoïque inférieur. Les isotopes de d'oxygène présents dans les sulfates ont été utilisés pour définir la concentration de CO_2 atmosphérique et pour déduire la productivité à la fin du Précambrien et au début du Cambrien (Bao et al., 2008, 2009). Ce travail apporte de nouvelles perspectives sur la concentration de CO_2 atmosphérique à l'échelle des temps géologiques. Habituellement, la

mesure précise de la paléotempérature pour les échantillons géologiques les plus anciens n'est pas une chose facile, en raison de nombreux débats concernant les durées et les transitions des événements climatiques majeurs à l'échelle géologique, telle que la durée de la glaciation de la fin de l'Ordovicien. Dans le but de préciser les paléotempératures de l'Ordovicien, une microsonde à haute-résolution (SHRIMP) a été utilisée par mesurer les compositions isotopiques de l'oxygène de microfossiles de l'Ordovicien, comme les conodontes (Trotter et al., 2008). Ce travail a établi un nouveau protocole pour mesurer fiablement les paléotempératures d'échantillons géologiques anciens. Comme les changements climatiques, les niveaux de O_2 atmosphériques et océaniques ont joué un rôle important dans les premières évolution animales. Des isotopes de triple-soufre des roches sédimentaires ont été utilisés avec succès pour examiner l'évolution de la concentration en O_2 atmosphérique à la fin de l'Archéen et du Protérozoïque inférieur (e.g., Farquhar et al., 2000). La spéciation du Fe a déjà été employée pour déterminer l'état redox de l'océan au Protérozoïque (e.g., Canfield 1998). En outre, quelques éléments traces (e.g., Mo, V, Ni, Ce) et leurs rapports isotopiques (e.g., $^{98}Mo/^{95}Mo$, $^{187}Os/^{188}Os$) sont également utiles pour définir les états redox de l'eau de fond dans les océans précambriens et paléozoïques. À l'avenir, des investigations géochimiques plus détaillées devraient être faites pour micux définir la pCO_2 atmosphérique, la bioproductivité, les niveaux d'O_2 océaniques et atmosphériques, et les paléotempératures pour bien comprendre influence environnementale sur l'évolution animale de la fin du Précambrien et du Paléozoïque inférieur sur Terre.

BIBLIOGRAPHIE GÉNÉRALE

Aitken JD, 1989. Uppermost Proterozoic formations in central Mackenzie Mountains, Northwest Territories. *Geol Surv Can Bull* 368, 1-26.

Aitken JD, 1991. The Ice Brook Formation and post-Rapitan, Late Proterozoic glaciation, Mackenzie Mountains, Northwest Territories. *Geol Surv Can Bull* 404, 1-43.

Algeo, T.J., Wilkinson, B.H., Lohmann, K.C., 1992. Meteoric-burial diagenesis of Pennsylvanian carbonate: water/rock interactions and basin geothermics. J. Sediment. Petrol. 62, 652-670.

Algeo, T.J., Scheckler, S.E., 1998. Terrestrial-marine teleconnections in the Devonian: links between the evolution of land plants, weathering processes and marine anoxic events. Philos. Trans. R. Soc. Lond. (B) Biol. Sci. 353, 113-128.

Algeo, T. J., B. B. Ellwood, T. K. T. Nguyen, H. Rowe, and J. B. Maynard, 2007. The Permian-Triassic boundary at Nhi Tao, Vietnam: Evidence for recurrent influx of sulfidic watermasses to a shallow-marine carbonate platform. Palaeogeogr. Palaeoclimatol. Palaeoecol., 252, 304–327, doi:10.1016/j.palaeo.2006.11.055.

Arthur, M. A., Dean, W. E., Pratt, L. M., 1988. Geochemical and climatic effects of increased marine organic carbon burial at the Cenomanian/Turonian boundary. Nature 335, 714-717.

Bao, H., Lyons, J. R., Zhou, C., 2008. Triple oxygen isotope evidence for elevated CO_2 levels after a Neoproterozoic glaciation. Nature 453, 504-506.

Bao H., Fairchild I.J., Wynn P.M., Spötl C., 2009. Streching the Envelope of Past surface environments: Neoproterozoic glacial lakes from Svalbard. Science 323, 119-122.

Baud, A., W. T. Holser, and M. Magaritz, 1989. Permian-Triassic of the Tethys: Carbon isotope studies. Geol. Rundsch. 78, 649–677.

Becker, L., R. J. Poreda, A. G. Hunt, T. E. Bunch, and M. Rampino, 2001. Impact event at the Permian-Triassic boundary: Evidence from extraterrestrial noble gases in fullerenes. Science 291, 1530–1533.

Bergström, S.M., Chen, X., Schmitz, B., Young, S, Rong, J., Saltzman, M.R., 2009. First documentation of the Ordovician Guttenberg $\delta^{13}C$ excursion (GICE) in Asia: chemostratigraphy of the Pagoda and Yanwashan formations in southeastern China. Geol. Mag. 146, 1-11.

Berkner LV, Marshall J, 1965. On origin and rise of oxygen concentration in Earth's atmosphere. *J Atmos Sci* 22, 225-261.

Berner R.A., 1990. Atmospheric carbon dioxide levels over Phanerozoic time. Science 249, 1382-1386.

Berner, R.A., Kothavala, Z., 2001. GEOCARB III: A revised model of atmospheric CO_2 over Phanerozoic time. Am. J. Sci. 301, 182-204.

Berner, R. A., 2002. Examination of hypotheses for the Permo-Triassic boundary extinction by carbon cycle modeling. Proc.Natl. Acad. Sci. U.S.A. 99, 4172–4177.

Bowring, S. A., D. H. Erwin, Y. G. Jin, M. W. Martin, K. Davidek, and W. Wang, 1998. U/Pb zircon geochronology and tempo of the end-Permian mass extinction. Science 280, 1039–1045.

Bottjer, D.J., Droser, M.L., Sheehan, P.M., McGhee Jr., G.R., 2001. The ecological architecture of major events in the Phanerozoic history of marine life. In: Allmon, W.D., Bottjer, D.J. (Eds.), Evolutionary Paleoecology. The Ecological Context of Macroevolutionary Change. Columbia Univ. Press, pp. 35–61.

Bottjer DJ, Clapham ME, 2006. in: *Neoproterozoic Geobiology and Paleobiology,* eds Xiao S, Kaufman AJ (Springer, Dordrecht, Netherlands), pp 91-114.

Bowring SA, Myrow P, Landing E, Ramenzani J, 2003. Geochronological constraints on terminal Neoproterozoic events and the rise of Metazoans. *NASA Astrobiol Inst (NAI Gen Mtg Abstr)*:113-114.

Brenchley, P.J., Romano, M., Young, T.P., Stoch, P., 1991. Hirnatian glaciomarine diamicties-evidence for the spread of glaciation and its effect on Ordovician faunas. Geol. Surv. Can. 90-9,325-336.

Brenchley, P.J., Marshall, J.D., Carden, G.A.F., Robertson, D.B.R., Long, D.G.F., Meidla, T., Hints, L., Anderson, T.F.,1994. Bathymetric and isotopic evidence for a short-lived Late Ordovician glaciation in a greenhouse period. Geology 22, 295-298.

Brenchley, P.J., Carden, G.A.F., Marshall, J.D., 1995. Environmental changes associated with the 'first strike' of the Late Ordovician mass extinction. Modern Geology 20, 69-82.

Brenchley, P.J., Marshall J.D., 1999. Relative timing of critical events during the late Ordovician mass extinction-new data from Oslo. Acta Univ. Carol. Geol. 43,187-190.

Brenchley, P.J., Carden, G.A, Hints, L., Kaljo, D, Marshall, J.D., Martma T, Meidla, T., Nolvak J, 2003. High-resolution stable isotope stratigraphy of Upper Ordovician sequences: Constraints on the timing of bioevents and environmental changes associated with mass extinction and glaciation. Geol. Soc. Am. Bull. 115, 89-104.

Broecker, W. S., and G. H. Denton, 1989. The role of oceanatmosphere reorganizations in glacial cycles. Geochim. Cosmochim. Acta 53, 2465–2501.

Buggisch, W., Keller, M., Lehnert, O., 2003. Carbon isotope record of Late Cambrian to Early Ordovician carbonates of the Argentine Precordillera. Palaeogeogr. Palaeoclimatol. Palaeoecol. 195, 357-373.

Burns SJ, Matter A, 1993. Carbon isotopic record of the latest Proterozoic from Oman. *Eclogae Geol Helv* 86, 595-607.

Burton, K. W., H.-F. Ling, and R.-K. O'Nions, 1997. Closure of the Central American Isthmus and its effect on deep-water formation in the North Atlantic. Nature 386, 382–385.

Butterfield NJ, 2000. *Bangiomorpha pubescens* n. gen., n. sp.: implications for the evolution

of sex, multicellularity, and the Mesoproterozoic/Neoproterozoic radiation of eukaryotes. *Paleobiology* 26, 386-404.

Canfield DE, Raiswell R, Westrich JT, Reaves CM, Berner RA, 1986. The use of chromium reduction in the analysis of reduced inorganic sulfur in sediments and shale. Chemical Geology 54, 149–155.

Canfield DE, 1998. A new model for Proterozoic ocean chemistry. *Nature* 396, 450-453.

Canfield DE, Poulton SW, Narbonne GM, 2007. Late-Neoproterozoic deep-ocean oxygenation and the rise of animal life. *Science* 315, 92-95.

Chen M, Lu G, Xiao Z, 1994. Preliminary study on the algal macrofossils -- Lantian Flora from the Lantian Formation of Upper Sinian in southern Anhui. *Bull Inst of Geology, Academia Sinica* 7, 252-267.

Chen JY, *et al.*, 2004. Small bilaterian fossils from 40 to 55 million years before the Cambrian. *Science* 305, 218-222.

Chen, X., Rong, J., Wang, X., Wang, Z., Zhang, Y., Zhan, R., 1995. Correlation of Ordovician Rocks of China. International Union of Geol. Sci. Publ. 31, pp 104.

Chen, X., Rong, J., Mitchell, C.E., Harper, D.A.T., Fan, J., Zhan, R., Zhang, Y., Li, R., and Wang, Y., 2000. Late Ordovician to earliest Silurian graptolite and branchiopod zonation from Yangtze Region, South China with global correlation. Geological Magazine137, 623-650.

Chen, X., Rong, J., Li, Y., and Boucot, A. J., 2004. Facies patterns and geography of the Yangtze region, South China, through the Ordovician and Silurian transition. Palaeogeography, Palaeoclimatology, Palaeoecology 204, 353-372.

Chen, X., Melchin, M.J., Sheets, H.D., Mitchell, C.E., and Fan, J., 2005a. Patterns and processes of latest Ordovician graptolite extinction and recovery based on data from south China. Journal of Palaeontology 79, 842-861.

Chen, X., Fan, J.X., Melchin, M.J., Mitchell, C.E., 2005b. Hirnantian (latest Ordovician) graptolites from the upper Yangtze region, China. Palaeontology 48, 1-47.

Chen, X., Rong, J., Fan, J., Zhan, R., Mitchell, C., Harper, D.A.T, Melchin, M.J., Peng, P., Finney, S.C., Wang, X., 2006a. The global boundary stratotype section and point for the base of the Hirnantian Stage (the uppermost of the Ordovician System). Episodes 29, 183-196.

Chen, X., Zhang, Y., Fan, J., 2006b. Ordovician graptolite evolutionary radiation: a review. Geo. J. 41, 289–301.

Cramer, B.D., Saltzman, M.R., 2007. Early Silurian paired analyses from the Midcontinent of North America: Implications for paleoceanography and paleoclimate. Palaeogeogr. Palaeoclimatol. Palaeoecol. 256, 195-203.

Crowell, J.C., 1999. Pre-Mesozoic Ice Ages: Their Bearing on Understanding the Climate System. Geol. Soc. Am. Memoir 192, 106 pp.

Cloud P, 1972. Working model of primitive Earth. *Am J Sci* 272:537-548.

Condon D, *et al.*, 2005. U-Pb ages from the Neoproterozoic Doushantuo Formation, China. *Science* 308, 95-98.

Dalrymple RW, Narbonne GM, 1996. Continental slope sedimentation in the Sheepbed Formation (Neoproterozoic, Windermere Supergroup), Mackenzie Mountains, N.W.T. *Can J Earth Sci* 33, 848-862.

Day ES, James NP, Narbonne GM, Dalrymple RW, 2004. A sedimentary prelude to marinoan glaciation, Cryogenian (Middle Neoproterozoic) Keele Formation, Mackenzie Mountains, northwestern Canada. *Precambrian Res* 133, 223-247.

de Wit, M. J., J. G. Ghosh, S. de Villiers, N. Rakotosolofo, J. Alexander, A. Tripathi, and C. Looy, 2002. Multiple organic carbon isotope reversals across the Permo-Triassic boundary of terrestrial Gondwana sequences: Clues to extinction patterns and delayed ecosystem recovery. J. Geol. 110, 227–240.

Droser, M.L., Sheehan, P.M., 1997. Palaeoecology of the Ordovician Radiation; resolution of large-scale patterns with individual clade histories, palaeogeography and environments. Geobios 20, 221–229.

Elliot, M., L. Labeyrie, and J. C. Duplessy, 2002. Changes in North Atlantic deep-water formation associated with the Dansgaard-Oeschger temperature oscillations (60–10 ka). Quat. Sci. Rev. 21, 1153–1165.

Erwin, D. H., 1994. The Permo-Triassic extinction. Nature 367, 231–236.

Erwin, D. H., S. A. Bowring, Y.-G. Jin, 2002. End-Permian mass-extinctions: A review. in Catastrophic Events and Mass Extinctions: Impacts and Beyond, edited by C. Koeberl and K. G. MacLeod, Spec. Pap. Geol. Soc. Am. 356, 353–383.

Fan, J., Peng, P., Melchin, M.J., 2009. Carbon isotopes and event stratigraphy near the Ordovician-Silurian boundary, Yichang, South China. Palaeogeogr. Palaeoclimatol. Palaeoecol. 276, 160-169.

Farquhar, J., Bao, H., Thiemens, M.H., 2000. Atmospheric influence of Earth's earliest sulfphur cycle. Science 289, 756-758.

Fedonkin MA, Waggoner BM, 1997. The Late Precambrian fossil *Kimberella* is a mollusc-like bilaterian organism. *Nature* 388, 868-871.

Fedonkin MA, 2003. The origin of the Metazoa in the light of the Proterozoic fossil record. *Paleont Res* 7, 9-41.

Fike DA, Grotzinger JP, Pratt LM, Summons RE, 2006. Oxidation of the Ediacaran Ocean. *Nature* 444, 744-747.

Finney, S.C., Berry, W.B.N., Cooper, J.D., Ripperdan, R.L., Sweet, W.C., 1999. Late Ordovician mass extinction: a new perspective from stratigraphic sections in central Nevada. Geology 27, 215-218.

Freeman, K.H, 2001. Isotopic biogeochemistry of marine organic carbon. Rev. in Mineral. and Geochem. 43, 579-605.

Fu, K., 1982. The Ordovician of the Yangtze region. In: Lai, C. (Ed.), The Ordovician System of China. Stratigraphy of China 5. Geol. Publ. House, Beijing, pp. 92-131.

Gehling JG, Rigby KJ, 1996. Long expected sponges from the Neoproterozoic Ediacara fauna of South Australia. *J Paleont* 70, 185-195.

Gellatly AM, Lyons TW, 2005. Trace sulfate in mid-Proterozoic carbonates and the sulfur isotope record of biospheric evolution. *Geochim Cosmochim Acta* 69, 3813-3829

Gibbs, M.T., Barron, E.J., Kump, L.R., 1997. An atmospheric pCO2 threshold for 535 glaciation in the Late Ordovician. Geology 27, 447-450.

Goldberg T, Poulton SW, Strauss H, 2005. Sulphur and oxygen isotope signatures of late Neoproterozoic to early Cambrian sulphate, Yangtze Platform, China: Diagenetic constraints and seawater evolution. *Precambrian Res.* 137, 223–241

Goldhaber, M. B., and I. R. Kaplan,1974. The sulfur cycle, in The Sea, vol. 5, Marine Chemistry, edited by E. D. Goldberg, pp. 569–655, John Wiley, New York.

Goodfellow, W.D., and Jonasson, I.R., 1984. Ocean stagnation and ventilation defined by secular trends in pyrite and barite, Selwyn Basin, Yukon. Geology12, 583-586.

Goodfellow, W.D., Nowlan, G.S., McGracken, A.D., Lenz, A.C., Grégoire, D.C., 1992. Geochemical anomalies near the Ordovician-Silurian boundary, north Yukon, Canada. Hist. Biol. 6, 1-23.

Gradstein, F., Ogg, J., Smith, A., 2004. A Geologic Time Scale. Cambridge Univ. Press, pp. 589.

Grice, K., C. Cao, G. D. Love, M. E. Bo¨ttcher, R. J. Twitchett, E. Grosjean, R. E. Summons, S. C. Turgeon, W. Dunning, and Y. Jin, 2005. Photic zone euxinia during the Permian-Triassic superanoxic event. Science 307, 706–709.

Gorjan P, Veevers JJ, Walter MR, 2000. Neoproterozoic sulfur-isotope variation in Australia and global implications. *Precambrian Res* 100, 151-179.

Graham JB, 1988. Ecological and evolutionary aspects of integumentary respiration: Body size, diffusion, and the Invertebrata. *Am Zool* 28, 1031-1045.

Hallam, A., and Wignall, P., 1997, Mass extinctions and their aftermath: Oxford, Oxford University Press, p. 328.

Halverson GP, Hoffman PF, Schrag DP, Maloof AC, Rice AHN, 2005. Toward a Neoproterozoic composite carbon-isotope record. *Geol Soc Am Bull* 117, 1181-1207.

Halverson, GP, 2006. in *Neoproterozoic Geobiology and Paleobiology,* eds Xiao S, Kaufman, AJ (Springer, Dordrecht, Netherlands), pp 231-271.

Halverson GP, Hurtgen MT, 2007. Ediacaran growth of the marine sulfate reservoir. *Earth Planet Sci Lett* 263, 32-44.

Harland WB, Rudwick MJS, 1964. The great infra-Cambrian ice age. *Sci Am* 211, 28-36.

Hayes J.M., Popp B.N., Takigiku 540 R., Johnson M.W., 1989. An isotopic study of biogeochemical relationships between carbonates and organic carbon on the Greenhorn Formation. Geochim. Cosmochim. Acta 68, 4363-4379.

Hayes JM, Lambert IB, Strauss H, 1992. in *The Proterozoic Biosphere: A Multidisciplinary Study,* eds Schopf JW, Klein C (Cambridge University Press, Cambridge), pp 129-132.

Hayes, J.M., Strauss, H., Kaufman, A.J, 1999. The abundance of ^{13}C in marine organic matter and isotopic fractionation in the global biogeochemical cycle of carbon during the past 800 Ma. Chem. Geol. 161, 103-125.

Hays, L. E., T. Beatty, C. M. Henderson, G. D. Love, and R. E. Summons, 2007. Evidence for photic zone euxinia through the end-Permian mass extinction in the Panthalassic Ocean (Peace River Basin, Western Canada). Palaeoworld 16, 39–50.

Herrmann, A.D., Patkowsky, M.E., Pollard, D., 2003. Obliquity forcing with 8-12 times preindustrial levels of atmospheric pCO_2 during the Late Ordovician glaciation. Geology 31, 485-488.

Hillaire-Marcel, C., A. de Vernal, G. Bilodeau, and A. J. Weaver, 2001. Absence of deep-water formation in the Labrador Sea during the last interglacial period. Nature 410, 1073–1077.

Hofmann HJ, Narbonne GM, Aitken JD, 1990. Ediacaran remains from intertillite beds in Northwestern Canada. *Geology* 18, 1199-1202.

Hoffman PF, Schrag DP, 2002. The snowball Earth hypothesis: testing the limits of global change. *Terra Nova* 14, 129-155.

Hotinski, R. M., K. L. Bice, L. R. Kump, R. G. Najjar, and M. A. Arthur, 2001. Ocean stagnation and end-Permian anoxia. Geology 29, 7–10.

Hurtgen MT, Arthur MA, Suits NS, Kaufman AJ, 2003. The sulfur isotopic composition of Neoproterozoic seawater sulfate: implications for a snowball Earth? *Earth Planet Sci Lett* 203, 413-429.

Hurtgen MT, Arthur MA, Halverson GP, 2005. Neoproterozoic sulfur isotopes, the evolution of microbial sulfur species, and the burial efficiency of sulfide as sedimentary pyrite. *Geology* 33, 41-44.

Hurtgen MT, Halverson GP, Arthur MA, Hoffman PF, 2006. Sulfur cycling in the aftermath of a 635-Ma snowball glaciation: Evidence for a syn-glacial sulfidic deep ocean. *Earth Planet Sci Lett* 245, 551-570.

Ingalls, A.E, Aller, R. C., Lee, C., Wakeham S.G., 2004. Organic matter diagenesis in shallow water carbonate sediments. Geochim. Cosmochim. Acta 68, 4363-4379.

Isozaki, Y., 1997. Permo-Triassic boundary superanoxia and stratified superocean: Records from lost deep sea. Science 276, 235–238.

Jablonski, D., 1991. Extinctions: a paleontological perspective. Science 253, 754-57.

James NP, Narbonne GM, Kyser TK, 2001. Late Neoproterozoic cap carbonates: Mackenzie

Mountains, northwestern Canada: precipitation and global glacial meltdown. *Can J Earth Sci* 38, 1229-1262.

Johnston DT, *et al.*, 2005. Active microbial sulfur disproportionation in the Mesoproterozoic. *Science* 310, 1477-1479.

Jørgensen BB, Böttcher ME, Lüschen H, Neretin LN, Volkov II, 2004. Anaerobic methane oxidation and a deep H_2S sink generate isotopically heavy sulfides in Black Sea sediments. *Geochim Cosmochim Acta* 68, 2095-2118

Kah LC, Lyons TW, Frank TD, 2004. Low marine sulphate and protracted oxygenation of the Proterozoic biosphere. *Nature* 431, 834-838.

Kaiho, K., T. Kajiwara, T. Nakano, Y. Muira, H. Kawahata, K. Tazaki, M. Ueshima, Z. Chen, and G. R. Shi, 2001. End-Permian catastrophe by a bolide impact: Evidence of a gigantic release of sulfur from the mantle. Geology 29, 815–818.

Kaiho, K., Z.-Q. Chen, H. Kawahata, Y. Kajiwara, and H. Sato, 2006. Close-up of the end-Permian mass extinction horizon recorded in the Meishan section, south China: Sedimentary, elemental, and biotic characterization and a negative shift of sulfate sulfur isotope ratio. Palaeogeogr. Palaeoclimatol. Palaeoecol. 239, 396–405.

Kajiwara, Y., S. Yamakita, K. Ishida, H. Ishiga, and A. Imai, 1994. Development of a largely anoxic stratified ocean and its temporary massive mixing at the Permian-Triassic boundary supported by the sulfur isotope record. Palaeogeogr. Palaeoclimatol. Palaeoecol. 111, 367–379.

Kakuwa, Y., and R. Matsumoto, 2006. Cerium negative anomaly just before the Permian and Triassic boundary event: The upward expansion of anoxia in the water column. Palaeogeogr. Palaeoclimatol. Palaeoecol. 229, 335–344.

Kaljo, D., Hints, L., Hints, O., Martma, T., Nolvok, J., 1999. Carbon isotope excursions and coeval environmental and biotic changes in the Late Caradoc and Ashgill of Estonia. Acta Univ. Carol. Geol. 43, 507-510.

Kaljo, D., Hints, L., Martma, T., Nõlvak, J., 2001. Carbon isotope stratigraphy in the latest Ordovician of Estonia. Chemical Geology 175, 49-59.

Kaljo, D., Hints, L., Martma, T., Nõlvak, J., Oraspõld, A., 2004. Late Ordovician carbon isotope trend in Estonia, its significance in stratigraphy and environmental analysis. Palaeogeography, Palaeoclimatology, Palaeoecology 210, 165-185.

Kaljo, D., Martma, T., Saadre, T., 2007. Post-Hunnebergian Ordovician carbon isotope trend in Baltoscandia, its environmental implications and some similarities with that of Nevada. Palaeogeogr. Palaeoclimatol. Palaeoecol. 245, 138–155

Kaufman AJ, Knoll AH, Narbonne GM, 1997. Isotopes, ice ages, and terminal Proterozoic earth history. *Proc Natl Acad Sci USA* 94, 6600-6605.

Kershaw, S., L. Guo, A. Swift, and J.-S. Fan, 2002. Microbialites in the Permian-Triassic boundary interval in central China: Structure, age and distribution. Facies 47, 83–90.

Kiehl, J. T., and C. A. Shields, 2005. Climate simulation of the latest Permian: Implications for mass extinction. Geology 33, 757–760.

Knoll AH, Hayes JM, Kaufman AJ, Swett K, Lambert IB, 1986. Secular variation in carbon isotope ratios from Upper Proterozoic successions of Svalbard and East Greenland. *Nature* 321, 832-838.

Knoll, A. H., R. K. Bambach, D. E. Canfield, and J. P. Grotzinger, 1996. Comparative Earth history and Late Permian mass extinction. Science 273, 452–457.

Knoll AH, Caroll SB, 1999. The early evolution of animals: emerging views from comparative biology and geology. *Science* 284, 2129-2137.

Knoll AH, Walter MR, Narbonne GM, Christie-Blick N, 2006. The Ediacaran Period: a new addition to the geologic time scale. *Lethaia* 39, 13-30.

Knoll, A.H., Bambach, R.K., Payne, J.L., Pruss, S., Fischer, W.W., 2007, Paleophysiology and end-Permian mass extinction. Earth and Planetary Science Letters 256, 295–313.

Korte, C., H. W. Kozur, M. M. Joachimski, H. Strauss, J. Veizer, and L. Schwark, 2004. Carbon, sulfur, oxygen and strontium isotope records, organic geochemistry and biostratigraphy across the Permian/Triassic boundary in Abadeh, Iran. Int. J. Earth Sci. 93, 565–581.

Korte, C., P. Pande, P. Kalia, H. W. Kozur, M. M. Joachimski, and H. Oberhänsli, 2008. Massive volcanism at the Permian- Triassic boundary and its impact on the isotopic composition of the ocean and atmosphere. J. Asian Earth Sci.37, 293-311.

Krull, E. S., and G. J. Retallack, 2000. δ^{13}Corg depth profiles from paleosols across the Permian-Triassic boundary: Evidence for methane release. Geol. Soc. Am. Bull. 112, 1459–1472.

Krull, E. S., D. J. Lehrmann, D. Druke, B. Kessel, Y. Yu, and R. Li, 2004. Stable carbon isotope stratigraphy across the Permian-Triassic boundary in shallow marine carbonate platforms, Nanpanjiang Basin, south China. Palaeogeogr. Palaeoclimatol. Palaeoecol. 204, 297–315.

Kump, L.R., Arthur, M.A., 1999. Interpreting carbon-isotope excursions: carbonates and organic matter. Chem. Geol. 161, 181-198.

Kump, L.R., Arthur, M.A., Patzkowsky, M.E., Gibbs, M.T., Pinkus, D.S., Sheehan, P.M., 1999. A weathering hypothesis for glaciation at high atmospheric pCO_2 during the Late Ordovician. Palaeogeography, Palaeoclimatology, Palaeoecology 152,173–187.

Kump, L. R., A. Pavlov, and M. A. Arthur, 2005. Massive release of hydrogen sulfide to the surface ocean and atmosphere during intervals of oceanic anoxia. Geology 33, 397–400.

Kump LR, Seyfried WE, 2005. Hydrothermal Fe fluxes during the Precambrian: effect of low oceanic sulfate concentrations and low hydrostatic pressure on the composition of black smokers. *Earth Planet Sci Lett* 235:654-662.

Le Guerroué E, Allen PA, Cozzi A, Etienne JL, Fanning M, 2006. 50 Myr recovery from the

largest negative $\delta^{13}C$ excursion in the Ediacaran ocean. *Terra Nova* 18, 147-153.

Kutzbach, J. E., P. J. Guetter, and W. M. Washington, 1990. Simulated circulation of an idealized ocean for Pangaean time. Paleoceanography 5, 299–317.

Lehrmann, D. J., J. L. Payne, S. V. Felix, P. M. Dillett, H.Wang, Y. Yu, and J.Wei, 2003. Permian-Triassic boundary sections from shallow-marine carbonate platforms of the Nanpanjiang Basin, south China: Implications for oceanic conditions associated with the end-Permian extinction and its aftermath. Palaios 18, 138–152.

Li C, Chen JY, Hua T, 1998. Precambrian sponges with cellular structures. *Science* 279, 879-882.

Logan GA, Hayes JM, Hieshima GB, Summons R, 1995. Terminal Proterozoic reorganization of biogeochemical cycles. *Nature* 376, 53-56.

Lohmann, K.C, Walker, J.C.G., 1989. The $\delta^{18}O$ record of Phanerozoic abiotic marine calcite cements. Geophys. Res. Lett. 16, 319-322.

Long, D.G.F., 1993. Oxygen and carbon isotopes and event stratigraphy near the Ordovician—Silurian boundary, Anticosti Island Quebec. Palaeogeography, Palaeoclimatology, Palaeoecology 104, 49-59.

Love GD, *et al.*, 2006. Constraining the timing of basal metazoan radiation using molecular biomarkers and U-Pb isotope dating. *Geochim Cosmochim Acta (Goldschmidt Conf Abstr Suppl)* 70, A371.

Ludvigson, G.A., Witzke, B.J., Gonzalez, L.A., Carpenter, S.J., Schneider, C.L., Hasiuk, F., 2004. Late Ordovician (Turinian-Chatfieldian) carbon isotope excursions and their stratigraphic and paleoceanographic significance. Palaeogeogr. Palaeoclimatol. Palaeoecol. 210, 187-214.

Lyons TW, Severmann S, 2006. A critical look at iron paleoredox proxies based on new insights from modern euxinic marine basins. *Geochim Cosmochim Acta* 70, 5698-5722.

Marshall, J.D., Brenchley, P.J., Mason, P., Wolff, G.A., Astini, R.A., 1997. Global carbon isotopic events associated with mass extinction and glaciation in the Late Ordovician. Palaeogeography, Palaeoclimatology, Palaeoecology 132,195-210.

McCrea J.M, 1950. The isotope chemistry of carbonates and a paleotemperature scale. Journal of Chemical Physics 63, 563-566.

Melchin, M.J., Holmden, C., 2006. Carbon isotope chemostratigraphy in Arctic Canada: Sea-level forcing of carbonate platform weathering and implications for Hirnantian global correlation. Palaeogeography, Palaeoclimatology, Palaeoecology 234, 186-200.

Miller, A.I., 1997. Dissecting global diversity trends: examples from the Ordovician radiation. Ann. Rev. Ecology and Systematics 28, 85– 104.

Mitchell, C.E., Sheets, H.D, Belscher, K, Finney, S., Holmden ,C, Laporte, D.F., Melchin, M.J., Patterson W.P., 2007. Species abundance changes during mass extinction and the inverse signor-lipps effect: apparently abrupt graptolite mass extinction as an artifact of

sampling. Acta Palaeontologica Sinica 46 (Suppl.), 340-346.

Mu, E., 1980, Research on the graptolithina of China. Acta Palaeontologica Sinica 19, 143-151 (in Chinese with English abstract).

Mu, E., Li, J., Ge, M., Chen, X., Ni, Y., Lin, Y., 1981. Late Ordovician paleogeography of South China. Acta Stratigraphy Sinica 5, 165-170.

Mu, E., 1988, The Ordovician-Silurian boundary in China. Bulletin of British Museum of Natural History (Geology) 43, 117-131.

Mundil, R., K. R. Ludwig, I. Metcalfe, and P. R. Renne, 2004. Age and timing of the Permian mass extinctions: U/Pb dating of closed-system zircons. Science 305, 1760–1763.

Narbonne GM, Aitken JD, 1990. Ediacaran fossils from the Sekwi Brook area, Mackenzie Mountains, Northwestern Canada. *Palaeontology* 33, 945-980.

Narbonne GM, 1994. New Ediacaran fossils from the MacKenzie Mountains, Northwestern Canada. *J Paleont* 68, 411-416.

Narbonne GM, Kaufman AJ, Knoll AH, 1994. Integrated chemostratigraphy and biostratigraphy of the Windermere Supergroup, Northwestern Canada – Implications for Neoproterozoic correlations and the early evolution of animals. *Geol Soc Am Bull* 106, 1281-1292.

Narbonne GM, Aitken JD, 1995. Neoproterozoic of the Mackenzie Mountains, northwestern Canada. *Precambrian Res* 73, 101-121.

Narbonne GM, Gehling JG, 2003. Life after snowball: The oldest complex Ediacaran fossils. *Geology* 31, 27-30.

Narbonne GM, 2005. The Ediacara biota: Neoproterozoic origin of animals and their ecosystems. *Annu Rev Earth Planet Sci* 33, 421-442.

Newton, R. J., E. L. Pevitt, P. B. Wignall, and S. H. Bottrell, 2004. Large shifts in the isotopic composition of seawater sulphate across the Permo-Triassic boundary in northern Italy. Earth Planet. Sci. Lett. 218, 331–345.

Nielsen, J. K., and Y. Shen, 2004. Evidence for sulfidic deep water during the Late Permian in the East Greenland Basin. Geology 32, 1037–1040.

Nursall JR, 1959. Oxygen as a prerequisite to the origin of the Metazoa. *Nature* 183, 1170-1172.

Orth, C.J., Gilmore, J.S., Quintana, L.R., Sheehan, P.M., 1986. The terminal Ordovician extinction: Geochemical analysis of the Ordoviciane/Silurian boundary, Anticosti Island, Quebec. Geology 14, 433-436.

Pancost, R.D., Freeman, K.H., Patzkowsky, M.E., 1999. Organic-matter source variation and the expression of a late Middle Ordovician carbon isotope excursion. Geology 27, 1015-1018.

Patzkowsky, M.E., Slupik, L.M., Arthur, M.A., Pancost, R.D., Freeman, K.H., 1997. Late Middle Ordovician environmental change and extinction: Harbinger of the Late Ordovician or continuation of Cambrian patterns? Geology 25, 911-914.

Payne, J. L., D. J. Lehrmann, J. Wei, M. J. Orchard, D. P. Schrag, and A. H. Knoll, 2004. Large perturbations of the carbon cycle during recovery from the end-Permian extinction. Science 305, 506–509.

Payne, J. L., D. J. Lehrmann, D. Follett, M. Seibel, L. R. Kump, A. Riccardi, D. Altiner, H. Sano, and J. Wei, 2007. Erosional truncation of uppermost Permian shallow-marine carbonates and implications for Permian-Triassic boundary events. Geol. Soc. Am. Bull. 119, 771–784.

Poulton SW, Fralick PW, Canfield DE, 2004. The transition to a sulfidic ocean ~1.84 billion years ago. *Nature* 431, 173-177.

Qing, H., Veizer, J., 1994. Oxygen and carbon isotopic composition of Ordovician brachiopods: Implications for coeval seawater. Geochimica et Cosmochimica Acta 58, 4429-4442.

Raiswell R, Canfield DE, 1998. Sources of iron for pyrite formation in marine sediments. *Am J Sci* 298, 219-245.

Raiswell R, Newton R, Wignall PB, 2001. An indicator of water-column anoxia: Resolution of biofacies variations in the Kimmeridge Clay (Upper Jurassic, UK). *J Sediment Res* 71, 286-294.

Renne, P. R., Z. C. Zheng, M. A. Richards, M. T. Black, and A. R. Basu, 1995. Synchrony and causal relations between Permian-Triassic boundary crisis and Siberian flood volcanism. Science 269, 1413–1416.

Retallack, G. J., 1995. Permian-Triassic extinction on land. Science 267, 77–80.

Riccardi, A. L., M. A. Arthur, and L. R. Kump, 2006. Sulfur isotopic evidence for chemocline upward excursions during the end-Permian mass extinction. Geochim. Cosmochim. Acta 70, 5740–5752.

Riccardi, A., L. R. Kump, M. A. Arthur, and S. D'Hondt, 2007. Carbon isotopic evidence for chemocline upward excursions during the end-Permian event. Palaeogeogr. Palaeoclimatol. Palaeoecol. 248, 73–81.

Rong, J., Harper, D.A.T., 1988. A global synthesis of the latest Ordovician Hirnantian brachiopod faunas. Trans. Roy. Soc. Edinburgh (Earth Sci.) 79, 383-402.

Rong, J., Zhan, R., Harper, D.A.T., 1999. Late Ordovician (Caradoc-Ashgill) brachiopod faunas with Foliomena based on data from China. Palaio 14, 412-431.

Rong, J., Chen, X., Harper, D.A.T., 2002. The latest Ordovician Hirnantia Fauna (Brachiopoda) in time and space. Lethaia 35, 231-249.

Royer, D.L., 2006. CO_2-forced climate thresholds during the Phanerozoic. Geochim. Cosmochim. Acta 70, 5665-5675.

Runnegar B, 1982. Oxygen requirements, biology and phylogenetic significance of the late Precambrian worm Dickinsonia, and the evolution of the burrowing habit. *Alcheringa* 6, 223-239.

Saltzman, M. R., 2005. Phosphorus, nitrogen, and the redox evolution of the Paleozoic oceans. Geology 33, 573-576.

Saltzman, M. R., Young, S.A., 2005. Long-lived glaciation in the Late Ordovician? Isotopic and sequence-stratigraphic evidence from western Laurentia. Geology 33, 109-112.

Schmitz, B., Harper D.A.T., Peucker-Ehrenbrink B., Stouge S., Alwmark C.,Cronholm A., Bergstrom S.M., Tassinari M., Wang X., 2008. Asteroid breakup linked to the Great Ordovician Biodiversification Event. Nature Geoscience 1, 49-53.

Sephton, M. A., H. Brinkhuis, C. V. Looy, R. J. Veefkind, H. Visscher, and J. W. de Leeuw, 2002. Synchronous record of $\delta^{13}C$ shifts in the oceans and atmosphere at the end of the Permian, in Catastrophic Events and Mass Extinctions: Impacts and Beyond, edited by C. Koeberl and K. G. MacLeod, Spec. Pap., Geol. Soc. Am. 356, 455-462.

Sepkoski, J.J., 1991. Diversity in the Phanerozoic oceans: a partisan review. See Dudley 1991, 1: 210-236.

Sepkoski, J.J., 1996. Patterns of Phanerozoic extinction: a perspective from global data bases. In: Walliser O. H. (Ed.), Global Events and Event Stratigraphy in the Phanerozoic. Springer, Berlin, pp. 35-51.

Sepkoski, J.J., 1997. Biodiversity: past, present and future. J. Paleontol. 71, 533–539.

Servais, T., Harper, D.A.T., Li, J., Munnecke, A., Owen, A.W., Sheehan, P.M., 2009. Understanding the Great Ordovician Biodiversification Event (GOBE): Influences of paleogeography, paleoclimate, or paleoecology? GSA Today 19, 4-10.

Sheehan, P.M., 2001. The Late Ordovician mass extinction. Ann. Rev. Earth and Planetary Sci. 29, 331-364.

Shen Y, Canfield DE, Knoll AH, 2002. Middle Proterozoic ocean chemistry: Evidence from the McArthur Basin, northern Australia. *Am J Sci* 302, 81-109.

Shen Y, Knoll AH, Walter MR, 2003. Evidence for low sulphate and anoxia in a mid Proterozoic marine basin. *Nature* 423, 632-635.

Shen Y, Buick R, 2004. The antiquity of microbial sulfate reduction. *Earth-Sci Rev* 64, 243-272.

Shields, G.A., Garden, G.A.F., Veizer, J., Meidla, T., Rong, J., Li, R., 2003. Sr, C, and O isotope geochemistry of Ordovician brachiopods: A major isotope event around the Middle-Late Ordovician transition. Geochim. Cosmochim. Acta 67, 2005-2025.

Son, T. H., C. Koeberl, N. L. Ngoc, and D. T. Huyen, 2007. The Permian-Triassic boundary sections in northern Vietnam (Nhi Tao and Lung Cam sections): Carbon-isotope excursion and elemental variations indicate major anoxic event. Palaeoworld 16, 51–66.

Stanley, S.M., 1984. Temperature and biotic crises in the marine realm. Geology 12, 205-208.

Strauss, H., 1997, The isotopic composition of sedimentary sulfur through time. Palaeogeography, Palaeoclimatology, Palaeoecology 132, 97-118.

Strauss H, 2002. in *Precambrian Sedimentary Environments: A Modern Approach to Ancient Depositional Systems,* eds Altermann W, Corcoran PL (Blackwell Science, Oxford), pp 67-105.

Sun WG, 1986. Late Precambrian pennatulids (sea pens) from the eastern Yangtze Gorge, China: *Paracharnia* gen. nov. *Precambrian Res* 31, 361-375.

Towe KM, 1970. Oxygen-collagen priority and early metazoan fossil record. *Proc Natl Acad Sci USA* 65, 781-788.

Trotter, J.A., Williams, I.S., Barnes, C.R., Lecuyer, C., Nicoll, R, S., 2008. Did cooling oceans trigger Ordovician biodiversification? Evidence from conodont thermometry. Science 321, 550-554.

Twitchett, R. J., C. V. Looy, R. Morante, H. Visscher, and P. B. Wignall, 2001. Rapid and synchronous collapse of marine and terrestrial ecosystems during the end-Permian biotic crisis. Geology 29, 351–354.

Underwood, C.J., Crowley, S.F., Marshall, J.D., and Brenchley, P.J., 1997, High-resolution carbon isotope stratigraphy of the basal Silurian stratotype (Dob's Linn, Scotland) and its global correlation. Journal of Geological Society London154,709-718.

Wang, H., 1985. Atlas of the Paleogeography of China. Cartographic Publ. House, Beijing, pp.143

Wang, H., Chen, J., 1991. Late Ordovician and early Silurian rugose coral biogeography and world reconstruction of palaeocontinents. Palaeogeogr. Palaeoclimatol. Palaeoecol. 86, 3-21.

Wang, K., Orth, C.J., Attrep, M., Chatterton, B.D.E., Wang, X., Li, J., 1993a. The great latest Ordovician extinction on the South China Plate: Chemostratigraphic studies of the Ordovician-Silurian boundary interval on the Yangtze platform. Palaeogeogr. Palaeoclimatol. Palaeoecol. 104, 61-79.

Wang, K., Chatterton, B.D.E., Attrep, M., Orth, C.J., 1993b. Late Ordovician mass extinction in the Selwyn Basin, northwestern Canada. Can. J. Earth Sci. 30, 1870-1880.

Wang, K., Chatterton, B.D.E., Wang, Y., 1997. An organic carbon isotope record of Late Ordovician to Early Silurian marine sedimentary rocks, Yangtze Sea, South China: Implications for CO_2 changes during the Hirnantian glaciation. Palaeogeogr. Palaeoclimatol. Palaeoecol. 132, 147-158.

Wang, X., Hoffknecht, A., Xiao, J., Chen, S., Li, Z., Broche, R.B., Erdtmamm, B.D.,1993. Graptolite, chitinozoan and scolecodont reflectances and their use as indicators of thermal maturity. Acta Geol. Sinica 6, 93-105.

Webby, B.D., Paris, F., Droser, M.L.(eds.), 2004. The Great Ordovician Biodiversification Event. Columbia University Press, New York, pp.1-484.

Wignall, P. B., and R. J. Twitchett, 1996. Oceanic anoxia and the end Permian mass extinction. Science 272, 1155–1158.

Wignall, P. B., and R. Newton, 1998. Pyrite framboid diameter as a measure of oxygen deficiency in ancient mudrocks. Am. J. Sci. 298, 537–552.

Wignall, P. B., R. J. Twitchett, 2002. Extent, duration and nature of the Permian-Triassic superanoxic event, in Catastrophic Events and Mass Extinctions: Impacts and Beyond, edited by C. Koeberl and K. G. MacLeod, Spec. Pap. Geol. Soc. Am. 356, 395-413.

Wignall, P. B., R. Newton, and M. E. Brookfield, 2005. Pyrite framboid evidence for oxygen-poor deposition during the Permian-Triassic crisis in Kashmir. Palaeogeogr. Palaeoclimatol. Palaeoecol. 216, 183–188.

Wijsman JWM, Middleburg JJ, Herman PMJ, Böttcher ME, Heip CHR, 2001. Sulfur and iron speciation in surface sediments along the northwestern margin of the Black Sea. *Marine Chem* 74, 261-278.

Wilde, P., W. B. N. Berry, 1982. Progressive ventilation of the oceans---Potential for return to anoxic conditions in the post- Paleozoic, in Nature and Origin of Cretaceous Carbon-Rich Facies, edited by S. O. Schlanger and M. B. Cita, pp. 209–224, Academic, New York.

Wilde, P., Berry, W.B.N., Quinby-Hunt M.S., Orth, C.J., Quintana, L.R., Gilore, J.S., 1986. Iridium abundances across the Ordovician-Silurian stratotype. Science 233, 339-341.

Wilkin, R. T., H. L. Barnes, and S. L. Brantley, 1996. The size distribution of framboidal pyrite in modern sediments: An indicator of redox conditions. Geochem. Cosmochim. Acta, 60, 3897–3912.

Winguth, A. M. E., C. Heinze, J. E. Kutzbach, E. Maier- Reimer, U. Mikolajewicz, D. Rowley, A. Rees, and A. M. Ziegler, 2002. Simulated warm polar currents during the middle Permian. Paleoceanography, 17(4), 1057, doi:10.1029/2001PA000646.

Winguth, A. M. E., and E. Maier-Reimer, 2005. Causes of marine productivity and oxygen changes associated with the Permian-Triassic boundary: A reevalution with ocean general circulation models. Mar. Geol. 217, 283–304.

Wood DA, Dalrymple RW, Narbonne GM, Gehling JG, Clapham ME, 2003. Paleoenvironmental analysis of the late Neoproterozoic Mistaken Point and Trepassey formations, southeastern Newfoundland. *Can J Earth Sci* 40:1375-1391.

Xiao S, Zhang Y, Knoll AH, 1998. Three-dimensional preservation of algae and animal embryos in a Neoproterozoic phosphorite. *Nature* 391, 553-558.

Xiao S, Yuan X, Knoll AH, 2000. Eumetazoan fossils in terminal Proterozoic phosphorites? *Proc Natl Acad Sci USA* 97, 13684-13689.

Xiao S, Knoll AH, 2000. Phosphatized animal embryos from the Neoproterozoic Doushantuo Formation at Weng'An, Guizhou, South China. *J Paleont* 74, 767-788.

Xiao S, Shen B, Zhou C, Yuan X, 2005. A uniquely preserved Ediacaran fossil with direct evidence for a quilted bodyplan. *Proc Natl Acad Sci USA* 102, 10227-10232.

Xie, S., R. D. Pancost, H. Yin, H. Wang, and R. P. Evershed, 2005. Two episodes of microbial change coupled with Permo/Triassic faunal mass extinction. Nature 434, 494–497.

Yan, D., Chen, D., Wang, Q., Wang, J., Wang, Z., 2009. Carbon and sulfur isotopic anomalies across the Ordovician–Silurian boundary on the Yangtze Platform, South China. Palaeogeogr. Palaeoclimatol. Palaeoecol. 274, 32-39.

Yan Y, Jiang C, Zhang S, Du S, Bi Z, 1992. Research of the Sinian System in the region of western Zhejiang, northern Jiangxi, and southern Anhui provinces. *Bull of the Nanjing Inst of Geol and Mineral Resources, Chinese Acad. Geol Sci* 12, 1-105.

Yin L, *et al.*, 2007. Doushantuo embryos preserved inside diapause egg cysts. *Nature* 446, 661-663.

Yuan X, Hofmann HJ, 1998. New microfossils from the Neoproterozoic (Sinian) Doushantuo Formation, Wengan, Guizhou Province, southwestern China. *Alcheringa* 22, 189-222.

Zhan, R., Rong, J., Cheng, J.H., Chen, P.F., 2005. Early-Mid Ordovician brachiopod diversification in South China. Science in China (Series D) 48, 662-675.

Zhan, R., Harper, D.A.T., 2006. Biotic diachroneity during the Ordovician radiation: evidence from South China. Lethaia 39, 211-226.

Zhan, R., Jin, J., Chen, P., 2007. Brachiopod diversification during the Early-Middle Ordovician: an example from Dawan Formation, Yichang, central China. Can. J. Earth Sci. 44, 9-24.

Zhan, R., Jin, J., 2007. Ordovician-Early Silurian (Llandovery) Stratigraphy and Palaeontology of the Upper Yangtze Platform, South China. Science Press, Beijing, 169 pp.

Zhan, R., Jin, J., 2008. Aspects of recent advances in the Ordovician stratigraphy and palaeontology of China. Paleoworld 17, 1-11.

Zhang, T., Shen, Y., Zhan, R., Shen, S., Chen, X., 2009. Large perturbations of the carbon and sulfur cycle associated with the Late Ordovician mass extinction in South China. Geology 37, 299-302.

Zhang, Y., Chen X., 2003. The Early Ordovician graptolite sequence of the Upper Yangtze region, South China. INSUGEO Serie Correlacion Geologia 17, 173-180.

Zhou C, Xiao S, 2007. Ediacaran $\delta^{13}C$ chemostratigraphy of South China. *Chem Geol* 237, 89-108.

Zhu M, Zhang J, Yang A, 2007. Integrated Ediacaran (Sinian) chronostratigraphy of South China. *Palaeogeogr Palaeoclimatol Palaeoecol* 254, 7-61.